Modeling the J-V Characteristics of Hybrid Solar Cells based on Planar-Silicon/PEDOT:PSS and SiNW/PEDOT:PSS

Seyed Mohammad Mehdi Mohebi

A Thesis
in
the Department
of
Electrical and Computer Engineering

Presented in Partial Fulfillment of the Requirements
for the Degree of Master of Applied Science at
Concordia University
Montréal, Québec, Canada

June 2014

CONCORDIA UNIVERSITY
SCHOOL OF GRADUATE STUDIES

This is to certify that the thesis prepared

By: Seyed Mohammad Mehdi Mohebi

Entitled: "Modeling the J-V Characteristics of Hybrid Solar Cells based on Planar-Silicon/PEDOT:PSS and SiNW/PEDOT:PSS"

Master of Applied Science (Electrical and Computer Engineering)

Complies with the regulations of this University and meets the accepted standards with respect to originality and quality.

Signed by the final examining committee:

_____ Chair
Dr. A. Amer

_____ Examiner, External
Dr. R. Sedaghati (MIE) To the Program

_____ Examiner
Dr. A. J. Al-Khalili

_____ Supervisor
Dr. M. Kahrizi

Approved by: _____
Dr. W. E. Lynch, Chair
Department of Electrical and Computer Engineering

_____20_____ _____
Dr. C. W. Trueman
Interim Dean, Faculty of Engineering
and Computer Science

ABSTRACT

Modeling the J-V Characteristics of Hybrid Solar Cells based on Planar-Silicon/PEDOT:PSS and SiNW/PEDOT:PSS

Seyed Mohammad Mehdi Mohebi

Solar cell devices have proven to be one of the promising energy resources in the future, owing to the following facts:

First and for most, solar energy is almost always available in all over the world and is an infinite source unlike fossil fuels or other finite resources. Secondly, the expenses associated with the fabrication of solar cell devices, are much less than the fabrication costs of other energy generators. This is because the sun energy is free of charges. Besides, the materials that are used in the solar cell structure are mainly from the most abundant elements on the earth such as silicon. Thirdly, this source of energy is not in conflict with the issue of natural environment pollution. In turn, it helps in eliminating the concern of contamination production, which is a direct result of fossil fuel consumption.

Having investigated for the benefits of these photovoltaic devices, we were motivated to do some significant work in improving the efficiency of these renewable energy resources. Therefore, searching for the best solar cell configurations (planar-Si and SiNW) from the literatures and modeling the optoelectrical characteristics of them by the commercial software was the first step taken in this area. In broad terms, in this work we

investigated the optical and electrical characteristics of the hybrid solar cells as well as analyzing the simulation results for investigating the optimum characteristic of the device for having a higher efficiency and cost effective solar cell.

In this study, we have shown that increasing the trap density reduces the short circuit current, open circuit voltage and the FF in the planar-Si structure. Note that, the same results have been obtained in the SiNW structure except for the short circuit current which did not change by altering the trap density in the SiNW cell configuration. Furthermore, it is demonstrated that increasing the Si material length, enhances the solar cell efficiency, in both SiNW and planar-silicon structures when the dopant concentration of the silicon is $1\times10^{16}\,cm^{-3}$. However, it is found that when Si is doped with $6\times10^{18}cm^{-3}$ atoms, increasing the Si material thickness, does not change the current density and FF in the planar-Si structure while it improves the short circuit current and the cell efficiency in the SiNW based solar cells. By investigating the effect of dopant concentration on the planar configuration, we found that Si substrates with higher dopant concentrations did not result in a better solar cell efficiency. While, in the SiNW structure, the wires with higher dopant concentrations have shown to have a better cell efficiency. Finally, PEDOT: PSS polymer has been found to be a good candidate as the p-type material, since it can make a good heterojunction with silicon in the form of nanowires.

Therefore, this work enables the correlation of silicon material height, dopant concentration and trap density to the end solar cell performance.

ACKNOWLEDGEMENTS

At first, I would like to express my special appreciation and thankfulness to my supervisor Dr.Kahrizi for his constant support along with patience during my research work in the master program.

Besides, I would like to thank my parents who have always been providing me with their Spiritual and material supports throughout my life.

Last but not the least, I would like to thank my wife for all of her supports and sacrifices that she has made on my behalf.

TABLE OF CONTENTS

LIST OF FIGURES

LIST OF TABLES

LIST OF ABBREVIATIONS

ASTM	-	American Society for Testing and Material
IEA	-	International Energy Agency
Si	-	Silicon
ITO	-	Indium Tin Oxide
AL	-	Aluminum
PEDOT:PSS	-	Poly(3,4-ethylenedioxythiophene) Polystyrene sulfonate
AM	-	Air Mass
2D	-	Two Dimensional
HOMO	-	Highest Occupied Molecular Orbital
LUMO	-	Lowest Occupied Molecular orbital
P3HT	-	Poly(3-hexylthiophene)
EHP	-	Electron and Hole Pair
CdTe	-	Cadmium Telluride
CdS	-	Cadmium Sulfied
CIGS	-	Copper Indium Gallium Selenide
NREL	-	National Renewable Energy Laboratory
PV	-	Photo Voltaic
SRH	-	Shockley Read Hall
IQE	-	Internal Quantum Efficiency

PCE	-	Power Conversion Efficiency
EQE	-	External Quantum Efficiency
VLS	-	Vapor Liquid Solid
RIE	-	Reactive Ion Etching
IPCE	-	Incident Photo-Current Conversion Efficiency
CO_2	-	Carbon Dioxide
SiNW	-	Silicon Nano Wire
FF	-	Fill Factor

LIST OF SYMBOLS

J_d	-	Dark current density
J_L	-	Photo current density
J_{sc}	-	Short circuit current
L_n	-	Diffusion length of electrons
L_p	-	Diffusion length of holes
V_{oc}	-	Open circuit voltage
P_{max}	-	Maximum output power
$\alpha(\lambda)$	-	Absorption coefficient
$F(\lambda)$	-	The number of incident photons
$R(\lambda)$	-	The fraction of reflected photons
K	-	Imaginary part of complex refractive index
E_g	-	Band gap
χ	-	Electron affinity
ϵ_r	-	Relative Permitivity
N_a	-	Acceptor concentration
N_d	-	Donor concentration
N_c	-	Effective density of states in conduction band
N_v	-	Effective density of states in valence band

CHAPTER 1

INTRODUCTION

More recently global warming has been accepted as a serious problem originated from fossil fuels such as coal, petroleum and gases. In 2011 approximately 9,000 million short tons of coal were consumed for releasing the energy [1]. Since one ton of coal creates 2.86 tons of CO_2 for creating energy [2], about 25,000 million tons of CO_2 has been produced only during this year. Most scientists believe that the growth in the production rate of CO_2 is responsible for climate changes and global warming which can have adverse effects on human being's life style. Furthermore, every day people are demanding for more energy, which is basically due to the increase in their population. Researchers have found that today around 7 billion people are living on the earth while the population of world is predicted to be around 9 billion in 2040. Besides, the international energy outlook 2013, has forecasted that the energy consumption will grow by 56% in 2040 compared to 2010. Therefore, if the rate of energy consumption is going to further increase, we would be run out of gas and oil reserves in the future. As a result, the problem of global warming and lack of resources would be an issue. Consequently, human being is looking for alternative energy sources such as solar cells, wind, biomass and so on. Since the source of energy for running solar cell devices is the sun, they can be considered as simple and low cost sources for energy production. Furthermore, the energy of the incident light per 1 hour to the earth is more than the whole humans energy

consumption per year [3], that further emphasizes on the choice of solar cells as a promising source of energy in the near future.

1.1. Photovoltaic Devices

Solar cell is a semiconductor device, which consists of two regions with different dopant concentrations, where in the n-type region the concentration of electrons and in the p-type region, the concentration of holes is dominated. In other words, solar cell is a p-n junction device, which has been developed for capturing the incident light in order to produce power for many applications, such as space crafts. Note that, the first solar cell, which converted the incident light to the power, was fabricated and designed in Bell Laboratories in 1955. Nevertheless, currently solar cell devices face cost and efficiency barriers to become one of the widespread energy resources in the industry.

1.2. First Generation solar cells

Bulk silicon and $III-V$ compound semiconductors such as, GaAs are put under the umbrella term of "first generation solar cells". In this type of solar cell, single crystalline Si is much more attractive for manufacturers due to its high efficiency and reliability among other elements during the past 50 years [4]. However, some high cost and high temperature problems exist in the manufacturing processes of this kind of solar cell. Note that, the exploited silicon in the first generation solar cells had to have a minimum thickness of 100μm, due to its indirect band-gap and low absorption coefficient for capturing the incident light [5].

As illustrated in Figure 1.1, the power conversion efficiency of the best crystalline silicon solar cell is about 27.6% which is very close to the theoretical Shockley-Queisser limit of 31% for a single junction solar cell [6].

One way to increase the efficiency in the first generation solar cells is to decrease the surface recombination. This method can be implemented by adding a high-doped layer at the back surface. The reason is that this layer can make a barrier for minority carriers to recombine at the back surface, which leads to an increase in the efficiency of the solar cell. The other solution in reducing the reflection from the surface is to create pyramids by texturing the surface of the device. In the textured silicon surface, when the light strikes the surface, reflects to other pyramids rather than reflect back to the air. As a result, reflection can be reduced from 35% for flat surface to 20% for texture surface of the bulk silicon [7]. Therefore, the short circuit current can increase and improve the efficiency. However, there is not much room to decline the fabrication cost, since the silicon technology is almost developed. The rate of production of multi and mono crystalline silicon solar cells is predicted to be above 80% among all the photovoltaic manufactures during 2014 despite the high cost in their manufacturing processes [8]. This is an issue that should be solved by the second-generation solar cells.

1.3. Second generation solar cells

The production of the second-generation solar cells is dramatically cheaper than the first generation however, second generation solar cells have lower power conversion efficiencies compared to the first generation solar cells. Thin film and organic solar cells are two examples of the second-generation solar cells, which are explained below:

1.3.1. Thin film solar cells

Second-generation solar cells are mainly based on thin films. The goal of thin film solar cell is to reduce the manufacturing cost by using thin layers of semiconductors such as, silicon (Si), cadmium telluride (CdTe), copper indium gallium selenide (CIGS) and so on. As it can be seen in Figure 1.1 their efficiencies can reach to values higher than 20%. These layers can be deposited on at substrate by various methods like plasma evaporation, plating and vapor growth [7]. These solar cells, benefit from the low cost of thin films but at the same time suffer from a large amount of defects inside the Si materials and short term stability [9]. One of the base materials for fabrication of the second-generation solar cells is CdTe [8]. In 2013 Reports by First Solar, showed that the manufacturing cost of a CdTe solar cells is $0.59 per installed watt. However, CdTe is proven to be a toxic material which creates a barrier for further development of it in solar cell application.

1.3.2. Organic solar cells

Another kind of second-generation solar cells are the organic-base photovoltaic. Organic solar cells have some benefits such as, high optical absorption coefficient, flexibility and lower prices compared to the inorganic solar cells like Silicon-base PVs. However, organic solar cells suffer from low conversion efficiency which is due to their low carrier mobility and low diffusion lengths [10]. On the other hand, they are in need of high energies for dissociation of excitons compared to the inorganic PVs. The reason is that in the organic materials the incident photons create mobile excited states instead of free electron hole pairs. Moreover, organic materials have a low dielectric constant which results in excitons with high binding energies [11].Therefore, using heterojunction solar

cells can be considered as a solution to this problem, since this structure can develop a high potential for dissociation of the excitons. This potential is due to the presence of organic materials with different electron affinities in the heterojunction solar cells. Because of this potential in heterojunction solar cells, electrons can be captured by the n-type material and holes by the p-type material, after dissociation of the exitons [11]. As shown in Figure 1.1 the power conversion efficiency of these kinds of solar cells is in the range of 1%-11% with the best performance of 11.1%, which is obtained from organic cells (various types).

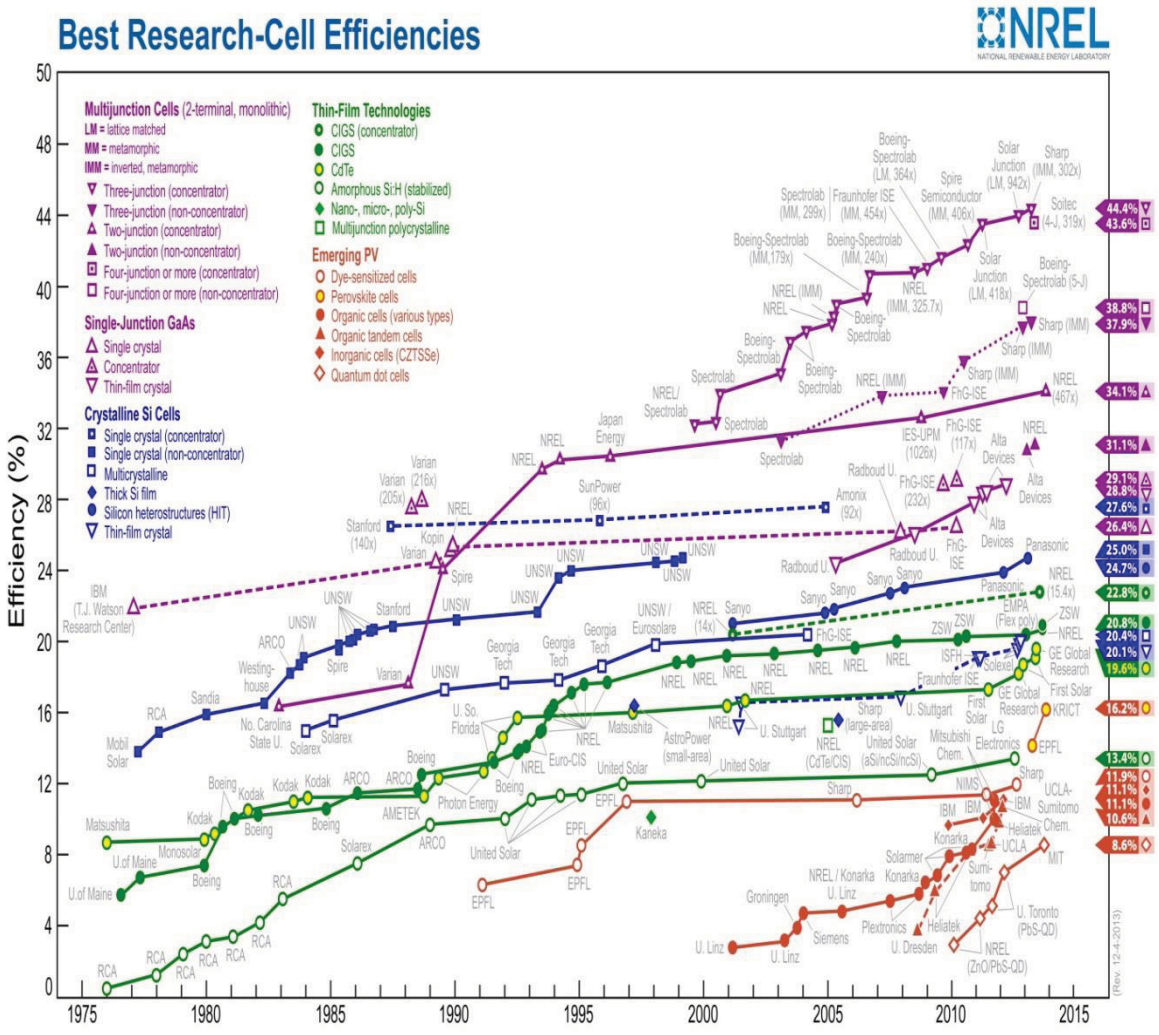

Figure 1.1 The trend of solar cells' efficiency variations during 1975 to 2015 [12].

1.4. Third generation solar cells

Third generation solar cells are still in research work and they are the state of art of the photovoltaic devices. That is due to their capability in increasing the efficiency compared

to the second generation and reducing the cost compared to the first generation solar cells. As shown in Figure 1.2 in this category of solar cells, the power conversion efficiency can increase to a value higher than the Shockley and Queisser limit in the single junction solar cell by some typical methods. These methods consist of tandem solar cells (multi junction solar cells) and using hot carriers through impact ionization [13]. In the former method, different band gap materials can absorb photons with different energies. While in the latter method, photons with high energies can produce other EHPs through impact ionization. Therefore, these methods can help in improving the power conversion efficiency in the third generation solar cells.

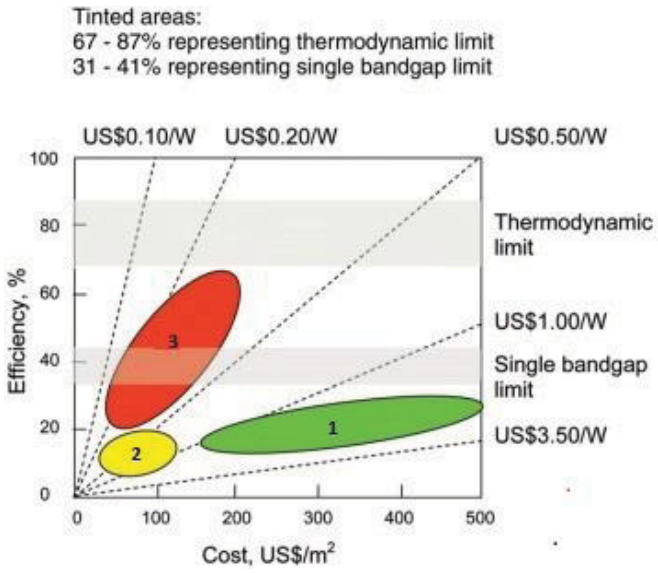

Figure 1.2 Efficiency versus cost for the first (1), second (2) and third (3) generation solar cells [14].

Below are the examples of the third generation solar cells:

1.4.1. Radial homojunction Silicon nanowires (SiNW) solar cells

SiNWs are structures that can be implemented in the fabrication of solar cells with lower light reflection from the surface. Radial homojunction SiNW solar cells have indicated to have a higher conversion efficiency than the conventional solar cells or the first generation solar cells which is due to a shorter collection length for EHPs [5] and a reduction in the reflection from the surface without using anti-reflection coatings. However, the high cost of manufacturing and high temperature doping methods prevents them to be one of the commercialized solar cells [15].

1.4.2. Multi-exciton generation solar cells

In 1961 Shockley and Queisser calculated the maximum thermodynamic efficiency for a single junction solar cell to be approximately 31% [6]. This maximum conversion efficiency was achieved for semiconductors with band gaps ranging from about 1.2 to 1.4 eV. On the other hand, photons in the solar spectrum have energies ranging from nearly 0.5 to 3.5 eV. Therefore, photons with energies less than the band gap the semiconductor do not have the sufficient energy to be absorbed by that semiconductor, While photons with energies higher than the band gap can be absorbed and create electron hole pairs (EHPs) in the semiconductor. Furthermore, photons with energies higher than the band gap create an excess kinetic energy that can be calculated by the difference between the photon energy, which is incident to the semiconductor, and the band gap energy. Note that, Carriers which are created after the absorption of photons might have a temperature 10 times higher than the lattice temperature of 300 K [16]. This excess kinetic energy of the hot carriers can be lost as heat by phonon emission. The phonon lost is one of the major factors, which limit the conversion efficiency. One way in reducing the phonon

lost is to implement materials with different band gaps (tandem solar cell) along the incident light. However the manufacturing cost of these kinds of solar cells is very high [17]. The other solution is to exploit hot carriers before their recombination in their respective band gap. In this case, hot carries can produce the second electron-hole pair through impact ionization [18]. In order to use hot carries for increasing the photocurrent, the rate of impact ionization should be higher than other rates of relaxation processes. Note that, the carrier-cooling rate can be slowed down in the quantum dot semiconductors compared to the bulk semiconductors, which is due to the presence of discreet quantized energy levels in the quantum dot semiconductors [17].

1.4.3. Hybrid solar cells

The performance of the organic solar cells is limited by the low diffusion length of carriers, poor carrier mobility, and low dissociation probability of the EHPs [19]. These issues can be resolved by adding inorganic materials such as CdSe, ZnO and Si which have a higher carrier mobility and a wider absorption spectrum [20]. There are three types of heterojunctions (organic/inorganic) to be used in the solar cell devices: 1) an organic material as the active layer and an inorganic material for transferring carriers to the contacts. 2) Both organic and inorganic materials as the active layer for transferring the photo generated carriers 3) an inorganic material as the active layer and the organic material as a transparent material and as the material for the selective contacts. The latter type of heterojunction solar cell is more attractive because of its high carrier mobility and wide band absorption spectrum of the inorganic materials [21]. Basically, there are two approaches in creating the heterojunction structure between the silicon and PEDOT:PSS polymer. The planar-Si/PEDOT:PSS solar cells have some disadvantages such as, low

absorption coefficient in Si and poor carrier mobility in polymers. However, in SiNW/PEDOT:PSS structure the increase in the area junction of the device results in an improvement in the carrier collection efficiency. Furthermore, the lattice mismatch problem which was observed in the planar-Si/PEDOT:PSS structure can be resolved by the SiNW/PEDOT:PSS radial junction configuration [15]. Moreover, the core/shell junction helps charge carriers to travel a shorter distance to reach the junction, which enhances the collection efficiency of photo-generated carriers. The short collection length in the radial SiNW/PEDOT:PSS junction, is highly beneficial specially in materials with short minority carrier diffusion lengths. Therefore, in SiNW/PEDOT:PSS hybrid solar cells, silicon materials with lower quality or more defects can be used which decreases the high cost of fabrication [22]. In addition in this solar cell configuration, the direction of the light absorption is orthogonal to the carrier separation therefore, each nano-wire can be long in the direction of incident photons to absorb more photons [5].

1.4.3.1. Fabrication of hybrid solar cells

Shiu et al. [23] have examined the specifications of the vertically aligned SiNW/PEDOT:PSS heterojunction solar cells by varying SiNWs lengths. They used an n-type 1-10 Ω-cm Si (100) wafer through an aqueous electroless etching method to create SiNWs [24]. They showed that through a solution based method the PEDOT and SiNW create a core-sheath heterojunction device. The advantage of this device is that the area of the junction has been increased while, the carrier diffusion length has been decreased therefore the carrier collection efficiency has risen significantly. The series resistance of this structure is about 1.47 Ωcm^2 and the power conversion efficiency is around 5.09%. Hybrid solar cells based on polymer and semiconductor materials have some advantages

in their fabrication procedure such as, low-temperature, low cost and easy fabrication techniques. In this category of solar cell devices, a conductive polymer (PEDOT:PSS) has been used as the p-type material and SiNWs as the n-type material to form a p-n junction. Note that, PEDOT has been used due to its desirable electrical and optical properties. The highest occupied molecular orbital (HOMO) energy of PEDOT:PSS is around ~5.1 eV which is near the valence band of the silicon. The interface between polymer and silicon creates a good heterojunction to transfer holes from silicon to polymer. Moreover, the PEDOT:PSS polymer is used to connect the whole SiNWs directly to the ITO electrode, which improves the transport of charge carriers instead of conventional metal fingers. This may decrease the series resistance since carriers have to travel a shorter distance for reaching the electrodes. Furthermore, in the SiNW/PEDOT:PSS structure incident photo-current conversion efficiency (IPCE) is also improved, which is a result of an increase in the collection rate of EHPs and also existence of light trapping effect.

HE et al. [20] found that when there is an increase in the length of the wires the PEDOT:PSS cannot cover the whole surface of the SiNWs, that leads to a reduction in the power conversion efficiency. In this work SiNW arrays which are fabricated by electroless etching technique, are interpenetrated into PEDOT:PSS polymer because of its high conductivity and good transparency. As a result of this good coverage, carrier collection efficiency has been increased. This structure has the power conversion efficiency of 9%.

Ozdemir et al [15] have created SiNW/PEDOT:PSS heterojunctions in a simple and cost effective method. They compared the performance of the SiNW/PEDOT:PSS and planar-

silicon/PEDOT:PSS which are created under the same method as [20] and [23]. The results illustrated that the performance of the SiNW/PEDOT:PSS is much better than the planar heterojunction. In this study, the variation in the lengths of SiNWs has also been examined. The SiNWs are made from the electroless etching method with the n-type monocrystalline silicon wafer (100) and 1-10 Ωcm resistivity.

Lu et al [22] also fabricated SiNW/PEDOT:PSS core-shell junction as the hybrid solar cells. They used a solution and drying method in achieving this structure. SiNWs are made from n-type Si (100) wafer (1-10Ω cm) by silver-assisted chemical etching method. In this structure the performance of the device is limited by the recombination at the interface of the SiNW/PEDOT:PSS junction. The author mentioned that the SiNW arrays are vertically aligned with the height of 2.9 μm. They found that the theoretical limit of V_{oc} in their SiNW/PEDOT:PSS junction solar cell is about 0.56 V. They obtained the ideality factor and the saturation current density to be 2.1 and 3.26 μm cm^{-2}, respectively. The author stated that a high interfacial state density results in a high ideality factor (n). Interfacial states can also be increased, by increasing the dangling bonds at surface of the SiNWs. The higher the interfacial states the higher would be the direct recombination rate, which results in decreasing the short circuit current. Results illustrated that SiNW/PEDOT:PSS solar cells have a lower V_{oc} compared to the planar Si/PEDOT hybrid solar cells. Lower V_{oc} is a result of higher J_s (reverse saturation current). In fact, a high J_s is a result of higher area junction in the SiNW/PEDOT:PSS configuration compared to the planar structure.

HE et al. [25] also fabricated hybrid solar cells using n-type silicon-nano wires spin coated with a conductive polymer (PEDOT:PSS). SiNWs are made by electroless

chemical etching, with a 2.2 μm long silicon-wire as the absorber layer. They compared the performance of the SiNW/PEDOT:PSS with the planar-silicon/PEDOT:PSS solar cells. Results showed that the power conversion efficiency and short circuit current density of SiNW/PEDOT:PSS solar cells has increased compared to the planar-silicon/PEDOT:PSS. They also mentioned that the electroless chemical etching method is a faster and easier method in fabricating SiNWs than other methods such as, vapor liquid solid (VLS) and reactive ion etching (RIE) technics. In addition the author mentioned that the planar-Si/PEDOT:PSS hybrid solar cells are also much more cost effective than the bulk silicon solar cells. In this study it was demonstrated that the power conversion efficiency (PCE) of the planar-Si/PEDOT:PSS has been limited by their low short circuit current (J_{sc}). This is because long-wavelength photons cannot be absorbed completely within the 2.2μm thin film silicon.

H.-J. Syu et al [26] have developed SiNW/PEDOT:PSS hybrid solar cells with conversion efficiency of 8.40% and short circuit current of 24.24 mA/cm^2. They fabricated SiNWs from single crystalline silicon (100) with a resistivity of 1-10 Ω cm. They implemented metal assisted chemical wet etching method in the fabrication of SiNWs and spin coating technique for depositing PEDOT on the SiNWs. These methods are solution process and less costly than other fabrication methods. The author mentioned that SiNW solar cells have some advantages in comparison with the conventional solar cells. The first one is that, SiNWs can be used as an anti-reflection coating as a result there is no need to use anti-reflection coatings to decrease the reflection anymore. Besides, SiNWs in this configuration decrease the series resistance as a result of higher area junction and lower path length which is required for carriers to reach the junction.

However, the open circuit voltage in the SiNW solar cells did not show to be improved compared to the planar structure. This result is due to two reasons: firstly, the open circuit voltage depends on the ideality factor (n), photo generation current density (J_p), reverse saturation current density (J_0) and shunt resistance (R_{sh}). The other reason is that the minority carrier lifetime in the planar solar cell is almost two times greater than the minority carrier lifetime in the SiNW structure. Therefore, the rate of recombination is higher in the SiNW structure and consequently, SiNWs have a higher saturation current density and lower V_{oc}. In this work, it was also illustrated that by increasing the length of SiNWs the performance of the cell has been degraded. Since, as mentioned earlier by increasing the length of wires the PEDOT polymer cannot penetrate into the bottom of the wires, therefore, the junction between the PEDOT and silicon decreases. Furthermore, as it was mentioned before by increasing the length of the silicon nanowire, surface state density and consequently recombination rate increases which result in a reduction in the lifetime.

He et al. [27] investigated the effect of a native oxide layer on the surface of silicon in characteristics of the Si- base solar cell. In this study, the hydrogen-terminated Si surface and oxygen-terminated Si surface solar cells have been examined. Results showed that oxygen-terminated silicon has a better power conversion efficiency (PCE) than the hydrogen-terminated silicon. This is due to the creation of a positive dipole on the surface of silicon in the oxygen-terminated Si, which helps in the separation of charges. The planar-silicon, which was used in this experiment, was made from an n-type single crystalline silicon and had a resistivity of 0.6-1 Ω cm and length of 575 μm. Furthermore, the conductive polymer PEDOT (Baytron PH500) which was mixed with dimethyl

sulfoxide, was spin coated on the surface of silicon. The author stated that the polarity of the created dipoles on the surface of silicon layer could alter its affinity. Because, the covalent bond of hydrogen induces a negative dipole of 0.12 eV on the surface of silicon, the electron affinity of Si which is 4.05 eV, will change to 4.17 eV when hydrogen terminated silicon is considered. This effect creates a bending down of the Si energy bands at the silicon and PEDOT junction, which attributes in the creation of a barrier for holes to enter the PEDOT that leads to an increase in the recombination rate at the junction. Whereas, the covalent bond of oxygen induces a positive dipole of 0.15 eV on the surface of silicon. Consequently, the electron affinity of Si decrease to 3.9 eV, which creates a bending up at the junction of silicon and PEDOT. Therefore, holes can easily travel from silicon to PEDOT, which leads to an increase in the short circuit current (J_{sc}). S. woo et al. [28] have investigated the effect of silicon conductivity on the performance of the hybrid n-type SiNW/PEDOT:PSS polymer. The n-type SiNWs have been fabricated by silver nano-dot-mediated micro electrochemical redox reaction method, on the (100) silicon wafer with a resistivity of 1-10 Ω cm^2 or 0.01-0.02 Ω cm^2. This study illustrated that the junction between Si and PEDOT:PSS polymer makes a stable rectifying solar cell. Furthermore, they showed that the device in which the silicon resistivity is 0.01-0.02 Ω cm^2 (Doping concentration~$10^{18}cm^{-3}$) has a better conversion efficiency than the one with resistivity of 1-10 Ω cm^2 (Doping concentration~10^{15} - $10^{14}cm^{-3}$). This is because, when the dopant concentration is higher (resistance is lower) charges can be easily transferred and collected at the junction. Furthermore, the author said that low performance in this device structure is due to two main reasons: 1) Formation of silicon dioxide at the surface of silicon that creates some defects, which

increase the recombination of minority carrier and 2) the poor coverage of SiNW sidewalls by PEDOT:PSS, which makes a separation between the SiNW and ITO electrode. Note that the latter effect was observed in the SEM images of the device. This observation that the formation of junction between PEDOT:PSS and SiNWs is not complete, illustrates that only a small part of SiNW contributes in the photocurrent production.

F Zhang et al. [29] have fabricated a hybrid schottky diode by using SiNWs and PEDOT. In this work SiNWs are fabricated thorough metal assisted chemical etching technique in which the length of wires are dependent to the etching time. The fabricated hybrid schottky-diode devices are based on SiNWs with different lengths and various spaces between adjacent wires. In this structure, the NWs are spin coated with PEDOT polymer. In this work, SiNWs have been implemented for hybrid solar cells due to their large area junction and capability to induce light trapping effect in the device, which leads to higher light absorption. The author also mentioned that the direction of light absorption is perpendicular to the carrier collection direction, which makes it different from the planar configuration in which these directions are parallel to each other. Because of this orthogonality in the radial junction, the length of nano wires can be long enough so that the maximum light absorption can be achieved and at the same time, nano-wires can be thin enough to minimize the carrier separation length. In other words, in the radial junction structure the maximum of light absorption and carrier separation can be achieved. Due to high collection rate, or minimum collection length in the radial junction configuration, SiNWs can be fabricated based on low purity silicon in which the carriers have low diffusion lengths. Therefore, the radial junction structure can be considered as a

high power conversion efficiency (PCE) based on low cost silicon materials. Furthermore, the external quantum efficiency (EQE) of hybrid solar cells has been measured in the same work. Results showed that over a spectral bandwidth ranging from 300 to 1100 nm, EQE for a solar cell based on SiNWs, which were immersed in a PCl_5 solution for 2 h, has achieved the value of 86% at 510 nm. Furthermore, a hybrid solar cell with smaller ideality factor (n) and reverse saturation current (I_S) and higher Shottky barrier (Φ_{bi}) showed to have a higher power conversion efficiency. The author mentioned that by knowing the ideality factor parameter, one can obtain the mechanism of the charge carrier transport in the device. For example n=1 interprets that the voltage is dependent to the Schottky barrier, and n>1 shows the recombination current in the space charge region. Therefore, the power conversion efficiency will be improved when n approaches unity.

Chen et al. [30] have studied hybrid heterojunction solar cells which were based on micro textured n-type silicon wafer coated with PEDOT polymer. In this work, PCE had a value of 9.84%. Note that, investigation about the output electrical characteristics of the 1-dimensionel model in this work, showed a value of 20% for the power conversion efficiency. Furthermore, the effect of surface recombination, defect density, doping density and band alignment on this kind of solar cells was examined. Results showed a relation between the spin coating rate and the performance of the device in the hybrid heterojunction solar cell based on an n-type mono-crystalline silicon with a thickness of 200 μm and a resistivity of 2 Ω-cm. For instance, it was shown that, when the spin coating rate of PEDOT on silicon was low, the interface contact was very poor. However, a reasonable interface contact could be achieved when the PEDOT coverage on silicon

was good as a result of high spin coating rate. Consequently, the best performance of the device was achieved at the highest spin coating rate (8000 rpm). The author mentioned that in the planar-silicon/PEDOT heterojunction, the short circuit current density and FF are limited due to the high reflection from the surface and finite surface area or high series resistance, respectively. He also mentioned that, PEDOT:PSS due to its low refractive index can be considered as an antireflection coating which helps in improving the short circuit current of the micro-textured hybrid solar cells. In this structure, the internal quantum efficiency (IQE) of the device has been measured to be over 95% in the range of the short wavelengths attributed to the large band gap of PEDOT:PSS which hinders electrons recombination at the polymer side of the device. However, IQE has a lower value in the range of longer wavelengths which results in the recombination in the silicon side of the device. In this work, an electronic model of hybrid solar cell has been also developed to solve the 1-dimensional Poisson and continuity equation, so that a better understanding of the relation between the charge transport and material properties can be achieved. This model is capable of finding the currents, fields and carrier concentrations by calculating the electrostatic potential and quasi Fermi levels. Note that, in this work PEDOT:PSS is assumed as an inorganic material where the lowest unoccupied molecular orbit (LUMO) and the highest occupied molecular orbit (HOMO) are treated as the conduction and valence band, respectively. Therefore, the drift-diffusion model in a two terminal device under illumination or dark condition can explain the carrier transport mechanism. Since the PEDOT layer used in this model is thin and the exciton binding energy of it is lower than other organic materials, the electrical model can be used in order to find the characteristics of solar cells without using too many

assumptions, which are usually used for modeling the organic cells. In addition, simulations have shown that, by increasing the interface and consequently defect density, open circuit voltage and therefore PCE will decrease. Therefore, Methyl groups or other organic molecules have been proven to be efficient in the passivation of the dangling bonds before depositing PEDOT. Moreover, FF can be specified by two mechanisms including, transport and recombination of carriers. Therefore, it can be improved by lowering the interface of PEDOT and increasing the doping concentration. On the other hand, in the same work it was stated that the short circuit current does not mainly depend on the interface and bulk defects, but on the reflection and metal shadow loss. Simulations showed that, the PEDOT polymer with the band gap of 3.6 eV and electron affinity of 3.6 eV has achieved an efficiency of 20.1%. Ultimately, the author predicted that the hybrid solar cells based on the conductive PEDOT polymer and micro textured silicon can achieve a PCE higher than 20% with decreasing the reflection losses and exploiting suitable material properties.

1.5. Research objective

The main objective of this work is to investigate the device operation of hybrid solar cells based on planar-silicon/PEDOT:PSS polymer and SiNW/PEDOT:PSS polymer by analysing the simulation results of both mentioned solar cell configurations. Therefore, this work consists of two sections including the study of: 1) planar-silicon/PEDOT:PSS and 2) SiNW/PEDOT:PSS solar cells.

In this work, Medici CAD tool has been used to simulate these hybrid solar cells. Medici program has been developed to simulate diodes, bipolar transistors and MOS [31]. Taurus Medici software is a 2-dimensional simulator, which models the semiconductor devices and can find the electrical characteristics associated with different biases. Note that, this software is mainly developed for simulating inorganic semiconductors such as Si and GaAs.

Nevertheless, in this work we could perform simulations on the PEDOT:PSS which is in fact an organic material. This ability in implementing organic materials in Medici has been achieved throughout useful information about the optical and electrical properties of PEDOT:PSS polymer, that could help us in finding their equivalent data in Medici.

One of the most important components in the simulation work is to have a complete knowledge about the optical and electrical characteristics of the materials, which are going to be modeled. However, these essential components which are namely: real and imaginary parts of the complex refractive index, band-gap energy, electron affinity, density of states for the conduction and valance band, doping density and electron and hole mobility are not easily found in data bases for organic materials. On the other hand,

since our work is based on organic polymers (PEDOT:PSS), it is vital to investigate the mentioned properties of these materials. As a result, we could finally find them from literature and defined them in the Medici software in order to be able to perform the subsequent simulations.

In broad terms, this work was a study of the effect of Si length, Si dopant concentration and silicon defect density on the principal characteristics of the hybrid solar cells. Besides, the external quantum efficiency, band diagram configuration and photo-generation of EHPs along the device in both SiNW and planar-Si solar cells are illustrated.

1.6. Thesis outline

In this chapter, we first stated the reasons for developing solar cells and explained demand for photovoltaic devices as a renewable energy source. Besides, a history of solar cells was described including the different types and generations of solar cell along with pointing to the advantages and disadvantages of any type and introducing solutions to overcome the problems associated with any solar cell generation. Finally, the third generation solar cells were introduced as the promising generation in the PV devices, owing to the fact that they are capable of having higher efficiencies as well as lower costs compared to other solar cell generations. In chapter 2, the physics and principal parameters of the solar cell devices are studied then the structures of the Hybrid solar cells that have been modeled in Medici are explained. The physical, chemical and optical properties of Si and PEDOT:PSS are described for a better understanding of why these materials have been exploited as the building blocks of our SiNW hybrid solar cells.

Finally, the J-V characteristics of the modeled solar cells have been explained to further clarify the performance of the device. Chapter 3 and 4 are the mainstream of this work since they include the results of the simulations, which are purely done in this research work. The simulations that were operated in this study were based on altering the physical characteristics of the unit cell and investigating the effect of these changes on the principal characteristics of the solar cell. In other words, we examined the effect of dopant concentration, carrier lifetime and Si length on V_{oc}, J_{SC}, FF and PCE in both SiNW and planar-Si configurations. In addition, the analysis of these results is brought in each of these chapters. The simulation results are basically, evaluated through fundamental equations that exist in the physics of semiconductor devices. Finally, chapter 5 is consisting of the conclusion of the total work and an introduction to pertinent research works that are suggested to be done in the future.

CHAPTER 2

BACK GROUND THEORY AND PHYSICAL STRUCTURE

The physics behind the photovoltaic devices, which includes the physics of diodes and an introduction to the major parameters of solar cells as well as the physical structure of the hybrid solar cell devices that has been modeled in this work, are brought in this chapter.

2.1. P-N junction solar cell

Basically, the solar cell is a p-n junction device that has been developed in order to absorb photons and produce power, for a wide range of applications. Photons with higher energies than the band gap of the semiconductor create electron hole pairs (EHPs) while others with lower energies than the band gap, pass the through the device. Figure 2.1 shows the equivalent circuit for the solar cell. There are two currents in the solar cell including dark and photo current. The characteristics of dark current (I_d) is similar to a p-n junction current which has the reverse saturation current in negative voltages and an exponential positive current in positive voltages. The dark current density and reverse saturation current density are illustrated in Equation 2.1 and Equation 2.2, respectively.

$$J_d = \left[\frac{eD_p P_{n0}}{L_p} + \frac{eD_n n_{p0}}{L_n}\right]\left[\exp\left(\frac{eV_a}{nKT}\right) - 1\right] \tag{2.1}$$

$$J_S = \left[\frac{eD_p P_{n0}}{L_p} + \frac{eD_n n_{p0}}{L_n}\right] \tag{2.2}$$

Where K is the Boltzmann constant, T is the absolute temperature, n is called the ideality factor, $n \approx 1$,when diffusion current dominates. Moreover in SRH and band to band recombination in low level injection, the ideality factor is equal to unity [32], the J_s is the ideal reverse saturation current density of the diode, L_n and L_p are the diffusion lengths of the minority carriers and V_a is the applied voltage across the junction, where $p_{n0} = n_i^2/N_d$ and $n_{p0} = n_i^2/N_a$ are thermal equilibrium carrier concentrations. n_i is the intrinsic carrier density, N_a and N_d are the acceptor concentration and donor concentration in p and n region, respectively.

When the light strikes the surface of the solar cell, electron hole pairs (EHPs) are created in its active layer. The separation of electron hole pairs is due to a built-in potential in the p-n junction that transfers these carriers to the electrodes, resulting in the photocurrent of the solar cell. The photocurrent has the opposite direction of the dark current, as a result when the photocurrent outweighs the dark current, J-V characteristics of the diode shifts to the negative currents. In this condition, the resulting power has a negative value, owing to the fact that power has been produced. Equation 2.3 shows the J-V characteristics of the solar cell:

$$J(v) = J_s\left(\exp\left(\frac{qv}{nkT}\right) - 1\right) - J_L \tag{2.3}$$

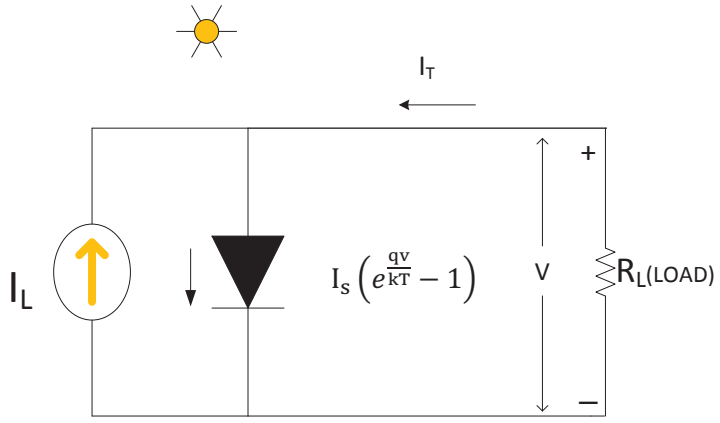

Figure 2.1 An illustration of the equivalent circuit for an ideal solar cell.

2.2. Short Circuit Current

One of the important parameters in the solar cells is the short circuit current density J_{sc}. For ideal solar cells that the series resistance is very low, the short circuit current and photocurrent are identical. Consequently, the maximum current, which is produced by the solar cell, is the short circuit current.

2.4 defines the short circuit current density for a solar cell with the constant generation rate, well-passivated surface and a much smaller depletion width than the carrier's diffusion lengths.

$$J_{sc} = qG(L_n + L_p) \tag{2.4}$$

Where L_n and L_p are the electron and hole diffusion lengths, respectively and G is the generation rate.

Furthermore, for a solar cell in which the diffusion length is much greater than the thickness of the cell, the short circuit current depends only on the generation rate and the diffusion lengths can be neglected.

As an example, silicon solar cells under AM 1.5 spectrums with the power density of 100 mw/cm^2 have a possible maximum current density of 46 mw/cm^2. Note that, market solar cells have a short circuit current density between 28 $mw/cm^2$and 35 mw/cm^2[32].

2.3. Solar Spectrum

The short circuit current is also dependent to the optical properties of the incident light. The energy of the incident light can be approximated by a 5800 K black body [33]. When the light strikes the atmosphere, its power reduces due to the water vapor absorption in the infrared and ozone absorption in the ultraviolet spectrum [33]. Air Mass (AM) is the normalized distance that light travels in the atmosphere. This quantity, which can be calculated by 2.5, identifies the power of the light that is reduced by passage through the atmosphere. Note that, Figure 2.2 is a good illustration of this concept.

$$AM = \frac{1}{\cos\ (\theta)} \tag{2.5}$$

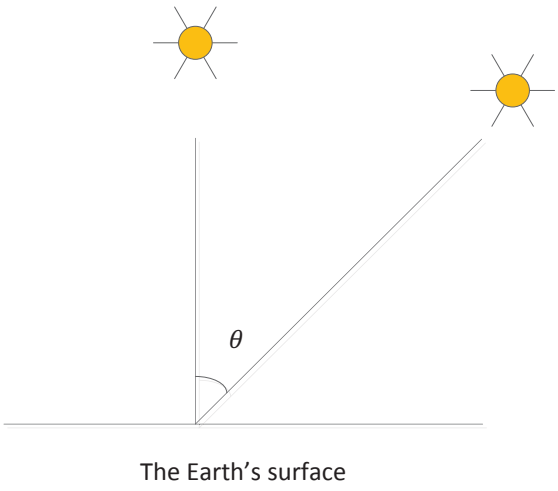

Figure 2.2 An illustration for explaining the Air Mass concept.

Where, θ is the angle from the vertical (zenith angle). For example when the solar spectrums is orthogonal to the solar panel, AM=1, however AM=1.5 refers to the

condition in which the angle of the incident light is about 48º , in this condition the power density has been approximated to be 84.4 mW/cm^2 [7].

Figure 2.3 is an illustration of the approximated spectral irradiation of the AM 1.5 solar spectrum versus different wavelengths which is obtained from the information in the ASTM [34]. This data has been exploited in Medici as the input power density.

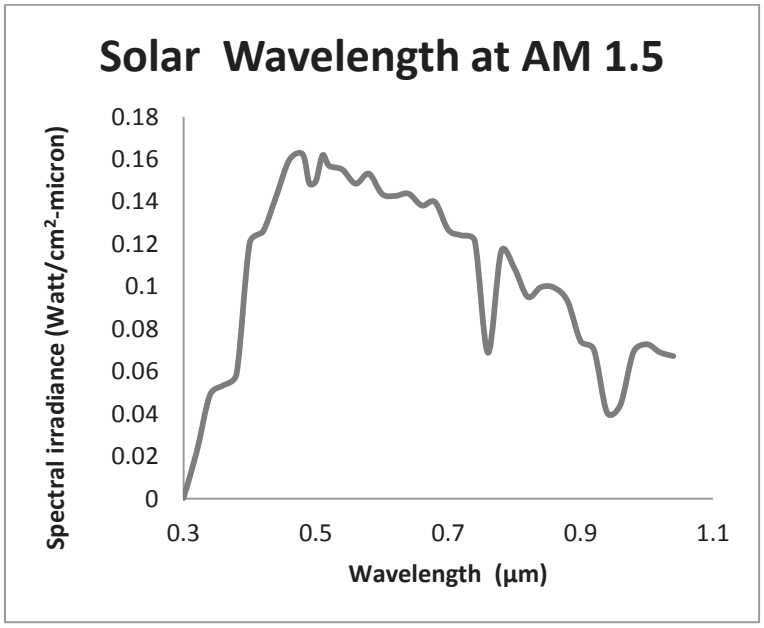

Figure 2.3 Spectral irradiance versus wavelength for AM 1.5 solar spectrum [34].

2.4. Electrical Field

2.4.1. Built-in potential

When a p-type and n-type semiconductor are brought together, excess electrons transfer from n-type to the p-type material and excess holes transfer from the p-type to the n-type material due to the diffusion mechanism. Transfer of electrons from the n-region to the p-region leaves behind positive ions in the n-type region, whereas diffusion of holes from p-region to the n-region leaves behind the negative ions in the p-type region.

Consequently, these ions create an electric field at the junction from positive ions to the negative ions that creates a built in potential at the junction. This built-in potential does not allow carriers to diffuse more however, there are still some carriers with high velocity and enough energy that can cross this electric field. Ultimately, the electric field depletes a certain region near the junction. The built-in potential is a barrier to the majority carriers to diffuse more to the opposite type region whereas, it eases the transfer of minority carriers of one region to the other region. That is, the electric field at the p-n junction impedes electrons (majority carriers) but at the same time helps holes (minority carriers) to travel from n-type region to p-type region. The passage of minority carriers throughout the electric field is called, drift current. In the thermal equilibrium condition, as shown in Figure 2.4, the total current in the p-n junction is zero. When a forward bias is applied to the p-n junction, the electric field across the junction drops to a value, which is the difference between the built in potential and the applied voltage. Reduction of the electric filed across the junction diminishes the barrier for the majority carriers, and increases the diffusion current. Due to the diffusion current holes, which are injected from p-region to the n-region, and electrons which are injected from n-region to the p-region, will recombine with the majority carriers in each side. As a result of this recombination, current flows from n-side to the p-side. Note that, this current is increased by increasing the rate of recombination. The saturation current density (J_s) is a measure of minority carrier recombination in the device. Therefore, a p-n junction with higher recombination rate will have a higher saturation current density (J_s).

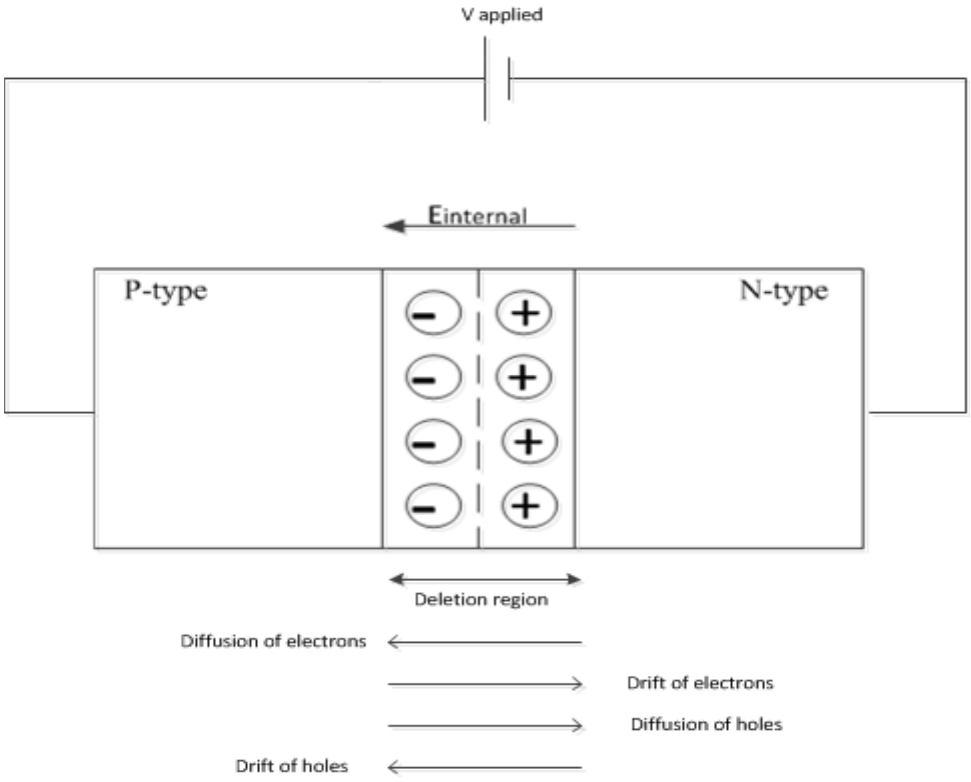

Figure 2.4 Illustration of the produced current in a simple diode.

2.4.2. Open Circuit Voltage

The other important parameter PV devices is the open circuit voltage (V_{oc}) which is demonstrated in Figure 2.5. This parameter is the maximum voltage that a solar cell can produce. The voltage of the solar cell is equal to V_{oc} when the short circuit current is zero. Therefore, the value of the open circuit voltage can be measured by putting the total current in 2.3 equal to zero. When light is exposed to the surface of the solar cell, electron-hole pairs are created. If minority carriers are swept by the electric field, then these carriers increase the number of holes in the p-region and also increase the number of electrons in the n-region. When a load is connected to a p-n junction device, the photo current flows in the external circuit and builds up a voltage across the load. The applied voltage across the load creates an electric field in the opposite direction of the internal

electric field, which was created at the junction before. Therefore, there would be a reduction in the internal electric field, and an increase in the diffusion currents. As a result, two currents will be present at the junction, including the diffusion current of the diode and the photo current, which are in opposite directions. The voltage in which the values of these two currents are equal to each other is called open circuit voltage. According to 2.6 by decreasing the value of J_s, open circuit voltage increases. In other words, J_s is a current that shows the recombination rate of the minority carriers, hence by decreasing this current the open circuit voltage should increase.

$$v_{oc} = \frac{nkT}{q} \ln\left(\frac{J_l}{J_s} + 1\right) \tag{2.6}$$

This equation illustrates the relation between the open circuit voltage, saturation current density and photocurrent of the solar cells. The photocurrent depends on the photons, which are absorbed by the solar cell and the reverse saturation current density (J_s) depends on the recombination rate of minority carriers of the solar cell.

2.5. Fill Factor

Fill factor is determined by the ratio of the maximum power produced by the solar cell to the product of open circuit voltage times short circuit current.

$$\text{FF} = \frac{P_{max}}{V_{oc} I_{sc}} = \frac{Area P_{max}}{Area\ P_{total}} \tag{2.7}$$

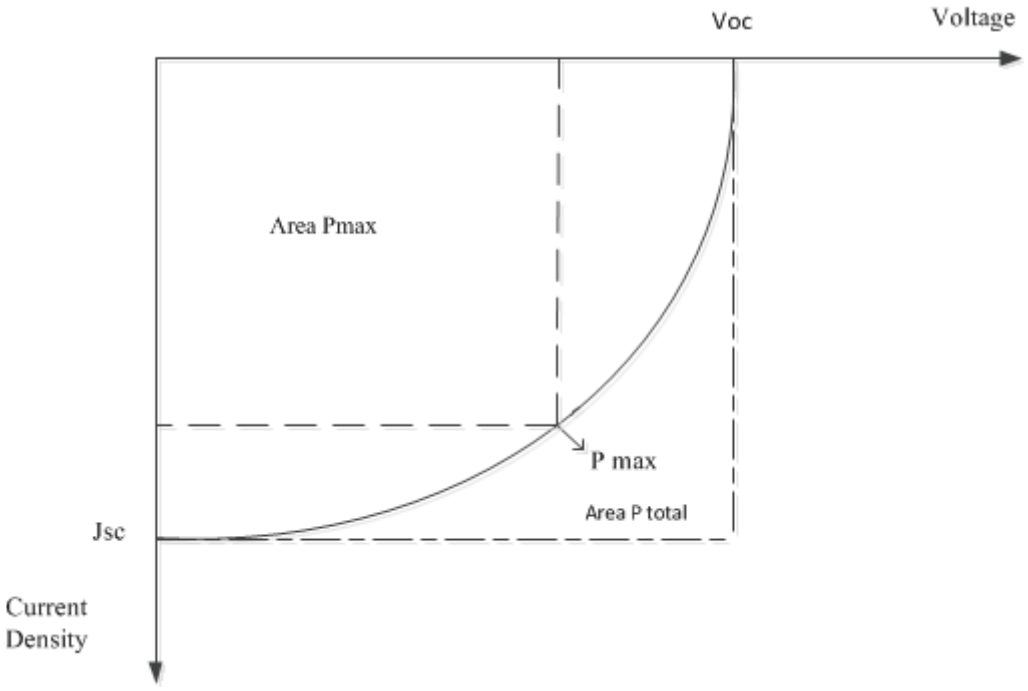

Figure 2.5 A schematic of the I-V characteristic of the solar cell.

Fill factor also depends on the ideality factor and series resistance in the solar cell [7]. The ideality factor is determined by the type of recombination and the quality of a junction in a device. For example, the ideality factor is equal to unity if the low-level injection and the SRH recombination are present in the device, whereas in high-level injection condition and Auger recombination the ideality factor is equal to 2 and 2/3,

respectively. Moreover by increasing the series resistance fill factor will decrease, which leads to a decrease in the convert efficiency of the solar cell [32].

2.6. Structure of planar hybrid solar cell based on thin film silicon and PEDOT:PSS

The physical structure of the device is shown in Figure 2.6. In this structure, electron hole pairs (EHPs) which are created in the n-type silicon will separate by a built-in potential at the junction. In other words, the built-in potential is created at the interface of the Si and PEDOT:PSS. After separation of the EHPs, holes and electrons will be collected by the ITO and AL contact, respectively [29]. The band gap energy of the PEDOT:PSS is ~ 1.6 eV and the highest occupied molecular orbit (HOMO) energy of the PEDOT:PSS is about 5.2 eV. Consequently, the HOMO energy of PEDOT is very close to the valence band energy of the silicon which is about 5.25 eV [23]. Since the PEDOT:PSS layer is very thin and is highly doped we can consider it as a conductive channel and neglect the created EHPs in this region. Since, the band gap energy of PEDOT:PSS is higher than the band gap of the silicon, photons with energies lower than 1.6 eV can be absorbed in the silicon. As shown in Figure 2.6 the ITO electrode has been used as the front contact because of high transparency, and the Al electrode as the back contact due to its high reflectivity.

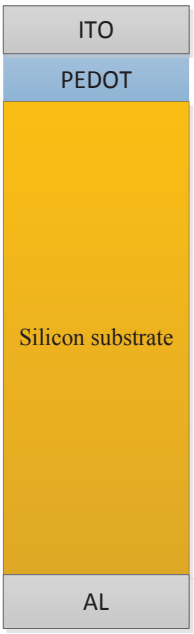

Figure 2.6 The structure of the planar hybrid solar cell.

2.7. The structure of the hybrid solar cell based on well-aligned silicon nano-wires

The structure of the hybrid solar cell based on ordered arrays of silicon nanowires dispersed in PEDOT:PSS polymer is shown in Figure 2.7 . In this kind of solar cell SiNWs with the length of sub-10 micron have been used. The reason is that the PEDOT polymer aggregates at the top of the SiNWs and cannot penetrate to the bottom to make a good junction with silicon, when SiNWs are too long [23][15]. The direction of the incident light is orthogonal to the diffusion direction of photo-generated carriers in the radial structure. As a result of the radial structure, photo-generated carriers have a high separation rate at the junction, which helps in exploiting low quality and low cost silicon

materials [22]. One of the benefits of this structure is the light trapping effect. Due to this effect, light can travel a larger distance in the device, therefore absorption and photocurrent will increase. For example, the SiNW/PEDOT:PSS structure which has been fabricated by reference [22] showed to absorb around 85% to 95 % of the photons in the range of 300-1100 nm of the AM 1.5 light. Note that the ITO film electrode collects holes from the PEDOT:PSS. In conventional solar cells holes should travel to the surface of the device and then be collected at the metal fingers which leads to an increase in the series resistance of the cell [23].

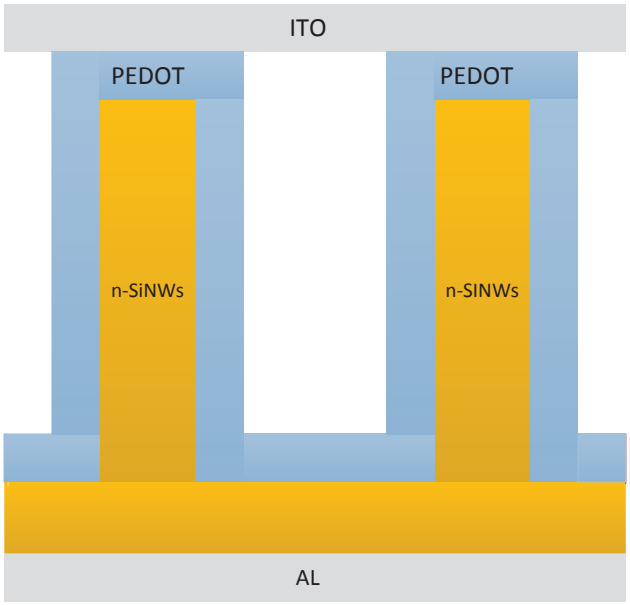

Figure 2.7 A schematic of a hybrid solar cell.

2.8. Silicon

Silicon materials are mainly the building blocks of solar cell devices due to several features such as: 1) second most abundant element on the Earth, 2) high stability and non-toxicity, 3) High carrier mobility and 4) well-established fabrication techniques [29]. Shockley-Queisser calculated the highest conversion efficiency for a single band gap solar cell. He showed that semiconductors with the band gap of about 1.34 eV have the highest conversion efficiencies. Therefore, silicon materials with a band gap of 1.1 eV are good candidates to be implemented in achieving the maximum efficiency of a solar cell device [35]. On the other hand, Si has some drawbacks such as, indirect band gap and low absorption. However, increasing the thickness of silicon material can increase the light absorption in the solar cell. Nevertheless, increasing the thickness of the Si substrate requires a large amount of Si, which leads to the high cost of fabrication due to the high price of the single crystalline silicon materials. In order to avoid the high cost of fabrication, an alternative method called “Si texturing” for reducing the reflectivity from the surface of silicon, has been proposed. As a result of texturing the surface of silicon, absorption will increase. One method in achieving textured surfaces is the inverted pyramids, which are created on the silicon surface by chemical wet etching technique. In this method porous silicon is formed at the starting pit of these inverted pyramids [36].

2.8.1. Silicon nano-wires

Nanowires (NWs) are one dimension (1-D) structure materials with a thickness in the order of nanometer and a high aspect ratio in the order of 100. In other words, the ratio of their length over their diameter is about 100. In addition, the energy levels in NWs differs from the energy levels in the bulk materials [37]. This is due to quantum confinement of

electrons in NWs. SiNW solar cells are highly recommended for the third generation of the photovoltaic devices, since they have some desirable optical and electrical properties due to their geometry. These properties are mainly: 1) minimal bulk recombination and efficient carrier separation in the radial p-n junction structure 2) a small amount of Si is required for SiNW fabrication 3) a reduction in the reflection of light from the surface of the device due to the light trapping effect [38].

2.9. PEDOT:PSS

A conductive polymer which is based on 3, 4-ethylenedioxythiophene or a polymer deposited on an EDOT is called PEDOT. PEDOT is a conductive, transparent, stable and moderate band gap polymer. Based on low solubility of PEDOT materials, they are usually mixed with Polystyrene sulfonate (PSS) so that a high solubility can be achieved. Therefore, PEDOT:PSS which is shown in Figure 2.8 , is a combination of two ion monomers or ionomers [39]. Based on this combination, Polystyrene sulfonate (PSS) carries negative charges and the other component, poly (3, 4-ethylenedioxythiophene) carries positive charges that these charged macromolecules make a macromolecule salt [40]. Note that, these materials are highly applicable in solar cells due to their high conductively.

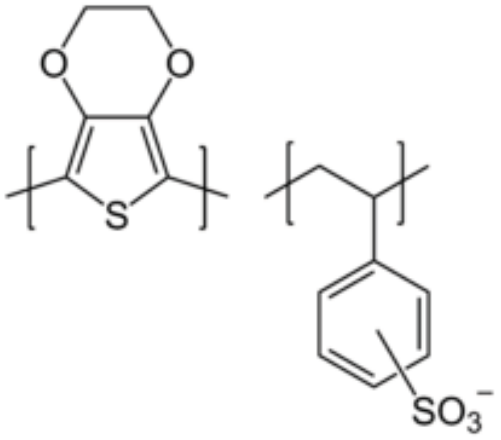

Figure 2.8 A schematic of the PEDOT:PSS polymer [41].

PSS was first mixed with PEDOT in order to make a Polyelectrolyte complex (PEC) in 1990 [39]. In addition to its solubility in water and commercial availability, PSS is almost a transparent material in the range of visible light [40].

As shown in Figure 2.9 the concentration of ionmers in the PEC defines the viscosity of the PEDOT:PSS. Major components in evaluating the quality of the PEDOT:PSS film are: viscosity, surface tension, and the adhesion to the substrate. Figure 2.9 is a good demonstration of the relation between solid concentration and viscosity. Furthermore, the ratio of PEDOT to PSS is one of the factors that should be considered in improving the viscosity, surface tension, and the adhesion to the substrate [39].

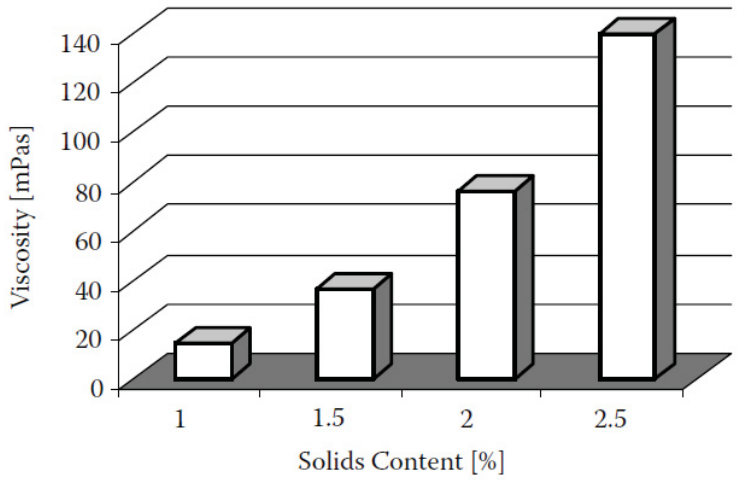

Figure 2.9 The relation between solid contents and viscosity [39].

Table 2.1 is a good comparison between the solid content, viscosity, particle size and conductivity of the PEDOT: PSS, which is presented in here for better perception.

Trade Name	Solids Content in Water (w/w) (%)	PEDOT:PSS Ratio (w/w)	Viscosity at 20°C (mPas)	Particle Size d_{50} (nm)	Conductivity (S/cm)
Clevios P	1.3	1:2.5	80	80	<10
Clevios PH	1.3	1:2.5	20	30	<10
Clevios P VP AI 4083	1.5	1:6	10	40	10^{-3}
Clevios P VP CH 8000	2.8	1:20	15	25	10^{-5}
Clevios PH 500	1.1	1:2.5	25	30	500
Clevios PH 750	1.1	1:2.5	25	30	750
Clevios PH 1000	1.1	1:2.5	30	30	1000

Table 2.1 The properties of the commercial PEDOT:PSS polymers dispersed in water [39].

As mentioned earlier, when the non-solvent PEDOT is mixed with the PSS, the product is soluble in the water. The soluble PEDOT:PSS mixture can be deposited on the desired surface by different coating techniques. Major coating techniques are namely: slit coating, drop casting, bar coating, spin coating, electro-spinning, and spraying. Among

all the mentioned techniques of coating, Spin coating has been shown to be the best in achieving uniform films with the thickness varying in the range of 0-300nm [39]. One of the major advantages of PEDOT:PSS is its flexibility compared to inorganic materials such as metal oxide films. In other words, PEDOT:PSS materials do not break upon bending [42]. The conductivity of PEDOT:PSS can be altered by: 1) changing the ratio of PEDOT to PSS, 2) the distribution of PEDOT:PSS gel particles in solution and 3) changing the PH value of solution [39],[43].

As shown in Equation 2.8, the conductivity parameter is a function of electron and hole concentrations and mobilities. Note that, unit of conductivity is $(\Omega cm)^{-1}$.

$$\sigma = e(\mu_n n + \mu_p P) \tag{2.8}$$

Since PEDOT:PSS is a p-type material, its conductivity is a function of the concentration and mobility of the holes, only. As a result concentration or mobility of electrons does not contribute into the overall current. Concentration of the holes can be calculated by using a geometrical configuration. For example, as it is demonstrated in Table 2.2, when the weight ratio of PEDOT to PSS is 1:2.5 we can get a highly conductive polymer as it is demonstrated in Table 2.1. The density of holes in the PEDOT:PSS polymer has been calculated by their molecular weight to be $3 \times 10^{20} cm^{-3}$. For highly conductive PEDOT:PSS polymers such as Clevios PH1000, the mobility of holes has been calculated to be 20 cm^2 /V-s [39].

2.10. Optical properties of Si and PEDOT:PSS

In order to investigate the electrical characteristics of the silicon-base optoelectronic devices such as solar cells, it is important to understand the optical properties of the

silicon materials. Therefore, exploring concepts such as light trapping, reflection, absorption and transmission in silicon is necessary in this study.

The absorption coefficient is defined as a parameter, which shows how far the incident light with a certain wavelength can penetrate into the materials. The distance is specified by absorption depth, which is inversely proportional to absorption coefficient (α). The absorption coefficient depends on the type of each material and the wavelength of the incident light. Based on Equation 2.9 a light with a higher energy or shorter wavelength has a higher absorption coefficient.

$$\alpha = \frac{4\pi K}{\lambda} \tag{2.9}$$

Where, K is the imaginary part of complex refractive index, λ is the wavelength and α is the absorption coefficient. Furthermore, the equation for the complex refraction indices is shown in 2.10.

$$N = n - iK \tag{2.10}$$

Where n and K are the real and imaginary parts of the complex refractive index, respectively. Note that, increasing the real part of N will result in higher reflection and increasing the imaginary part leads to an improvement in the absorption. The real and imaginary parts of the complex refractive index for silicon are obtained from the default values of Medici, however the optical properties of PEDOT:PSS are taken from the literatures [44] and are displayed in Figure 2.10. Based on this figure silicon has a higher absorption coefficient in a range below 600 nm, which means in this range the absorption depth has a lower value. Therefore, Si can be a good candidate for a low cost fabrication since there is no need for thick Si substrates and consequently excess silicon materials [32]. As it can be seen in Figure 2.10, the absorption coefficient of the PEDOT:PSS is

lower than the silicon in ultraviolet range, however in the visible and infrared range the absorption coefficient of PEDOT:PSS is higher than silicon. Hence, the combination of PEDOT:PSS and Si can be a noble structure for absorbing light in the whole range of light wavelengths.

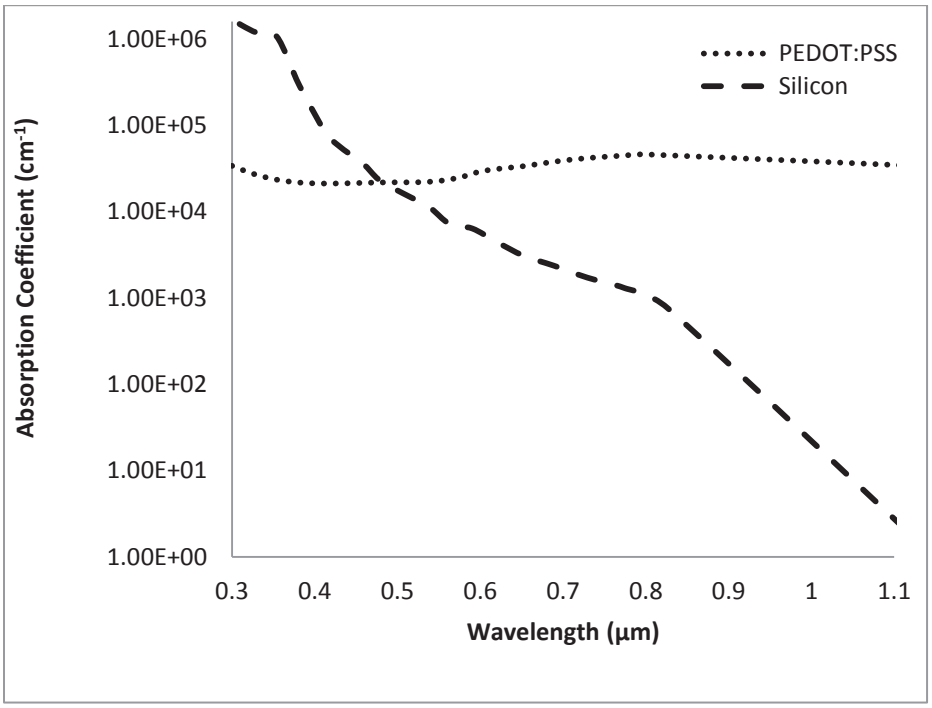

Figure 2.10 Absorption coefficient of silicon and PEDOT: PSS versus Wavelength.

2.11. Carrier transport in p-n junction solar cells

Figure 2.11 represents a p-n junction, in which the front contact is ITO and the back contact is Al. In order to investigate the number of carriers collected per photon at a certain wavelength, photocurrent and spectral response should be calculated. In order to do so, first the rate of generation is defined as the following equation:

$$G(\lambda, X) = \alpha(\lambda)F(\lambda)[1 - R(\lambda)]\exp[-\alpha(\lambda)x] \quad (2.11)$$

Where $\alpha(\lambda)$ is the absorption coefficient, $F(\lambda)$ the number of incident photons /cm^2/s per unit bandwidth and $R(\lambda)$ is the fraction of the reflected photons from the surface of the device.

In the quasi-neutral n-type and p-type regions of the device, excess carries are generated. From continuity equation, the distribution of minority carriers can be found in the n-type and p-type regions. In addition, the steady state continuity equation, under low-level injection and one-dimensional condition is:

$$G_n - \frac{n_p - n_{p0}}{\tau_n} + \frac{1}{q}\frac{dJ_n}{dx} = 0 \quad \text{(for minority carriers in p-type region)} \quad (2.12)$$

$$G_p - \frac{p_n - p_{n0}}{\tau_p} - \frac{1}{q}\frac{dJ_p}{dx} = 0 \quad \text{(for minority carriers in n-type region)} \quad (2.13)$$

Where J_n is the electron current density and J_p is the hole current density. G_n , G_p are the generation rates of n-type and p-type regions, respectively.

$\frac{n_p - n_{p0}}{\tau_n}$, $\frac{p_n - p_{n0}}{\tau_p}$ are the recombination rates for the electrons and holes in the quasi-neutral regions.

In order to solve the continuity equation, it is required to find a relation between the current densities and carrier densities. Furthermore, the current density, which is the summation of the drift and diffusion currents, is:

$$J_n = q\mu_n n_p E + qD_n \frac{dn_p}{dx} \quad \text{(for electrons)} \quad (2.14)$$

$$J_p = q\mu_p p_n E - qD_p \frac{dp_n}{dx} \quad \text{(for holes)} \tag{2.15}$$

In the following equations, it is considered that the electric field in the quasi neutral regions is zero. As a result, in the continuity equation only the diffusion currents in the quasi-neutral regions should be considered. After substituting electron current and the generation rate from the continuity equations 2.16 can be achieved.

$$D_n \frac{d^2 n_p}{dx^2} + \alpha F(1-R)\exp(-\alpha x) - \frac{n_p - n_{p0}}{\tau_n} = 0 \tag{2.16}$$

The general solution of Equation 2.16 is:

$$n_p - n_{p0} = C_2 \cosh\left(\frac{x}{L_n}\right) + C_3 \sinh\left(\frac{x}{L_n}\right) - \frac{\alpha F(1-R)}{\alpha^2 L_n - 1}\exp(-\alpha x) \tag{2.17}$$

Where, L_n is the diffusion length of electrons in p-type region and C_2 and C_3 are the constants of this equation. Note that, constants can be found by considering the boundary conditions of the device.

$$x = 0: D_n \frac{d(n_p - n_{p0})}{d_x} = s_n(n_p - n_{p0}) \tag{2.18}$$

$$x = x_j : n_p - n_{p0} \cong 0 \tag{2.19}$$

S_n is the recombination velocity at the surface. Electron current density, at the depletion edge can be calculated by 2.20.

$$J_n = qD_n \left(\frac{dn_p}{dx}\right) at\ X_j \tag{2.20}$$

By substituting holes current density and generation rate for n-type region in the continuity equation, 2.21 can be achieved.

$$D_p \frac{d^2 p_n}{dx^2} + \alpha F(1-R)\exp(-\alpha x) - \frac{p_n - p_{n0}}{\tau_p} = 0 \quad (2.21)$$

Similarly, applying the boundary conditions for holes in n-type region in the above equation:

$$x = x_{j+w} : p_n - p_{n0} \cong 0 \quad (2.22)$$

$$x = L: s_p(p_n - p_{n0}) = -D_p \frac{d(p_n - p_{n0})}{d_x} \quad (2.23)$$

Where, S_p is the recombination velocity at the bottom of the device, W is the width of the depletion region and L is the length of the device. The hole photo current density at the depletion edge is:

$$J_p = -qD_p \left(\frac{dp_n}{dx}\right) \; at \; X_{j+W} \quad (2.24)$$

And the current in the depletion region which is only from generation is:

$$J_{dr} = \int_{X_J+W}^{X_J} eGdx \quad (2.25)$$

$$J_{dr} = qF(1-R)\exp\left(-\alpha x_j\right)[1 - \exp(-\alpha W)] \quad (2.26)$$

Therefore, the total photo current can be calculated by the following equation:

$$J_{ph}(\lambda) = J_p(\lambda) + J_n(\lambda) + J_{dr}(\lambda) \quad (2.27)$$

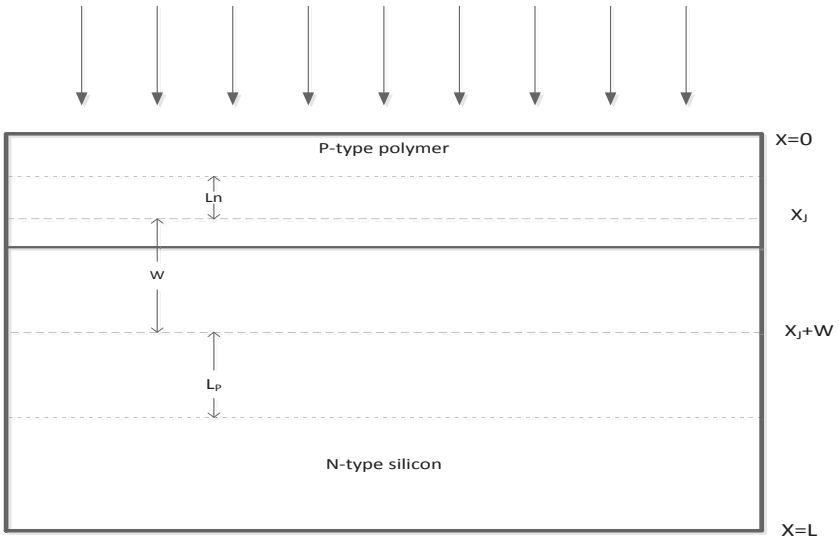

Figure 2.11 An illustration for expalining the solar cell equations.

2.12. J-V curves of Hybrid solar cells

The practical efficiency differs from the ideal one, since in practice, series and shunt resistances are added to the ideal configuration, which is shown in Figure 2.12. Series resistance consists of contacts resistance and the resistance, which is developed due to passage of electrons through the surface of the device, where the electrodes are placed. Note that, by increasing the series resistance, short circuit current decreases and consequently both FF and efficiency degrade. Shunt resistance is due to the presence of grain boundaries that leads to the recombination of carriers that tend to flow through the crystal. Note that, series resistance is more important to be considered than the shunt resistance unless, the density of the grain boundaries exceed a certain limit where the material is called polycrystalline [7].

In order to investigate the J-V characteristics of the device we should sum all the currents at a node in the circuit, which is illustrated in Equation 2.28.

$$I_L + I - I_D - I_p = 0 \tag{2.28}$$

Where:

$$I_D = I_S\left(e^{\frac{V-R_SI}{nv_t}} - 1\right), v_t = \frac{KT}{q} \tag{2.29}$$

And,

$$I_p = \frac{V - R_sI}{R_P} \tag{2.30}$$

Therefore, the total current is equal to:

$$I = I_s\left(e^{\frac{V-R_SI}{nv_t}} - 1\right) + \frac{V - R_sI}{R_p} - I_L \tag{2.31}$$

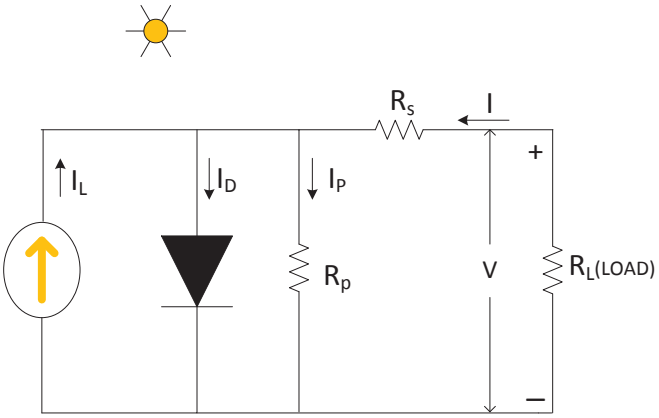

Figure 2.12 A schematic of the equivalent circuit of a practical solar cell.

CHAPTER 3

PLANAR-SILICON/PEDOT:PSS SOLAR CELL MODELING

A planar hybrid unit cell of a solar cell, based on silicon, coated with a 20 nm thick p-type polymer (PEDOT:PSS), has been simulated. Simulations are done by using finite element semiconductor device simulator software: Taurus Medici from Synopsys. In this hetrojunction, silicon layer thickness, dopant concentration and the concentration of defects was subjected to change, in order to examine the electrical characteristics of the device. The short circuit current density (J_{SC}) is shown to decrease by increasing the trap density (defects) in the silicon layer. As an example, when the trap density increased from$1 \times 10^{12} cm^{-3}$ to $1 \times 10^{17} cm^{-3}$, current density reduced by $11.01 mA/cm^2$. Moreover, by increasing the trap density, the open circuit voltage (V_{OC}) decreased from 0.65V to 0.275V and the power conversion efficiency (PCE) dropped by 7.87%, which is due to a reduction in the value of both short circuit current and open circuit voltage. It is investigated that, although increasing the thickness of the silicon layer helps for more photon absorption, in highly doped devices this increase in the dopant concentration will not lead into a higher short circuit current. Results show that the value of the open circuit voltage increases by increasing the dopant concentration of the silicon as a result of reduction in J_s (reverse saturation current). The maximum external quantum efficiency of the unit cells was measured to be 69% and 60% for the dopant concentration 1×10^{16}cm^{-3} and $6\times 10^{18} cm^{-3}$, respectively. Moreover, the simulation results show the impact of band alignment and photo generation in the unit cell.

3.1. Device Structure

In this work, a planar hybrid heterojunction solar cell based on silicon and PEDOT:PSS polymer, is simulated with the device modeling software Medici. The thickness, dopant concentration and the concentration of defects of these were subjected to change in order to find the electrical characterizations. Figure 3.1 represents the modeled structure of a planar-silicon based solar cell in which Aluminum and ITO are used as the back and front contact, respectively.

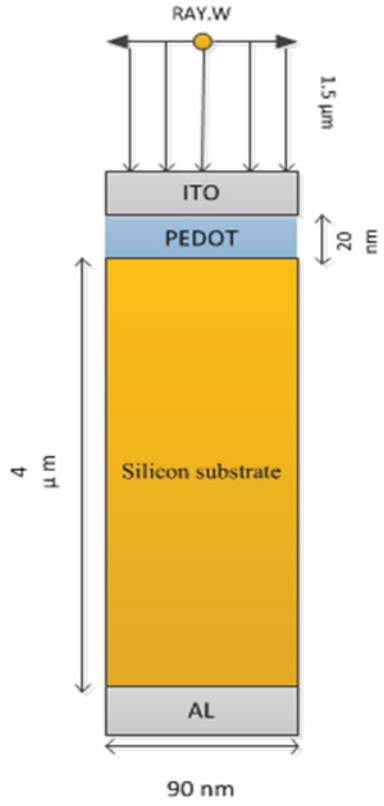

Figure 3.1 A schematic of the modeled planar-silicon based solar cell.

Note that, in the above structure, the thickness of the silicon layer is 4μm and its width is 90nm. Furthermore, a layer of p-type polymer (PEDOT:PSS) with a thickness of 20 nm, has been deposited on the top of n-type silicon layer in order to make a heterojunction.

A planar-Silicon/PEDOT:PSS hybrid solar cell, has been previously fabricated by He et al [25]. They first doped the silicon with a high concentration of about$1 \times 10^{20}\ cm^{-3}$. Afterwards, an epitaxial layer of single crystalline silicon with a dopant concentration of $1.5 \times 10^{16}\ cm^{-3}$ and thickness of 2.2 μm was grown on the n^{++} silicon substrate at 1000 °C. Finally, the PEDOT:PSS polymer was spin coted on the top of the whole silicon sample. Note that, a layer of Aluminum and silver has been evaporated on the planar structure as the back and front contact, respectively.

3.2. Simulation Parameters

Table 3.1Table 3.1 is an illustration of the electrical properties of the PEDOT:PSS polymer. In addition, silicon electrical properties are obtained from the default values of the Medici software and are shown in Table 3.2

Parameters	PEDOT:PSS Values	References
Permittivity(ε_r)	3.5	[45]
N_aDoping (cm^{-3})	10^{19}	[39]
Nc,Nv (cm^{-3})	2×10^{21}	[45]
Affinity(V)	3.6	[45]
E_g(eV)	1.6	[45]
μ_p ($\frac{cm^2}{V-S}$)	20	[39]

Table 3.1 PEDOT:PSS electrical properties which were used in the simulations.

Parameters	Silicon Values	References
Permittivity (ε_r)	11.8	[31]
N_dDoping (cm^{-3})	1×10^{16},6×10^{18}	[31]
Nc,Nv (cm^{-3})	2.8×10^{19},1.4×10^{19}	[31]
Affinity(eV)	4.17	[31]
E_g(eV)	1.08	[31]
μ_n ($\frac{cm^2}{V-S}$)	1076,113.6	[31]
σ_n, σ_p (cm^2)	1×10^{15}	[5]
v_{th} ($cm\ s^{-1}$)	1×10^{7}	[5]

Table 3.2 Silicon electrical properties, which were used in the simulations.

In order to investigate the relation between carrier transport and material properties, Medici software has been used to solve the Poisson equation and the electron and hole continuity equations in a 2-dimension distribution. Therefore, the current, electric field and carrier concentration can be computed. Taurus Medici software is a 2-dimensional simulator, which models the semiconductor devices. Medici can be used to design the p-n junction semiconductors and find the spectral response of the optical devices.

The electrical output characteristics of the planar-silicon and PEDOT:PSS unit cell with different thicknesses under the power density of 84mW/cm^2 have been examined. The light source used in the simulations is obtained from the solar spectrum ranging from 0.3μm to1.1μm, which is approximated from AM 1.5 solar spectrum from the ASTM [34].

In this work, in order to be able to implement PEDOT:PSS layer in the simulations, it was assumed as an inorganic material where the lowest unoccupied molecular orbit (LUMO) is considered as the conduction band and the highest occupied molecular orbit (HOMO) as the valence band [30]. Moreover, the Shockley-Read-Hall recombination from a single trap level at the mid-gap has been considered in this modeling .The materials which were used in the simulations were not heavily doped therefore, Auger recombination has not been considered in this model. In a real semiconductor due to the presence of defects in the crystal, some energy levels do exist in the band gap. Note that, Shockley, Read and Hall have analyzed this type of recombination. The following equation describes the recombination of the localized states which is derived by Shockley, Read and Hall, where U shows the net rate of recombination [46].

$$U = \frac{N_r v_{th} \sigma_n \sigma_p (pn - n_i^2)}{\sigma_p \left[p + n_i \exp(\frac{E_i - E_t}{KT})\right] + \sigma_n \left[n + n_i \exp(\frac{E_i - E_t}{KT})\right]} \quad (3.1)$$

Equation 3.1 shows that, if the cross section area of the electrons and holes be the same ($\sigma_p = \sigma_n = \sigma_0$) and $\tau_0 = (N_r V_{th} \sigma_0)^{-1}$, the following equation can be achieved:

$$U = \frac{pn - n_i^2}{\left[p + n + 2n_i \cosh\left(\frac{E_t - E_i}{kT}\right)\right] \tau_0} \quad (3.2)$$

Where, E_t is the trap level energy.

In this equation, the bracket in the denominator has its minimum value when $\cosh\left(\frac{E_t - E_i}{kT}\right)$ is equal to 1. This condition occurs when $E_t = E_i$, meaning that the traps or recombination states are in the middle of the band gap. Therefore, the maximum rate of recombination happens when traps are far from the edges (conduction or the valance bang edge). In other words, when the recombination states are close to the band edges electrons and holes can be easily re-emitted to the conduction band and valance band, respectively. In this case, these traps are not considered as effective recombination states. Since in this work the effect of recombination is studied, effective recombination states are considered.

One of the most important parameters in the solar cell, which determines the recombination rate, is the carrier lifetime of the excess minority carriers. In the depletion region, lifetime can be defined by the following equation:

$$\tau_{n0} = \tau_{p0} = \tau_0 = \frac{1}{\sigma_0 N_r \upsilon_{th}} \quad (3.3)$$

Where σ_0 is the cross section area of the holes and electrons. N_r is the density of the recombination centers, and υ_{th} is thermal velocity. We have assumed that the trap density in the depletion region and quasi-neutral regions are the same and constant. Hence, the lifetimes in the quasi-neutral regions and depletion region are the same. As shown in Equation 3.1lifetime is inversely proportional to the trap density. In the silicon N_r has been reported to be in the range of 7×10^{12} cm^{-3} and 7×10^{17} cm^{-3} [5]. Note that, defects have the same behavior as traps, since they degrade carrier transport by capturing carriers.

3.3. Simulation Results

3.3.1. Effect of trap density or carriers lifetime on Jsc, Voc and PCE

In this work, a planar hybrid unit cell of a solar cell with the thickness of 4μm and a width of 90 nm has been simulated. As shown in Figure 3.1 a 20 nm thick p-type polymer (PEDOT:PSS) has been coated on the planar-silicon as a p-type material to create a heterojunction with the n-type silicon, having a carrier concentration of $6 \times 10^{18} cm^{-3}$.

In general, an ideal semiconductor is the one that there are no energy levels within its forbidden gap. However, in a real semiconductor due to the presence of defects in the crystal, some energy levels do exist in this region [47]. Carrier lifetime, which was defined earlier, has a direct relationship with these allowed energy states, which are

formed within the forbidden gap. Therefore, this parameter, Carrier lifetime, can be defined by the Shockley-Read-Hall theory of recombination. The mentioned energy states within the forbidden gap, which are also known as traps, act as recombination centers. These traps or in other words recombination centers are states for capturing electrons and holes. Since the cross section area of these traps for electrons and holes is almost the same, the probability of capturing electrons and holes are nearly equal to one another [47]. As can be seen in Figure 3.2, reduction in the value of J_{sc} is the result of an increase in the trap density (N_r) and decrease in τ. Note that, electron and hole trap densities are assumed to be the same in the simulations.

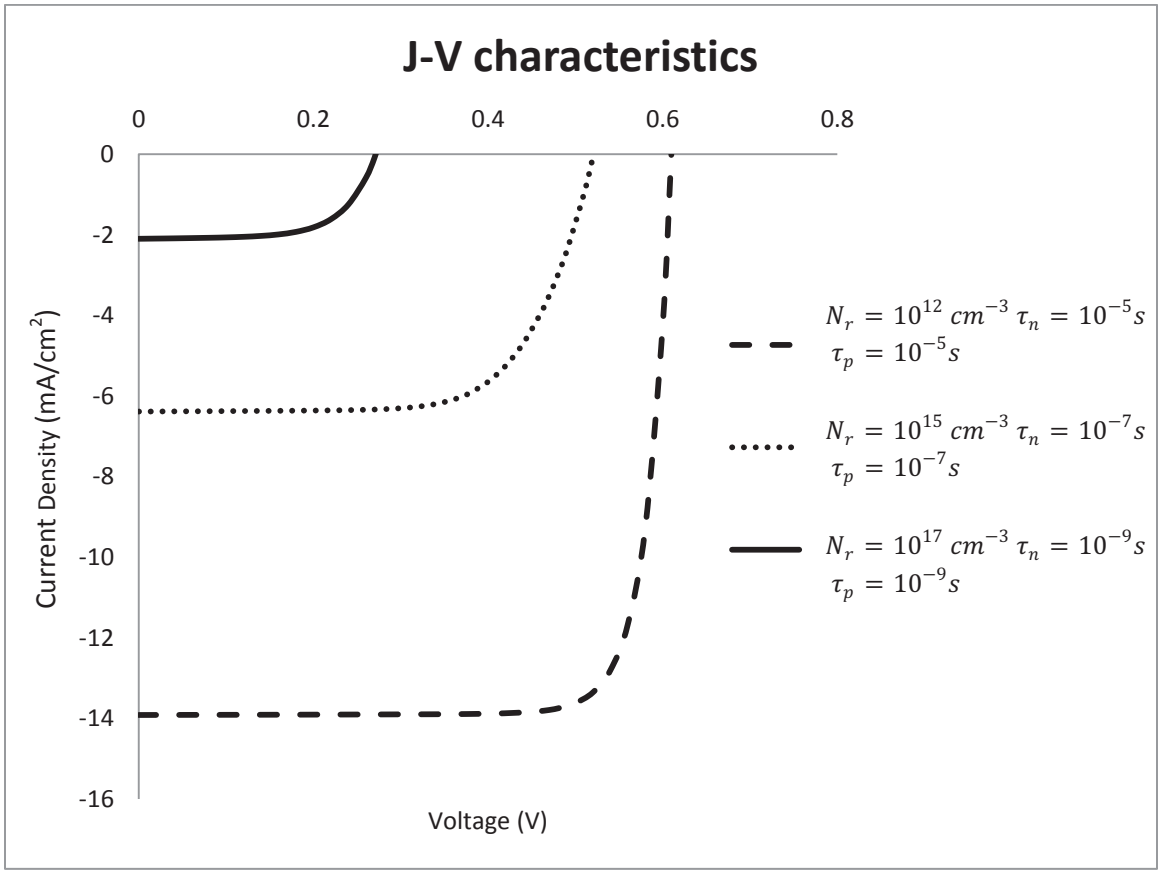

Figure 3.2 J-V Characteristics of the planar-silicon/PEDOT:PSS solar cell with a length of the 4μm and different trap densities.

Test	Silicon Trap Density (cm^{-3})	$electron\ life\ times(s)$	$Hole\ life\ times(s)$	V_{oc} (Volt)	J_{sc} (mA/cm^2)	FF (%)	PCE (%)
1	1×10^{12}	10^{-5}	10^{-5}	0.65	13.91	82.28	8.23
2	1×10^{15}	10^{-7}	10^{-7}	0.525	6.38	67.47	2.69
3	1×10^{17}	10^{-9}	10^{-9}	0.275	2.09	63.15	0.36

Table 3.3 The electrical charactestics of the planar-silicon/PEDOT:PSS solar cell for different silicon trap density.

Table 3.3 shows that, increasing the trap density decreases short circuit current (J_{sc}) which is in agreement with Equation 3.3. This equation says that, increasing the density of traps when the thermal velocities and cross section areas are constant reduces the lifetime. Based on 3.7 when mobility is assumed to be constant, lifetime (τ), which is defined as the average time that electron-hole pairs spend in an excited state before being recombined, is proportional to L^2. Therefore, reducing the lifetime will decrease the diffusion length (L). As a result, electron hole-pairs will travel a shorter distance and recombine before they reach the junction, where they have to be separated and generate the current. As an example from the mentioned table, when the trap density increases from $1 \times 10^{12} cm^{-3}$ to $1 \times 10^{17} cm^{-3}$, we have a current density reduction of $11.01 mA/cm^2$. Note that, trap density was assumed to be the same in the depletion and quasi-neutral region. Furthermore, there was a reduction in the open circuit voltage, which is

due to a lower photocurrent that was discussed above. Moreover, FF, which is determined by the recombination and carrier transport rate in the unit cell, decreased as a result of more recombination of minority carriers, when the tarp density was increased. Finally, the device efficiency dropped by 7.87%, when the trap density increased from $1 \times 10^{12} cm^{-3}$ to $1 \times 10^{17} cm^{-3}$. This is due to a reduction in the value of both short circuit current and open circuit voltage, which were just discussed.

Simulations showed that, decreasing the electron lifetime does not affect short circuit current, but decreased the open circuit voltage (V_{OC}) slightly. The reason is that, our sample is n-type silicon where the minority carriers are holes. In a semiconductor, current is carried by minority carriers therefore, varying the electrons lifetime, which are not the minority carriers of our sample, does not change the current and voltage. As an example, Table 3.4 shows that, when there was a decrease in the electron lifetime from 10^{-7}s to 10^{-9}s, short circuit current remained almost the same since by decreasing the electron lifetime, hole diffusion length remained constant at a value of about 0.4 μm. However, decreasing the hole lifetime by the same factor to 10^{-9}s, dramatically degraded the short circuit current and open circuit voltage. This is because, the reduction in the hole lifetime decrease the diffusion length of minority carriers from 0.4μm to 0.04μm.

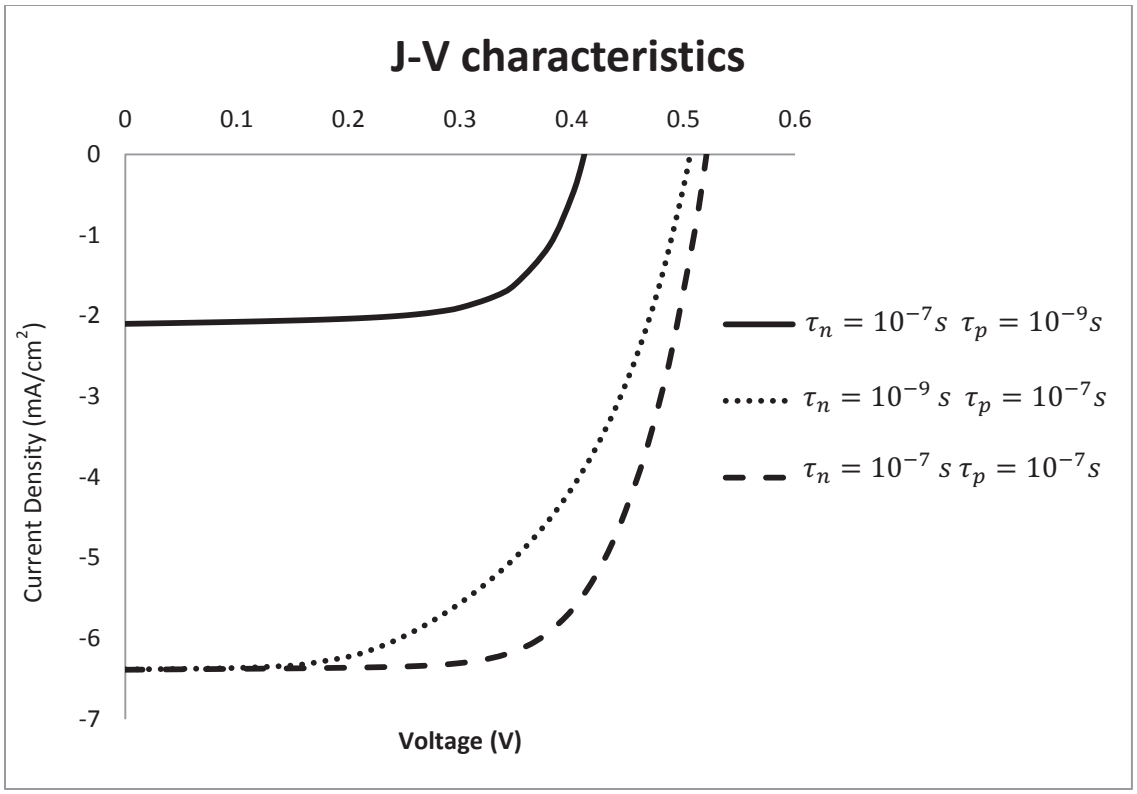

Figure 3.3 J-V Characteristics of a planar-silicon/PEDOT:PSS solar cell with a thickness of the 4µm and different electrons and holes lifetimes.

Test	$electron\ life\ times(s)$	$Hole\ life\ times(s)$	V_{oc} (Volt)	J_{sc} (mA/cm^2)	FF (%)	PCE (%)	diffusion length of holes in silicon(μm)
1	10^{-7}	10^{-7}	0.525	6.38	67.47	2.69	0.4
2	10^{-9}	10^{-7}	0.5	6.38	54.54	2.07	0.4
3	10^{-7}	10^{-9}	0.415	2.1	66.89	0.69	0.04

Table 3.4 The charactestics of the planar-silicon/PEDOT:PSS solar cell for different electron and hole lifetimes.

3.3.2. Effect of the Si layer thickness on Jsc, Voc and PCE

J-V characteristics for a planar-silicon and PEDOT:PSS polymer with a trap density of $10^{15} cm^{-3}$ have been obtained. J-V curves of three different thicknesses (including 2µm, 4µm and 8µm) of Si substrate with a dopant concentrations of $1 \times 10^{16} cm^{-3}$and $6 \times 10^{18} cm^{-3}$ are demonstrated in Figure 3.6 and Figure 3.7, respectively.

Based on 3.4 by increasing the thickness of the unit cell the current will increase.

$$J_l \propto (1 - e^{-\alpha L}) \tag{3.4}$$

In 3.4 α is the absorption coefficient of the silicon and L is the thickness of the substrate. Note that, increasing the thickness of the cell results in, more photon absorption.

The simulations are done in order to investigate the effect of thickness on the cell efficiency. Therefore, in all examinations, the only parameter that was subjected to change was the thickness of the cell, and the thickness of the PEDOT:PSS at the top of the cell was kept constant at the value of 20 nm. Note that, the thicknesses that are used in plotting these figures are without considering the thickness of the electrodes. In each simulation, three different thicknesses of Si layer including 2µm, 4µm, and 8µm have been examined.

Results show that, in a Si with the dopant concentration of $1 \times 10^{16} cm^{-3}$, by increasing the thickness of the Si layer, FF, V_{oc}, J_{sc} and the PCE has increased, which means that more photons have been be absorbed. The results of these simulations are illustrated in the Table 3.5 and Figure 3.4. Based on Table 3.5 and Figure 3.5, when the dopant concentration of the silicon substrate is $6 \times 10^{18}\ cm^{-3}$, results do not show the same trend. In this case, open circuit voltages, fill factor and short circuit current are almost the

same for all three different thicknesses. The reason is that, by increasing the dopant concentration, mobility will decrease because of the increase in the number of impurity scattering centers increased [47]. Moreover, based on Equation 3.5 diffusion constant will decrease by decreasing the mobility.

$$D_p = \frac{KT}{q}\mu_p \tag{3.5}$$

Based on the carrier-concentration dependent lifetime Equation 3.6, lifetime is a function of the dopant concentration where it decreases by increasing N_{total} (dopant concentration). In Equation 3.6 $TAUP0$ is the Shokley-Read-Hall hole lifetime and $NSRHP$ is the Shokley-Read-Hall concentration parameter for holes which are both assumed to have constant values in Medici [31].

$$\tau_P = \frac{TAUP0}{1 + N_{total}/NSRHP} \tag{3.6}$$

The assumed values for $TAUP0$ and $NSRHP$ in Medici software are stated bellow:

$$TAUP0 = \text{Hole lifetime} = 10^{-7}\ \text{s}$$

$$NSRHP = 5 \times 10^{16}\ cm^{-3}$$

Therefore, based on 3.5, 3.6 and 3.7, diffusion length will decrease when there is an increase in the dopant concentration. As a result of low diffusion length in highly doped Si substrates, varying the thickness of the Si layer does not really affect FF, V_{oc}, J_{sc} and the power conversion efficiency.

$$L_p = \sqrt{\tau_p D_p} \tag{3.7}$$

Where τ_p is the lifetime of minority carriers (hole) in the n-type quasi neutral region and D_p is the hole diffusion coefficient and L_p is the hole (the minority carrier) diffusion length.

When, $N_{total} = 1 \times 10^{16} cm^{-3}$:

$\tau_p = 4.54 \times 10^{-8}$s and mobility μ_p =460.9$\frac{cm^2}{V-S}$ then D_p =11.98 cm^{2}s^{-1}

So, the hole diffusion length L_p =7.37μm

And when, $N_{total} = 6 \times 10^{18} cm^{-3}$

$\tau_p = 8.26 \times 10^{-10}$s and mobility μ_p=74.5 $\frac{cm^2}{V-S}$ then D_p = 1.93 cm^{2}s^{-1}

So, the hole diffusion length L_p =0.4 μm

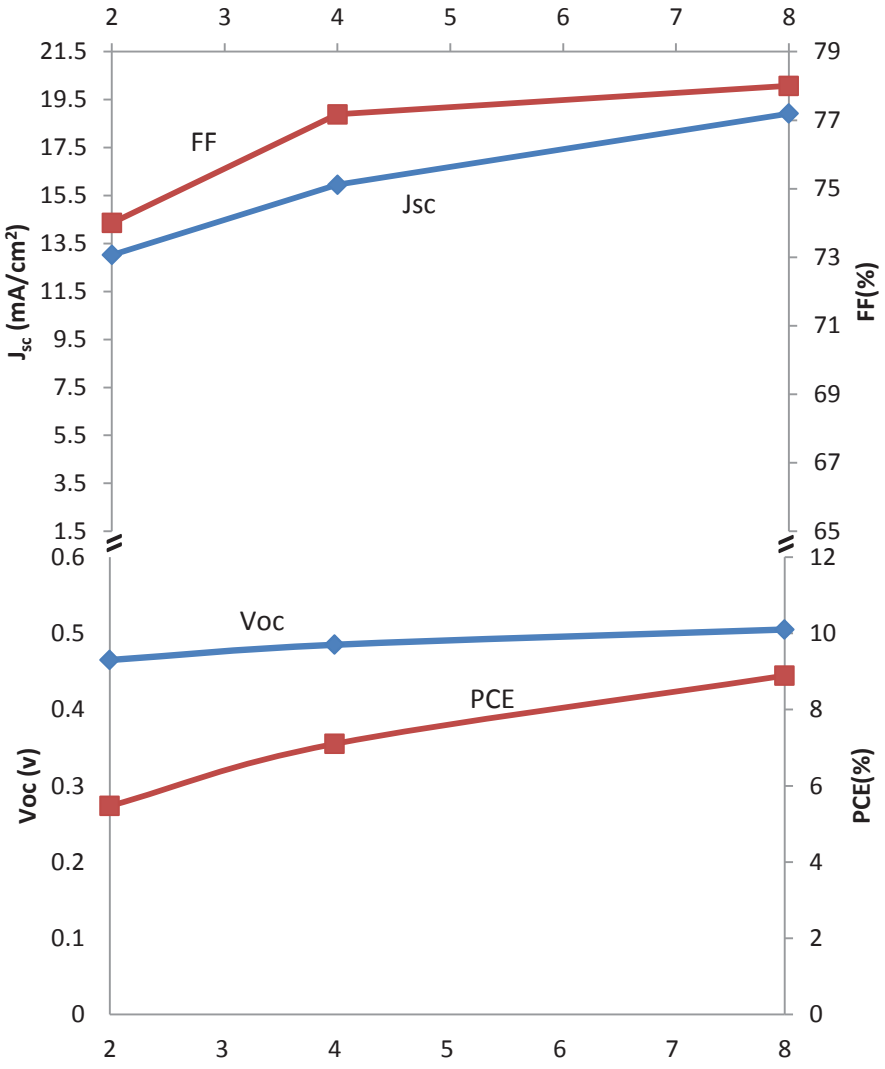

Figure 3.4 Calculated values of solar cell principal parameters based on different lengths at a constant dopant concentration of $1\times10^{16}cm^{-3}$.

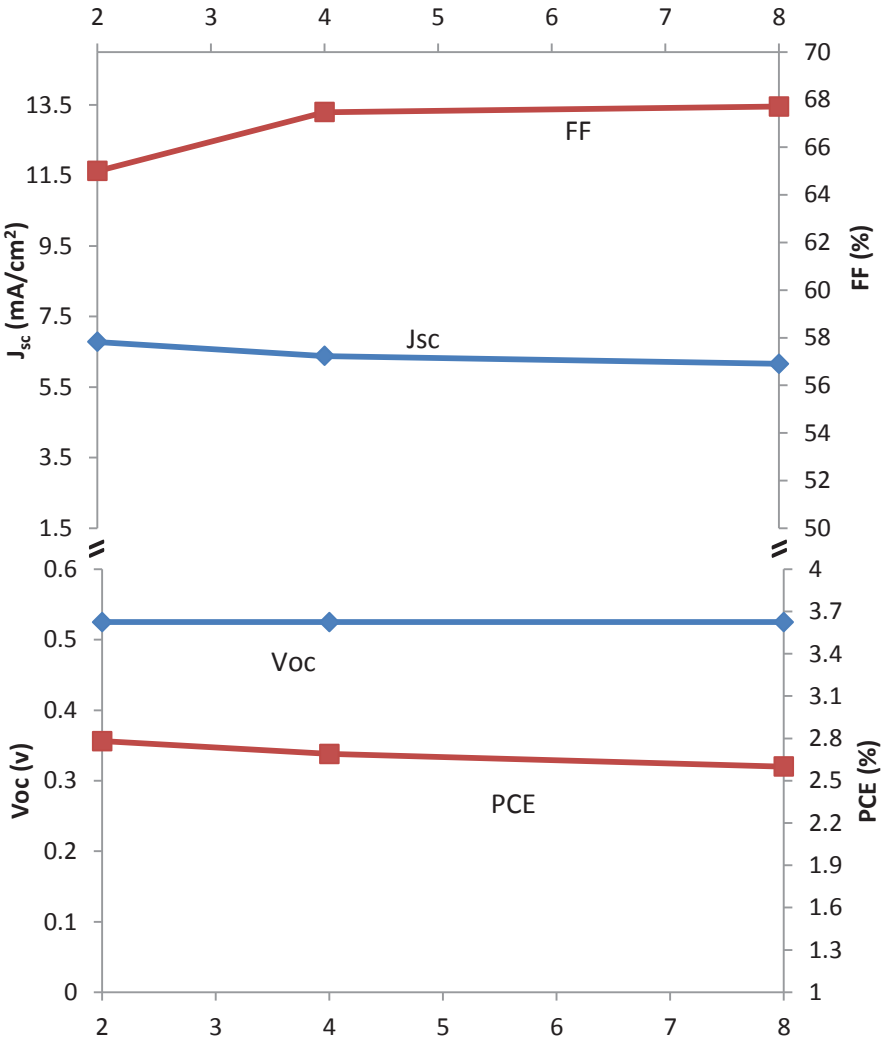

Figure 3.5 Calculated values of solar cell principal parameters based on different lengths at a constant dopant concentration of $6\times10^{18}cm^{-3}$.

3.3.3. Effect of dopant concentration on Jsc, Voc and PCE

The values of the V_{oc} , I_{SC}, power conversion efficiency and fill factor which are calculated by the simulation software are shown in Table 3.5. This table shows that, open circuit voltage values have increased with increasing silicon dopant concentration. The value of open circuit voltage depends on the reverse saturation current density and photo current density, in the active layer based on the following equation [26]:

$$V_{oc} = \frac{nKT}{q} \ln\left[\left(\frac{J_{ph}}{J_s}\right) + 1\right] \tag{3.8}$$

Where

$$J_{ph}=\mathrm{q}\ \mathrm{g(x)}\ (L_p + L_n + W) \tag{3.9}$$

$$\mathrm{J_s} = \mathrm{qn_i^2}\left[\left(\frac{1}{\mathrm{N_a}}\right)\sqrt{\frac{\mathrm{D_n}}{\tau_{\mathrm{n0}}}} + \left(\frac{1}{\mathrm{N_d}}\right)\sqrt{\frac{\mathrm{D_p}}{\tau_{\mathrm{p0}}}}\right] \tag{3.10}$$

Where n is the ideality factor; k is the Boltzmann constant; T is the temperature; q is the electron charge; J_{ph} is the photon generated current; J_s is the reverse saturation current density; g(x) is the generation rate of the electron-hole pairs and $L_p and\ L_n$ are minority carrier diffusion lengths in the n-type and p-type regions, respectively. W is the carrier diffusion length in the depletion region; n_i is the intrinsic carrier concentration; $N_a and\ N_d$ are the dopant concentrations in p-type and n-type regions, respectively. $D_n\ and\ D_p$ are diffusion coefficients of holes and electrons, respectively

and $\tau_{p0}\ and\ \tau_{n0}$ are minority carrier lifetimes of the holes and electrons, respectively. Based on 3.10, by increasing the dopant concentration, J_s decreases and because of the reduction in J_s, open circuit voltage (V_{oc}) will also increases.

According to 3.11, it is obvious that there is an increase in the built-in potential with the increase in the dopant concentration. Moreover, the maximum value of the open circuit voltage is determined by the value of the built-in potential. Therefore, silicon materials having higher dopant concentrations have a higher built-in potential and consequently a greater V_{oc} .

$$V_{bi} = \frac{KT}{q}\ln\left(\frac{N_a N_d}{n_i^2}\right) + \frac{\Delta E_c}{q} \tag{3.11}$$

In 3.11, ΔE_c is the conduction band offset. Energy band diagrams and Fermi level illustrate the difference in the V_{oc} of samples with two different dopant concentrations.

When the dopant concentration is $1 \times 10^{16} cm^{-3}$, for silicon layers with thicknesses of 2μm, 4μm, 8μm, results show the short current densities with values of 13.02, 15.95, and 18.92 mA/cm^2, respectively. However, the simulations showed that, unit cells with thicknesses of $2\mu m, 4\mu m\ and\ 8\mu m$ have the short current density of approximately 6 mA/cm^2 when the dopant concentration is $6 \times 10^{18} cm^{-3}$. Therefore, current density drops by increasing the dopant concentration.

The reason is that, when the dopant concentration increases, the mobility decreases and as a result, diffusion coefficient declines. Moreover, from 3.6, it can be concluded that by increasing the dopant concentration, lifetime of carriers decreases. Therefore, diffusion lengths of minority carriers have decreased from 7.42 μm to 0.4 μm. Note that, the relation between dopant concentration and the mobility is shown in Table 3.5.

As shown in Equation 3.12 output power efficiency, is a parameter, which is used in order to compare the performance of each unit cell. This parameter is defined as the ratio between the output power from the unit cell and the input energy from the incident light. In these experiments, we used the data from the NREL laboratory to introduce the AM 1.5 in Medici software as the input power.

$$\eta = \frac{V_m I_m}{P_{in}} \quad \text{or} \quad \eta = \frac{V_{oc} I_{sc} FF}{P_{in}} \tag{3.12}$$

Note that, the dopant concentration plays an important role in the performance of the unit cell. As shows in Table 3.5 and Figure 3.8 by increasing the dopant concentration of silicon from $1\times10^{16}cm^{-3}$ to $6\times10^{18}cm^{-3}$ although the open circuit voltage increased PCE decreased, which is attributed to the significant decrease in the value of $J_{sc}$by increasing the silicon dopant concentration.

On the other hand, FF is determined by the recombination and carrier transport rate in the unit cell [30]. Based on Figure 3.8, FF has dropped when the dopant concentration increased from a certain value. For instance, FF for a silicon substrate with a thickness of 4μm and dopant concentration of 1×10^{16} cm^{-3} is 77.17%, while it is about 67.47% for the same thickness but a different dopant concentration with a value of $6\times10^{18}cm^{-3}$. Note that, the difference between FF in all three different thicknesses having dopant concentrations of $1 \times 10^{16}\ cm^{-3} and\ 6 \times 10^{18} cm^{-3}$ is about 10%.

Besides, the output power versus resistivity of the unit cell having a thickness of 8μm for silicon with the dopant concentration of $1\times10^{16}cm^{-3}$ and $6\times10^{18}cm^{-3}$ are shown in Figure 3.9 and Figure 3.10, respectively.

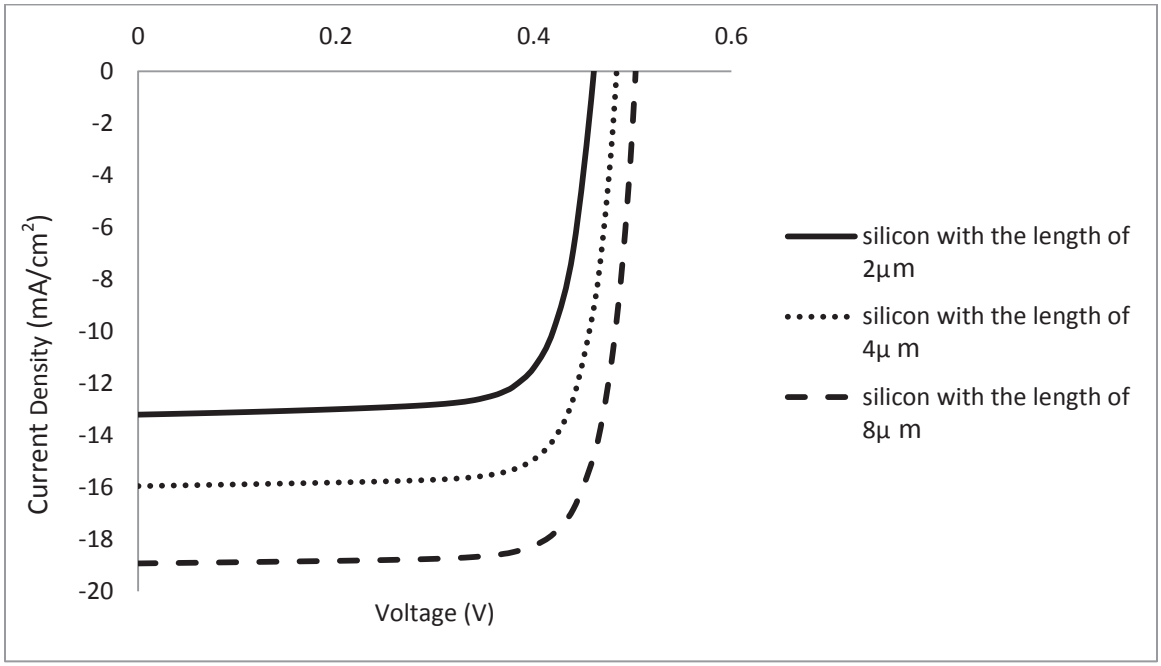

Figure 3.6 J-V characteristics of a planar-silicon/PEDOT:PSS solar cell by varying the thickness of silicon substrate with a dopant concentration of 1×10^{16} cm^{-3}.

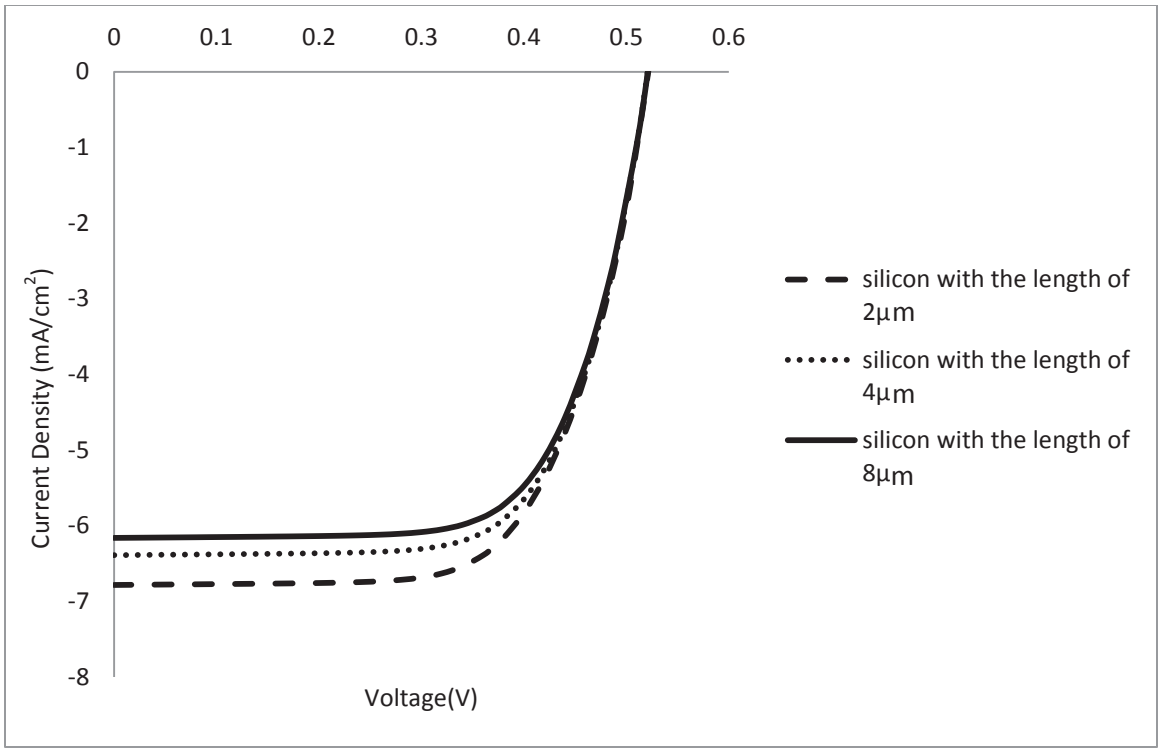

Figure 3.7 J-V characteristics of a planar-silicon/PEDOT:PSS solar cell by varying the thickness of silicon substrate with a dopant concentration of 6×10^{18} cm^{-3}.

Simulation results of planar structure with thickness of 2µm

Test	n-type Silicon (cm^{-3})	$\mu_n(\frac{cm^2}{V-S})$ Si	$\mu_p(\frac{cm^2}{V-S})$ Si	p-type PEDOT:PSS (cm^{-3})	V_{oc} (Volt)	J_{sc} (mA/cm^2)
1	1×10^{16}	1076	460.9	5×10^{19}	0.465	13.02
2	6×10^{18}	113.6	74.5	5×10^{19}	0.525	6.78

Test	n-type Silicon (cm^{-3})	MX.Output Power mW/cm^2	FF (%)	PCE (%)
1	1×10^{16}	4.6	74	5.47
2	6×10^{18}	2.34	65	2.78

Simulation results of planar structure with thickness of 4µm

Test	n-type Silicon (cm^{-3})	$\mu_n(\frac{cm^2}{V-S})$ Si	$\mu_p(\frac{cm^2}{V-S})$ Si	p-type PEDOT:PSS(cm^{-3})	V_{oc} (Volt)	J_{sc} (mA/cm^2)
1	1×10^{16}	1076	460.9	5×10^{19}	0.485	15.95
2	6×10^{18}	113.6	74.5	5×10^{19}	0.525	6.38

Test	n-type Silicon (cm^{-3})	MX.Output Power mW/cm^2	FF (%)	PCE (%)
1	1×10^{16}	5.97	77.17	7.1
2	6×10^{18}	2.26	67.47	2.69

Simulation results of planar structure with thickness of 8µm

Test	n-type Silicon (cm^{-3})	$\mu_n(\frac{cm^2}{V-S})$ Si	$\mu_p(\frac{cm^2}{V-S})$ Si	p-type PEDOT:PSS(cm^{-3})	V_{oc} (Volt)	J_{sc} (mA/cm^2)
1	1×10^{16}	1076	460.9	5×10^{19}	0.505	18.92
2	6×10^{18}	113.6	74.5	5×10^{19}	0.525	6.16

Test	n-type Silicon (cm^{-3})	MX.Output Power mW/cm^2	FF (%)	PCE (%)
1	1×10^{16}	7.47	78	8.89
2	6×10^{18}	2.19	67.71	2.60

Table 3.5 Simulation results of planar-silicon/PEDOT:PSS unit cells with different thicknesses and dopant concentrations.

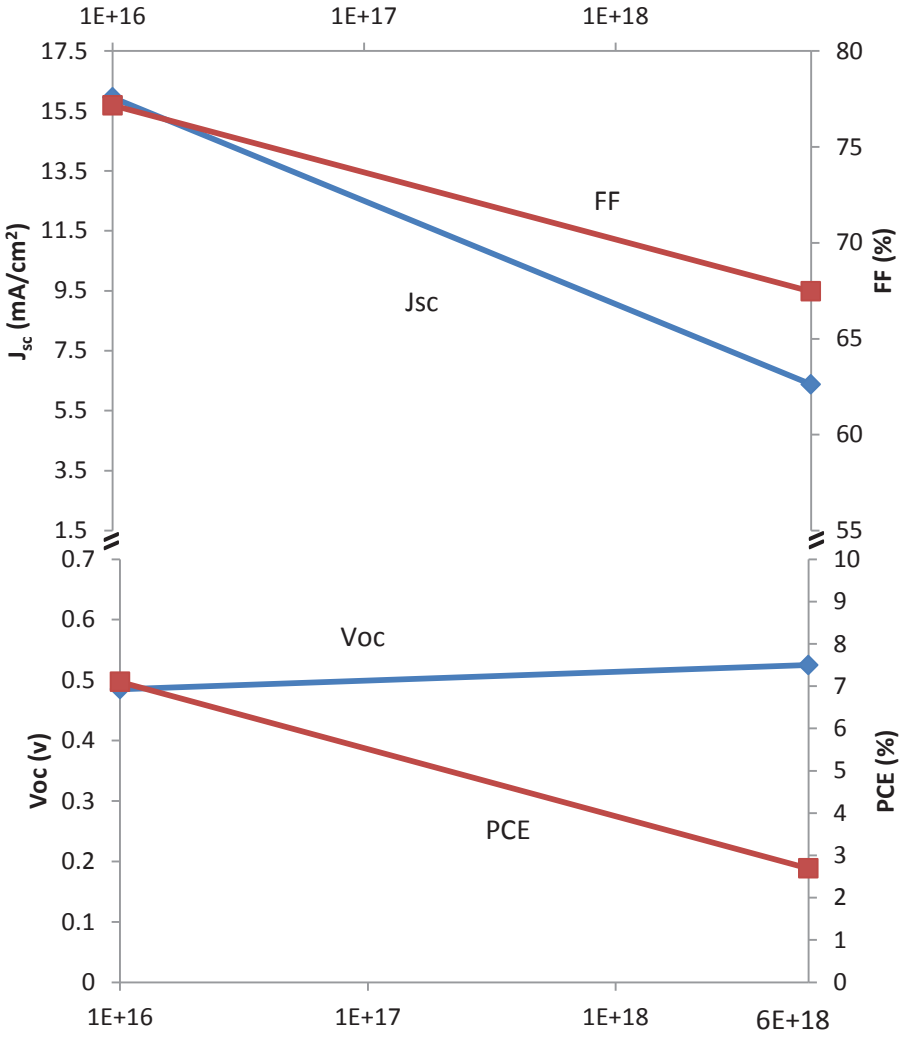

Figure 3.8 Calculated values of solar cell principal parameters based on different dopant concentrations at a constant length of 4μm.

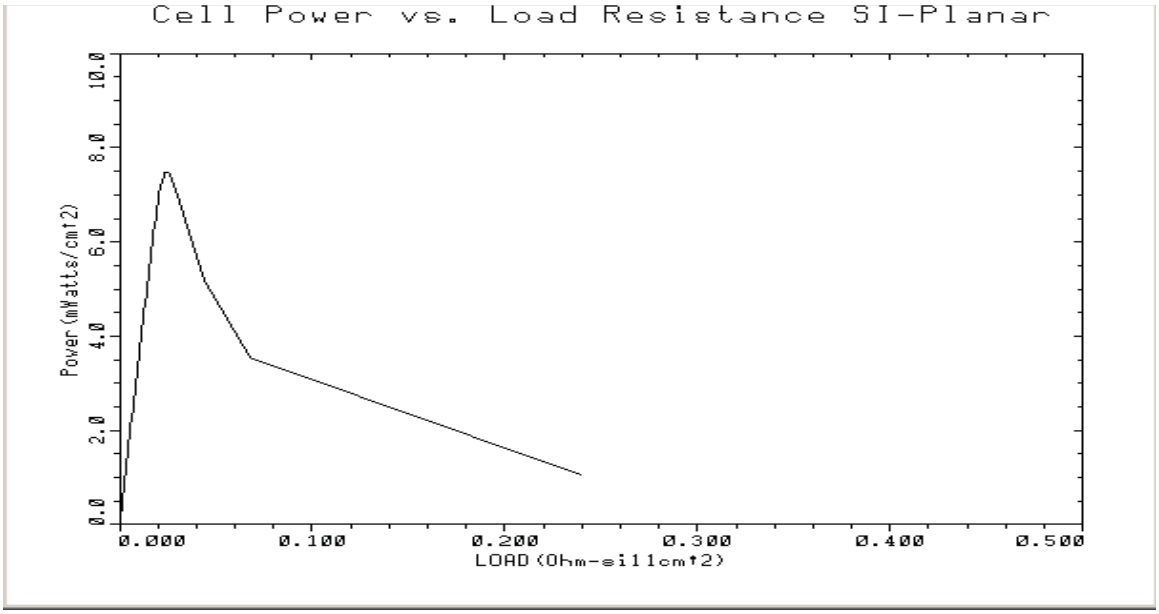

Figure 3.9 The power versus the load resistance for a planar-silicon with a thickness of 8μm and dopant concentration of $1\times10^{16}cm^{-3}$.

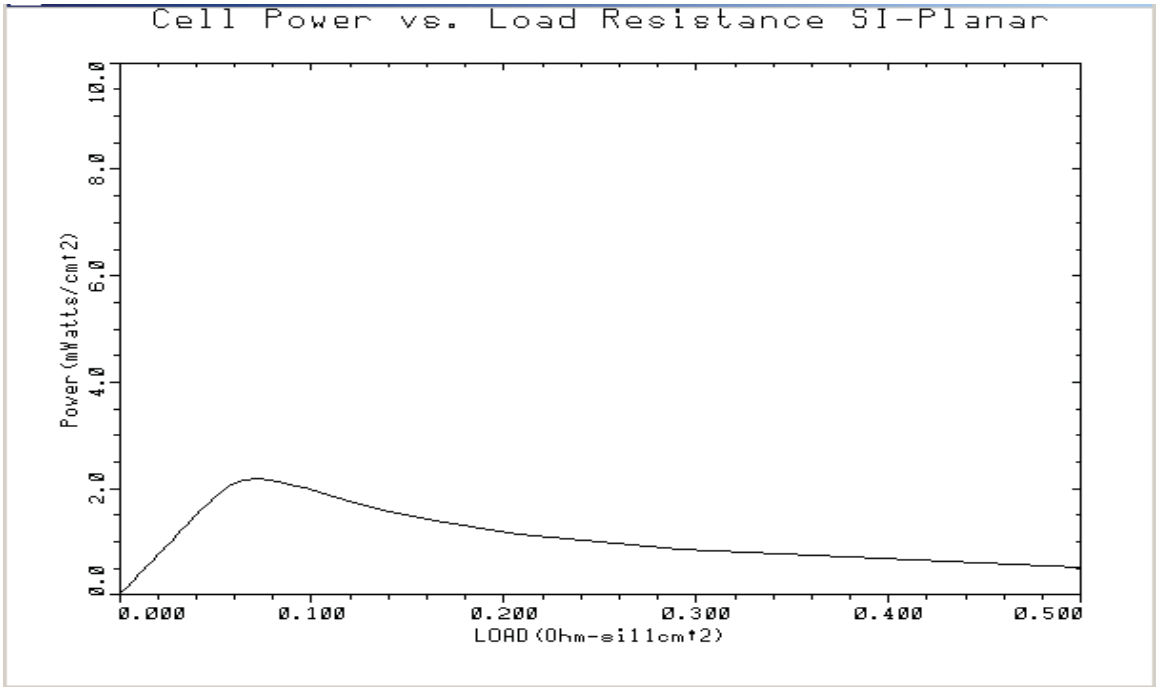

Figure 3.10 The power versus the load resistance for a planar-silicon with a thickness of 8μm and dopant concentration of $6\times10^{18}cm^{-3}$.

3.4. External Quantum Efficiency

External quantum efficiency (EQE) is defined as the ratio of the number of charges collected by the electrode over the number of incident photons. Note that, only the fraction of light, which is in the range of 0.3-1.1μm, can generate current which is due to the band-gap energy of Si. The external collection efficiency of a planar solar cell with a dopant concentration of $1\times 10^{16} cm^{-3}$ and $6\times 10^{18} cm^{-3}$ and a thickness of 2μm are plotted in the Figure 3.11 and Figure 3.12 , respectively. Based on Figure 3.11, the maximum collection efficiency is 69% when the wavelength of the incident light is 450 nm and the dopant concentration of the unit cell is $1\times 10^{16} cm^{-3}$. Whereas for a unit cell with a dopant concentration of $6\times 10^{18} cm^{-3}$ the maximum collection efficiency is about 60% at λ=450nm. These figures indicate that the external collection efficiency at the near infrared range decreases gradually for the unit cell with a dopant concentration of $1\times 10^{16} cm^{-3}$, while declines rapidly for the unit cell with the dopant concentration of $6\times 10^{18} cm^{-3}$. Therefore, the incident light in the near infrared range should be absorbed at the bottom of the planar-silicon and the light in the visible range, should be absorbed at the top of the planar-silicon [29]. In the case of the lower dopant concentrations, the minority carrier has a higher lifetime therefore; electron hole pairs (EHPs) can travel a longer distance. While, the unit cell with a higher dopant concentration has a lower lifetime and EHPs can travel a shorter distance. As a result, EQE values can be determined by the minority carrier lifetimes as well as the absorption coefficient of the material.

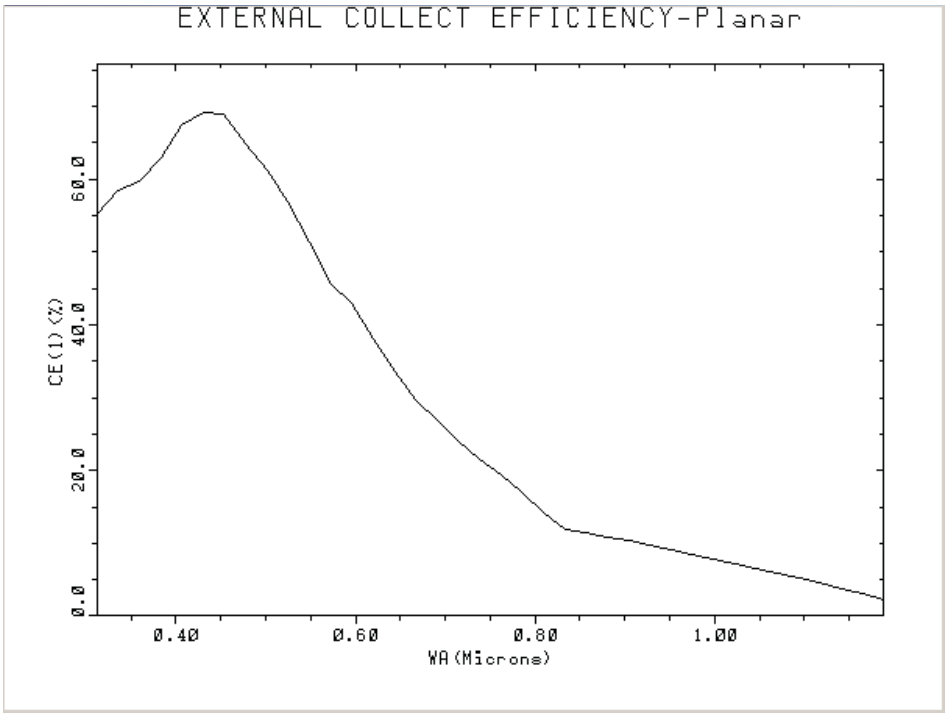

Figure 3.11 External collection efficiency of a planar-silicon/ PEDOT:PSS solar cell with a thickness of 2μm and dopant concentration of 1×10^{16} cm^{-3}.

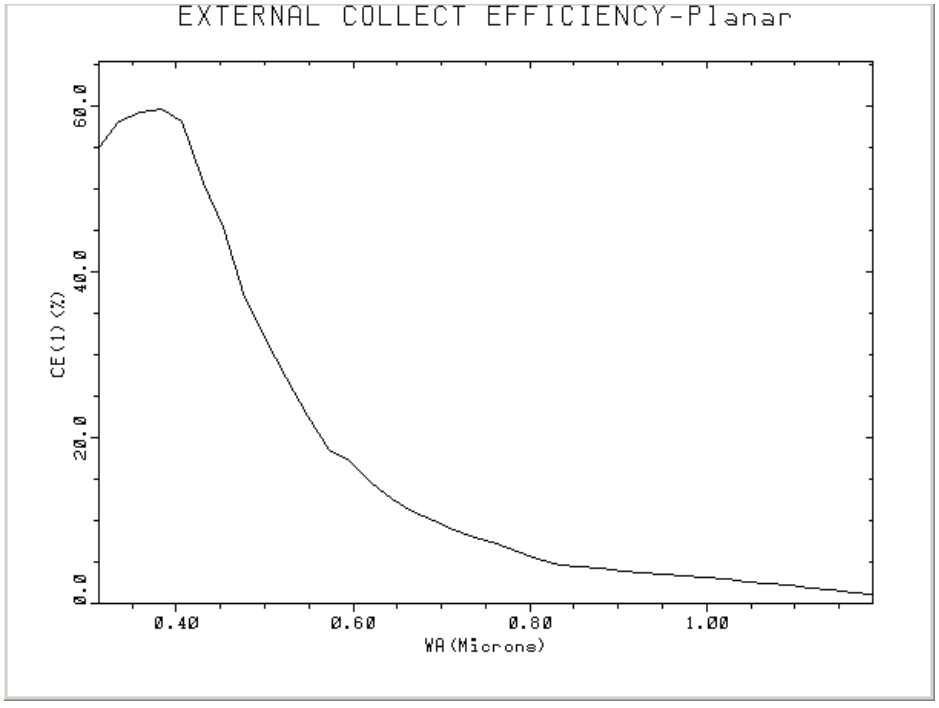

Figure 3.12 External collection efficiency of a planar-silicon/ PEDOT:PSS solar cell with a thickness of 2μm and dopant concentration of $6\times10^{18}$$cm^{-3}$.

3.5. Band Diagram

The band diagrams for the unit cell of the planar-Si with PEDOT:PSS for two different dopant concentrations of 1×10^{16}cm^{-3} and 6×10^{18}cm^{-3} are illustrated in Figure 3.13 and Figure 3.14, respectively. The modeled structure is a planar solar cell, in which a PEDOT:PSS polymer with a thickness of 20 nm is deposited on the top of it. The photo generated carriers can be separated at the planar-silicon and PEDOT:PSS polymer junction by a built-in potential. In addition, the direction of the incident light and hole transport are orthogonal. The PEDOT:PSS is one of the conductive polymers and has some intrinsic advantages such as high conductivity, high transparency in the visible light, stability and solution process [39]. Moreover the HOMO energy of the PEDOT:PSS is about 5.2eV, which is almost similar to the valence band energy of the silicon. Consequently, the interface between polymer and silicon forms a good p-n junction to collect the excess minority carriers [28]. The energy band diagram of the PEDOT:PSS with a band gap of 1.6 eV and electron affinity of 3.6 eV is shown in Figure 3.13. This band diagram shows that a large conduction band offset can make a barrier for electrons to be recombined in the front (PEDOT) surface however, the small valence band offset can ease the hole transport [30]. As shown in Figure 3.14 by increasing the dopant concentration, the depletion region width decreases. Note that, this simulation results can be proven by the bellow equation:

$$x_n + x_p = \left[\frac{2\varepsilon_s V_{bi}}{q}\left(\frac{1}{N_a}+\frac{1}{N_d}\right)\right]^{\frac{1}{2}} \tag{3.13}$$

In this equation we can see that the space charge width depends on the dopant concentration.

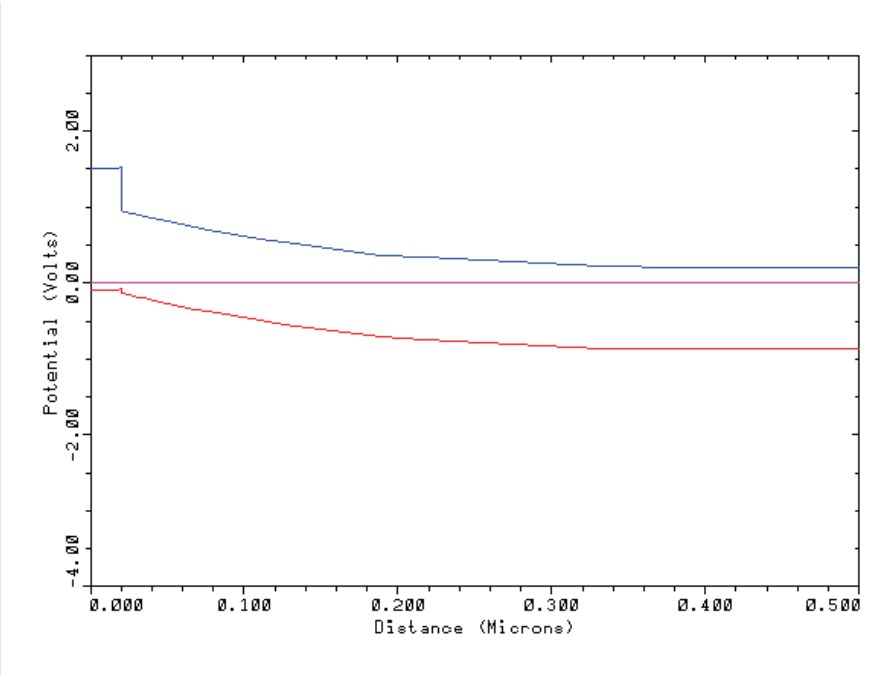

Figure 3.13 The energy band diagram of a hybrid PEDOT:PSS/n-type planar-Silicon, solar cell with a dopant concentration of 1×10^{16} cm^{-3}.

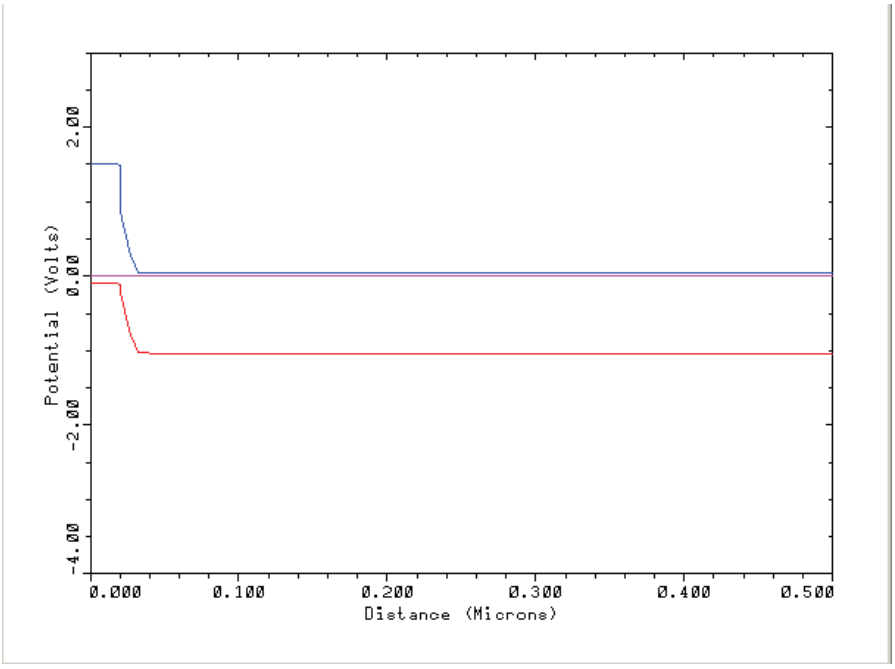

Figure 3.14 The energy band diagram of a hybrid PEDOT:PSS/n-type planar-Silicon, solar cell with a dopant concentration of 6×10^{18} cm^{-3}.

3.6. Photo generation

The generation rate determines the number of electrons generated at each point in the unit cell, which is related to the absorption coefficient of the material. The amount of the incident light, which can be absorbed by a material, depends on the absorption coefficient and the thickness of those materials. In addition, the intensity of light can be calculated from 3.14:

$$I = I_0 e^{-\alpha x} \tag{3.14}$$

Where, α is the absorption coefficient, x is the distance that the light travels in the material before being absorbed and I_0 is the initial intensity.

From3.14, the number of electron-hole pairs, which are generated either in the polymer or in the silicon, can be calculated. If we assume that the internal quantum efficiency equals 1, it means that the entire incident light has generated EHPs. Therefore, generation rate (G) can calculated from 3.15:

$$G = \alpha N_0 e^{-\alpha x} \tag{3.15}$$

Where N_0 is the photon flux at the surface with the unit of (photons/area/second). From this equation, we can figure out that by increasing x, the generation rate decreases exponentially, meaning that the generation rate is higher at the surface of the device.

In this work, the position of the light source and the incident angle has been also changed in order to investigate the effect of the position of the light source on the short circuit current. However, results showed that these changes do not affect the short circuit current as long as the ray width covers the whole surface of the device. However, the short circuit

current decreases when the tilted angle is large enough so that, a small portion of light gets out of the surface of the cell.

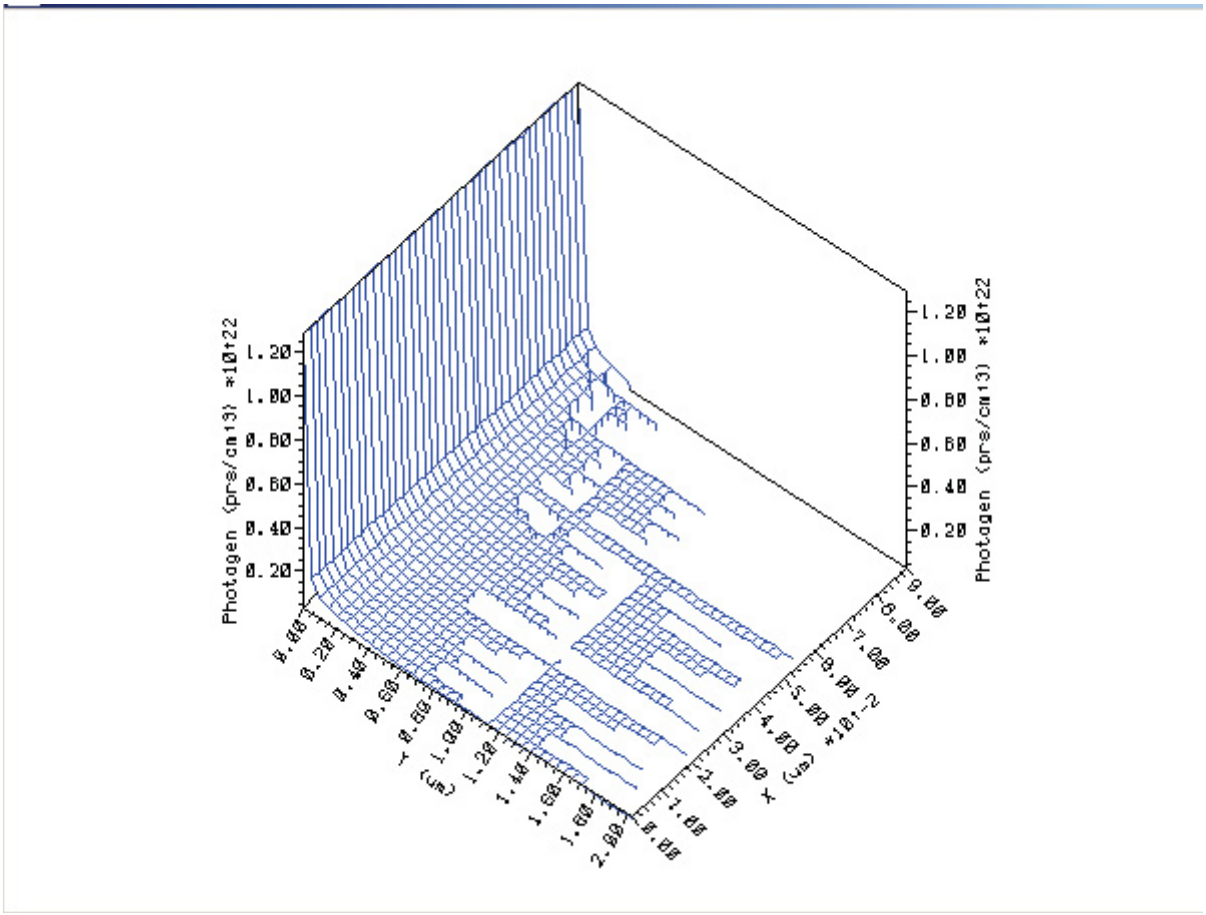

Figure 3.15 Generation rate of EHPs in a planar-Si/PEDOT:PSS unit cell as a function of distance.

3.7. Conclusion

In this work, hybrid planar solar cells based on silicon and PEDOT:PSS polymer, have been simulated with the device modeling software Medici. The thickness, dopant concentration and the concentration of defects of these planer-silicon solar cells were subjected to change in order to find the electrical characterizations of the device.

For our purpose, two Si layers with two different dopant concentrations of $1\times10^{16}cm^{-3}$ and $6\times10^{18}cm^{-3}$ were considered. For each certain dopant concentration, we had three different Si substrates thicknesses including, 2µm, 4µm and 8µm. The reason of this choice is that, we wanted to have the same study on the SiNW based solar cells being 2µm, 4µm and 8µm long and compare the results with the planar structure. Therefore, it was necessary to choose the same thicknesses for silicon substrates in the planar structure as the SiNW configuration.

Moreover, it was shown that there was a reduction in the value of J_{sc} as a result of an increase in the trap density (N_r) and decrease in the lifetime (τ). Therefore, due to the decrease in the photocurrent there was a reduction in the open circuit voltage. Furthermore, FF, which is determined by the recombination and carrier transport rate in the unit cell, decreased as a result of more recombination of minority carriers, when the tarp density was increased. Finally, the device efficiency dropped by 7.87%, when the trap density increased from $1\times10^{12}cm^{-3}$ to $1\times10^{17}cm^{-3}$. This is due to a reduction in the value of both short circuit current and open circuit voltage, which were discussed above.

Although results showed an increase in the cell efficiency for thicker samples when Si was doped with $1\times10^{16}cm^{-3}$ atoms, it is demonstrated that in solar cells based on Si with

a dopant concentration of $6\times10^{18}cm^{-3}$ PCE did not improve in cells based on thicker Si substrates. In broad terms, in highly doped silicon substrates results showed that, current density, PCE and FF were almost the same for all the selected thicknesses of the silicon layer.

By investigating the effect of dopant concentration on Si samples with the same thicknesses, it was understood that Si layers with higher dopant concentrations did not contribute into better cell efficiency. Although V_{oc} increased in a sample with a dopant concentration of $6\times10^{18}cm^{-3}$ compared to its counterpart having a dopant concentration of $1\times10^{16}cm^{-3}$, the current decreased dramatically in the highly doped one, as a result, the unit cell with the lower dopant concentration showed a higher cell efficiency.

Therefore, we can conclude that as the dopant concentration of the Si substrate increases, the effect of the substrate thickness becomes less dominant on the cell efficiency.

CHAPTER 4

SiNW/PEDOT:PSS Solar Cell Modeling

In this work, the finite-element semiconductor-device software "Taurus Medici" from Synopsys is used to investigate the structure and functions of hybrid solar cells based on vertically well-aligned silicon nanowires (SiNWs) coated with a 20 nm long p-type polymer. Note that, the length, dopant concentration, and concentration of defects of the silicon were subjected to change in each simulation. Short circuit current density (J_{SC}) has been shown to remain constant by increasing the trap density (defects) in the silicon layer. This is due to the radial junction providing short collection lengths, which makes photo generated carriers with low diffusion lengths to be separated at the junction. As an example, when the trap density increased from $1 \times 10^{12} cm^{-3}$ to $1 \times 10^{17} cm^{-3}$, the J_{SC} remained constant about 12 $\mathrm{mA/cm^2}$ while the open circuit voltage decreased from 0.435 V to 0.125 V. J_{SC} has also increased by growing the SiNW length because by increasing the length of SiNWs more photons can be captured by the active layer. However, increasing the length of the SiNW has decreased the open circuit voltage when the dopant concentration of SiNW was $6\times10^{18}\mathrm{cm^{-3}}$ due to the increase in the area junction. Results show that V_{OC} and J_{SC} have increased by increasing silicon dopant concentration for all three different lengths of the silicon. The maximum external quantum efficiency of the unit cells was measured to be about 41% for the both dopant concentration $1\times 10^{16} cm^{-3}$ and $6\times 10^{18} cm^{-3}$, respectively. Moreover, the simulation results illustrate the effect of band alignment and photo generation on the electrical characteristics of the unit cell.

4.1. Device Structure

In this work, a unit cell of a hybrid solar cell consisting of ordered arrays of Silicon nanowires dispersed in PEDOT:PSS polymer is modeled with Medici software. The silicon nanowires are supposed to be vertically aligned and connected to the Al and ITO as the back and front electrode, respectively. Furthermore, the silicon nanowires were assumed to have uniform spacing and uniform dimensions.

Figure 4.1 is a schematic illustration of the device modeling in which the SiNWs are 4µm long and 50nm wide. As shown in Figure 4.2, due to the presence of symmetry in this structure, it can be divided into basic repeating unit cells.

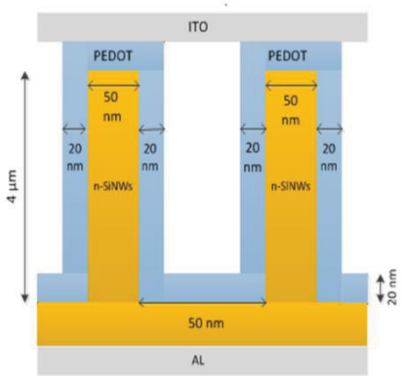

Figure 4.1 Schematic of a hybrid solar cell.

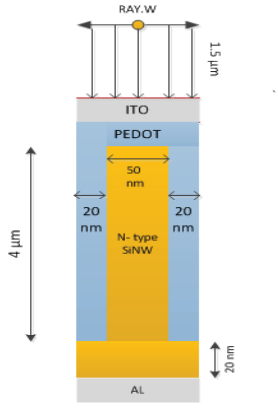

Figure 4.2 A schematic of the SiNW/PEDOT:PSS unit cell, which is implemented in the simulations.

Note that, in each unit cell the Si core is surrounded by PEDOT:PSS polymer with a thickness of 20 nm. The mentioned configuration is almost similar to the work done by Shiu et al [23]. In his work, the cell was a core-sheath heterojunction structure, fabricated from the well-aligned silicon nanowires SiNW/PEDOT:PSS. In other words, the cell structure can be defined as: ITO/PEDOT:PSS/SiNW/Al. PEDOT: PSS which is a hole conductive polymer has coated the SiNWs as the p-type material to create a heterojunction with the n-type silicon core. SiNW arrays have been fabricated by electroless etching technique, from an n-type, 1-10 Ω-cm silicon wafers.

In [23] the length of the SiNWs, PEDOT:PSS thickness and an average SiNW diameter is approximately to be 2.78μm, 20nm and 50nm, respectively. In addition, the spaces between the SiNWs have been reported to be about 100 nm to 200 nm.Note that, PEDOT:PSS and Si properties are illustrated in Table 3.1and Table 3.2, respectively.

4.2. Simulation Results

4.2.1. Effect of trap density or carriers lifetime on Jsc, Voc and PCE

In this work, SiNW/PEDOT:PSS hybrid solar cells with the length of 4μm and thickness of 50nm have been studied. As shown in Figure 4.2, the 20 nm thick PEDOT sheath is used as a p-type material to create a heterojunction with the n-type silicon with a carrier concentration of $6\times10^{18}cm^{-3}$. As can be seen in Figure 4.3, in the SiNW structure like the planar configuration, increase in the value of N_r (trap density) decreases the open circuit voltage while, the short circuit current J_{SC} remains constant. This is again, due to the radial junction, which provides a short collection length for the photo-generated carriers with low diffusion lengths, to be collected at the junction. As can be seen in 4.1 and 4.2

V_{oc} is dependent to the diffusion length. Therefore, when the trap density increases, or in other words L (diffusion length) decreases, due to the constancy of J_{ph}, V_{oc} degrades [5].

$$V_{oc} = \frac{nKT}{q} \ln\left(\frac{J_{ph}}{J_s} + 1\right) \tag{4.1}$$

$$J_s = \left[\frac{eD_p p_{n0}}{L_p} + \frac{eD_n n_{p0}}{L_n}\right] \tag{4.2}$$

For example, when the trap density increases from $1\times10^{12} cm^{-3}$ to $1\times10^{17} cm^{-3}$, the open circuit voltage will decrease from 0.435V to 0.125V, however, the short circuit current remains almost the same in this condition. As mentioned in Equation 3.3 and 3.7, by increasing the trap density the electron and hole lifetimes will decrease and as a result, diffusion length decreases. Moreover, as it is demonstrated in Table 4.1, power conversion efficiency (PCE) has decreased by increasing the tarp density. The reason is that, by increasing the trap density J_{sc} remained almost constant while V_{oc}decreased, therefore PCE decreased.

Based on Table 4.2, when there is a decrease in the 'electron' (majority carriers) lifetime from 10^{-7}s to 10^{-9}s, short circuit current remains almost the same because, by decreasing the lifetime of the majority carriers, hole (minority carriers) diffusion length will remain constant. However, open circuit voltage decreases from 0.35V to 0.275V because; V_{oc} dramatically depends on the trap density in the depletion region. Note that, trap densities are assumed to be the same in the depletion region and the quasi neutral region. Moreover, by decreasing the 'hole' lifetime to 10^{-9}s, the short circuit current remained almost the same while, the open circuit voltage decrease from 0.275 V to 0.235 V. This is due to the short collection length in the radial junctions.

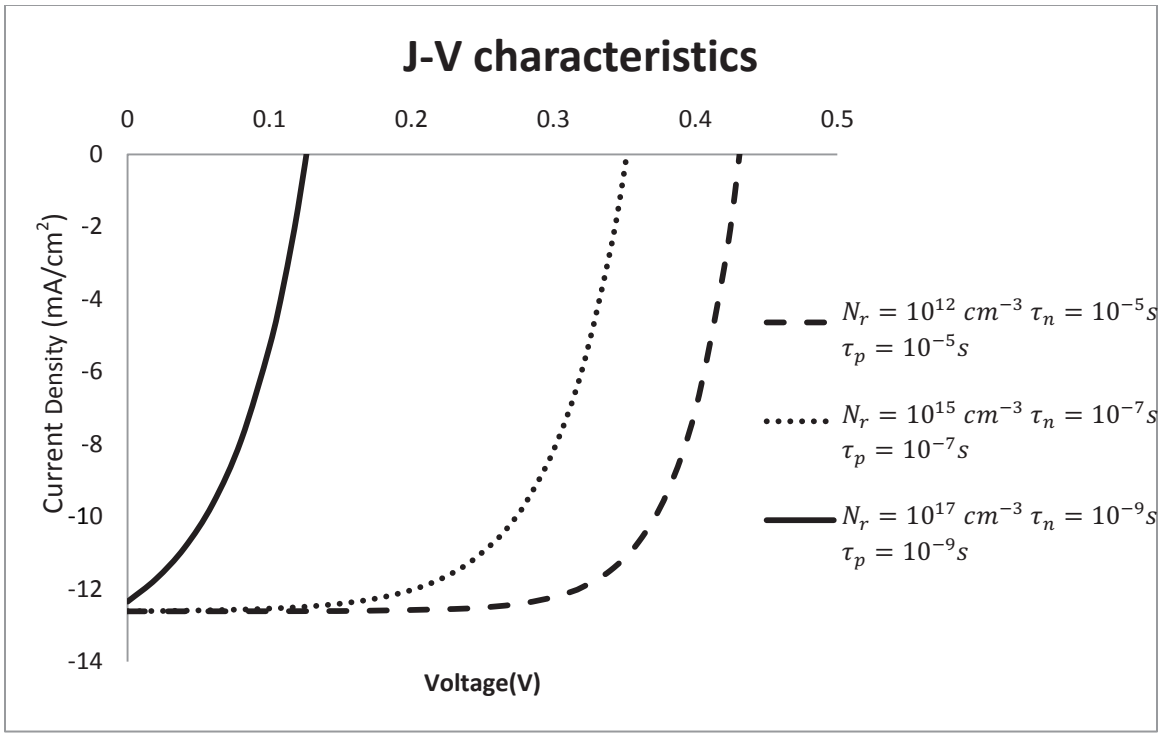

Figure 4.3 J-V characteristics of the SiNW/PEDOT:PSS solar cell with the length of 4µm and different trap densities.

Test	Silicon Trap Density (cm^{-3})	$electron\ life\ times(s)$	$Hole\ life\ times(s)$	V_{oc} (Volt)	J_{sc} (mA/cm^2)	FF (%)	PCE (%)
1	1×10^{12}	10^{-5}	10^{-5}	0.435	12.611	55	4.65
2	1×10^{15}	10^{-7}	10^{-7}	0.355	12.6	61	3.28
3	1×10^{17}	10^{-9}	10^{-9}	0.125	12.34	40	0.75

Table 4.1 Electrical charactestics of the SiNW/ PEDOT:PSS heterojunction solar cell for different silicon trap densities.

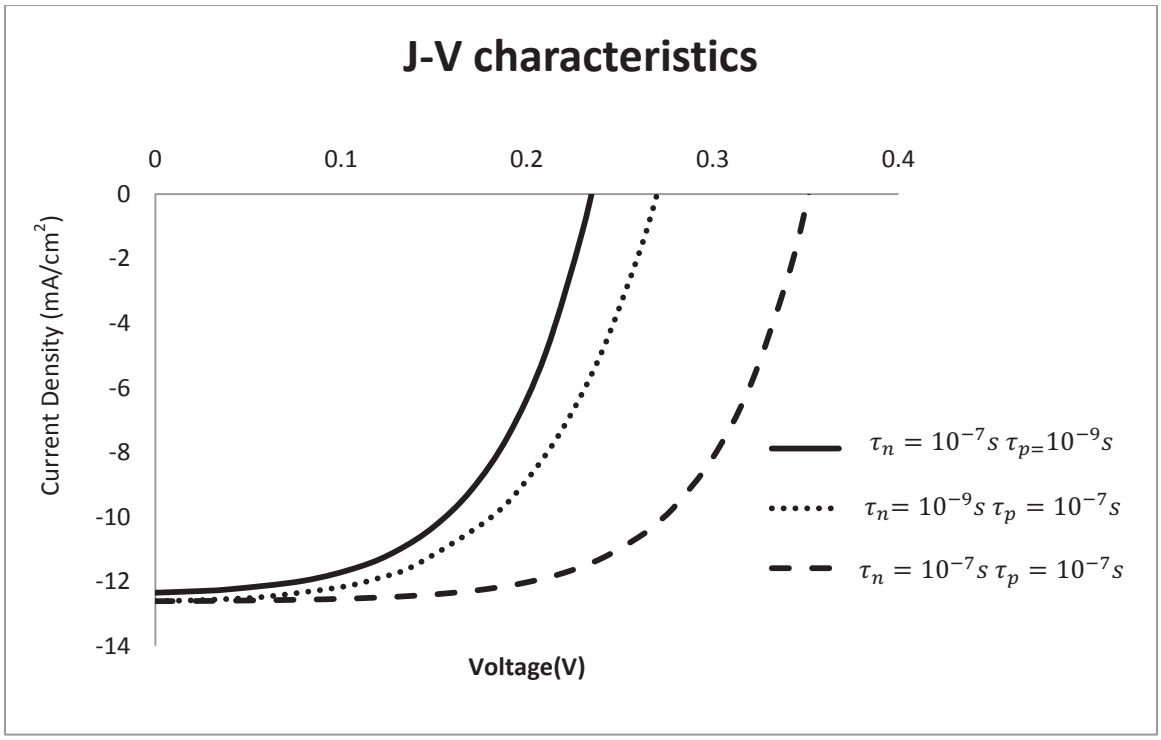

Figure 4.4 J-V characteristics of the SiNW/PEDOT:PSS solar cell with lengths of the 4μm and different electron and hole lifetimes.

Test	$electron\ life\ times(s)$	$Hole\ life\ times(s)$	V_{oc} (Volt)	J_{sc} (mA/cm^2)	FF (%)	PCE (%)	diffusion length of holes in silicon(μm)
1	10^{-7}	10^{-7}	0.35	12.6	61	2.36	0.4
2	10^{-9}	10^{-7}	0.275	12.6	52.23	2.15	0.4
3	10^{-7}	10^{-9}	0.235	12.34	53.1	1.83	0.04

Table 4.2 The charactestics of the SiNW/PEDOT:PSS solar cell with different electron and hole lifetimes.

4.2.2. Effect of the SiNW length on Jsc, Voc and PCE:

Based on a trap density of 10^{15} cm^{-3}, J-V characteristics of a silicon nano wire (SiNW) coated with the PEDOT:PSS polymer is simulated. J-V curves of three different lengths of SiNW, including 2µm, 4µm and 8µm with dopant concentrations of $1\times10^{16}cm^{-3}$ and $6\times10^{18}cm^{-3}$ are demonstrated in Figure 4.7and Figure 4.8, respectively.

These simulations analyze the effect of increasing the length of SiNW on the short circuit current, open circuit voltage and power conversion efficiency. In each figure, the only parameter that was subjected to change was the unit cell length, and the PEDOT sheath maintained its thickness in all experiments. Note that, the lengths that are demonstrated in these figures are without considering the height of the electrodes.

Figure 4.5 in which the dopant concentration is $1\times10^{16}cm^{-3}$, shows that when the length of SiNW increases from 2µm to 8µm, the short circuit current density (J_{sc}) increases from 9.08 $mA/cm^2$to 12.06 mA/cm^2. The reason is that by increasing the length of SiNW more photons can be captured by the active layer. However, the open circuit voltage (V_{OC}) has remained almost the same in these simulations. Furthermore, in radial P-N junction SiNWs, the collection length is short. Hence photo generated carriers with low diffusion lengths, can be collected. However, in the highly doped ($6\times10^{18}cm^{-3}$) sample open circuit voltage decreased by increasing the length due to an increase in the area junction. Note that, as it is demonstrated in Table 4.3 and Figure 4.5 in both dopant concentration conditions ($1\times10^{16}cm^{-3}$ and $6\times10^{18}cm^{-3}$) PCE has increased by increasing the length of the nano-wire. Finally, by increasing the SiNWs length FF has remained nearly constant in $1\times10^{16}cm^{-3}$ dopant concentration mode and reduced in $6\times10^{18}cm^{-3}$ as a result of reduction in the value of the open circuit in longer wires.

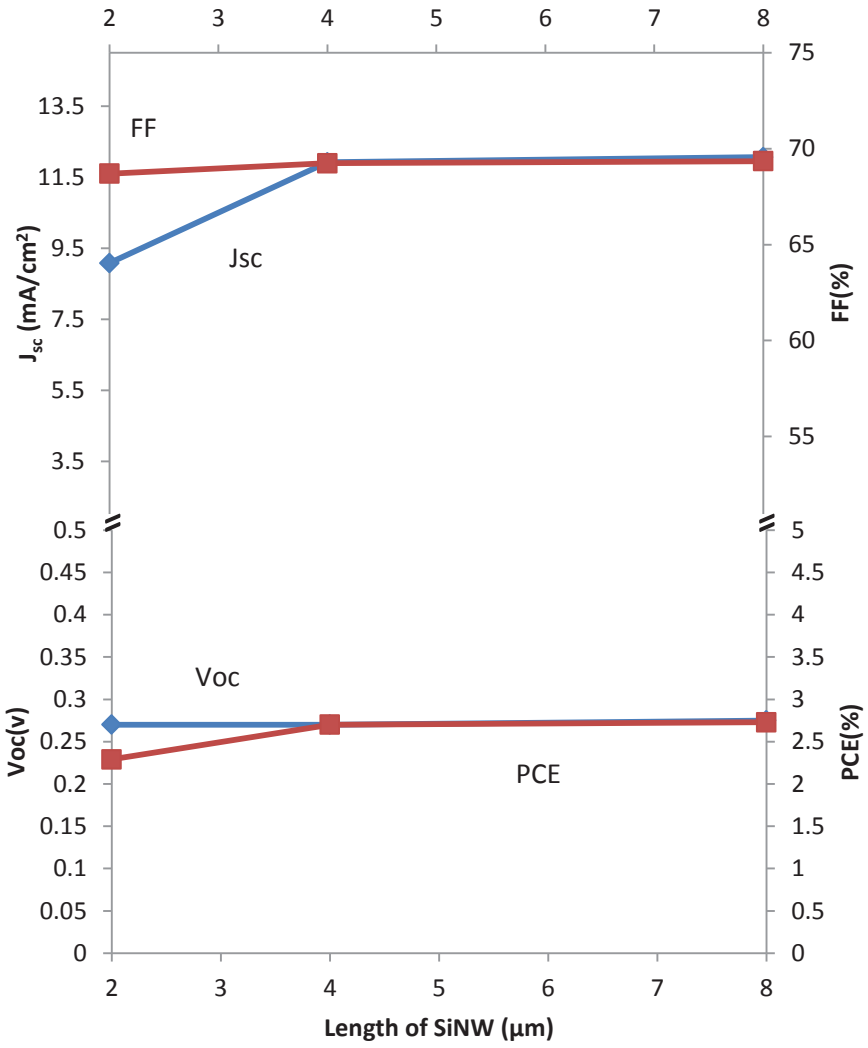

Figure 4.5 Calculated values of solar cell principal parameters based on different lengths at a constant dopant concentration of $1\times10^{16}cm^{-3}$.

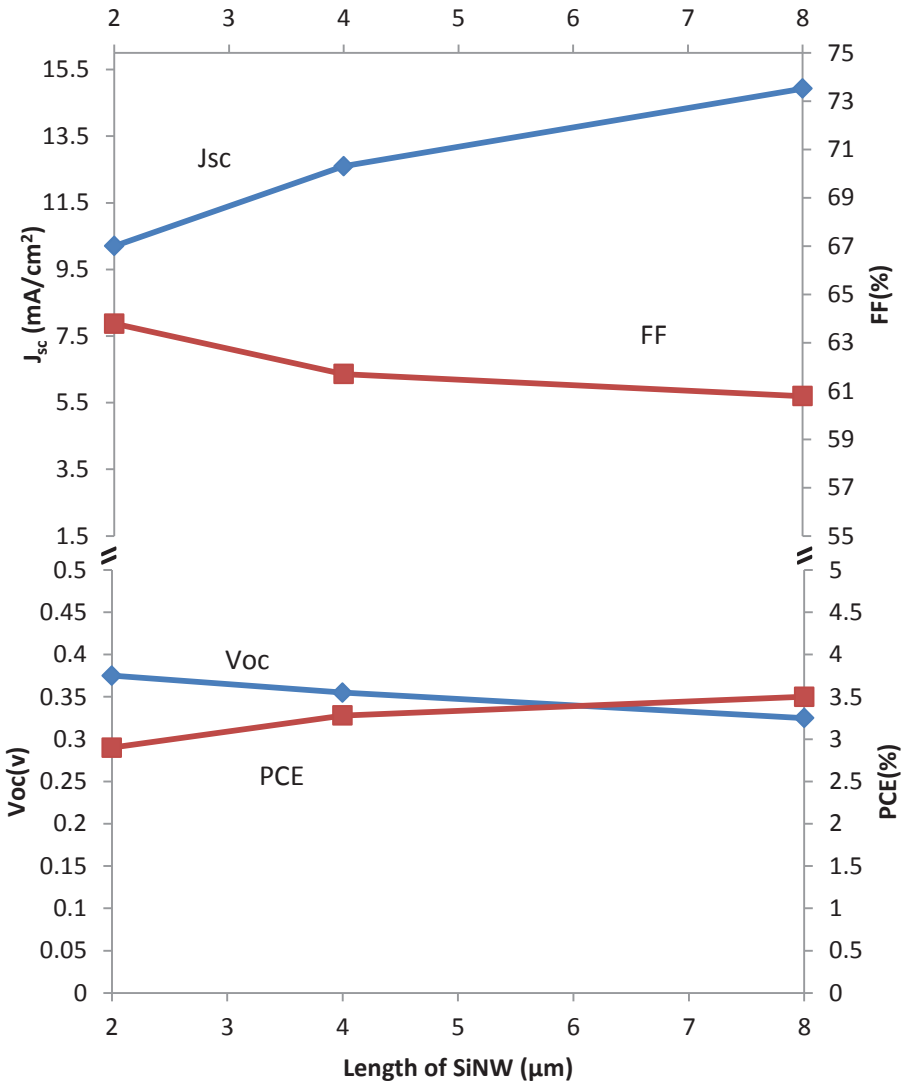

Figure 4.6 Calculated values of solar cell principal parameters based on different lengths at a constant dopant concentration of $6\times10^{18}cm^{-3}$.

4.2.3. Effect of dopant concentration on Jsc, Voc and PCE

Values of V_{oc} , I_{SC}, power conversion efficiency and the fill factor for different dopant concentrations, which are calculated by the simulation software, are shown in Table 4.3 and Figure 4.9. These table and figure show that, the open circuit voltage increases by increasing the dopant concentration of the silicon, in all three different lengths. The reason is that by increasing the dopant concentration, the built in potential will increase and hence open circuit voltage rises.

Results from Figure 4.9 show that, by increasing the dopant concentration, short circuit current will increase in the SiNW unit cell. The reason is that, when the dopant concentration increases, the conductivity of the device will increase, as a result J_{sc} increases.

As shown in Table 4.3 and Figure 4.9 by increasing the dopant concentration from $1\times10^{16}\ cm^{-3}$ to $6\times10^{18}cm^{-3}$ the Power Conversion Efficiency (PCE) increases. This is because J_{SC} and V_{OC} increase by increasing the dopant concentration. Results show that, the power conversion efficiency (PCE) of the hybrid solar cell, based on silicon with the length of 8μm, has increased from 2.7% to 3.5% when the dopant concentration increased from 1×10^{16}cm^{-3} to 6×10^{18}cm^{-3}. As it is shown in Table 4.3 and Figure 4.9, fill factor (FF), which is determined by the recombination and carrier transport rate in the unit cell [30], has decreased by increasing the dopant concentration. For instance, FF for a SiNW with a length of 2μm and with dopant concentration of 6×10^{16}cm^{-3} is 69%, while the FF for the same length of Si but a different dopant concentration with a value of $6\times10^{18}cm^{-3}$ is about 64%.

The output power versus resistivity of a SiNW unit cell, with a length of 8µm and a dopant concentration of 1×10^{16}cm^{-3} and $6\times10^{18}\ cm^{-3}$ are shown in Figure 4.10 and Figure 4.11, respectively.

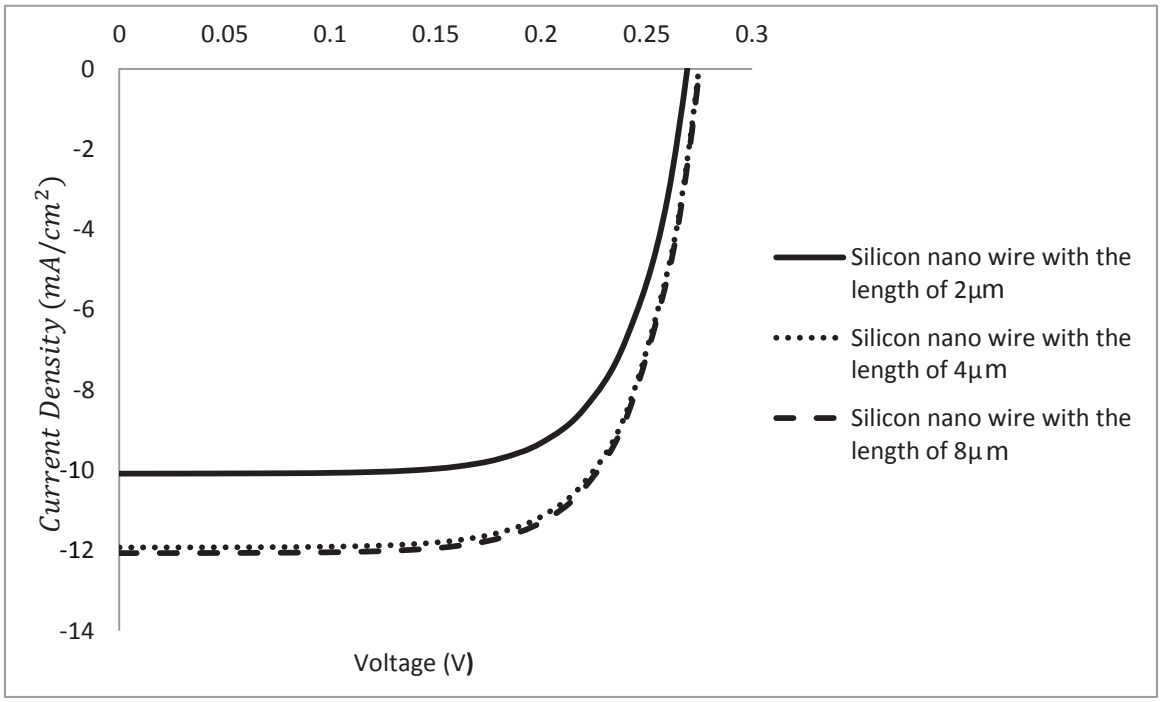

Figure 4.7 J-V characteristics of the SiNW/PEDOT:PSS solar cell by varying the length of silicon nano wire with a dopant concentration of 1×10^{16} cm^{-3}.

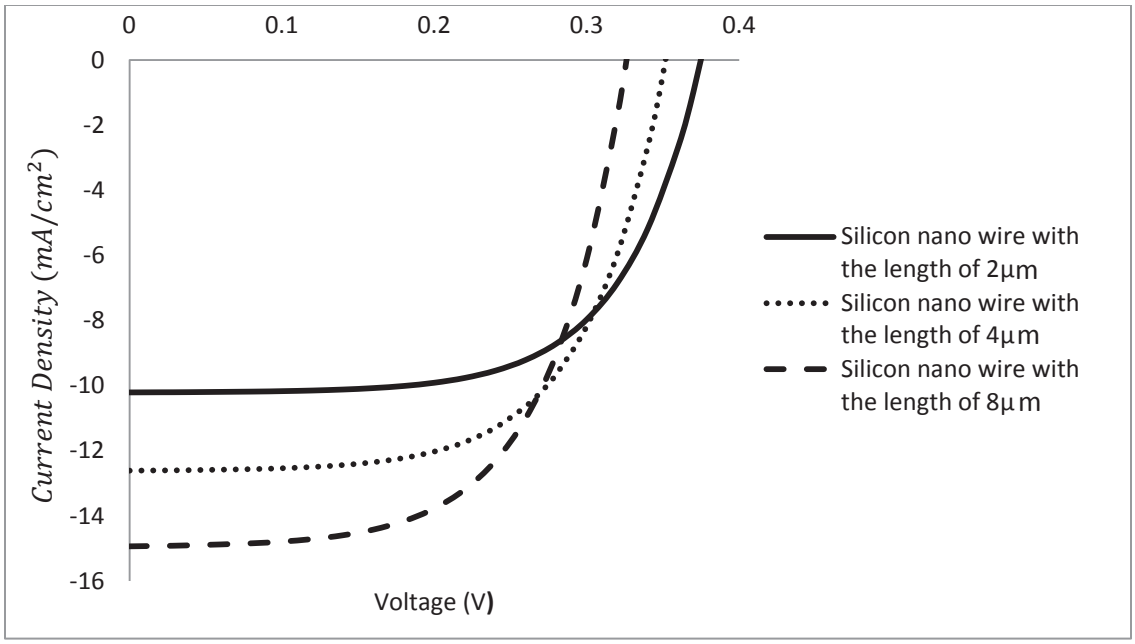

Figure 4.8 J-V characteristics of the SiNW/PEDOT:PSS solar cell by varying the length of silicon nano wire with a dopant concentration of 6×10^{18} cm^{-3}.

Simulation results of SiNW structure with length of 2µm

Test	n-type Silicon (cm^{-3})	$\mu_n(\frac{cm^2}{V-S})$ Si	$\mu_p(\frac{cm^2}{V-S})$ Si	p-type PEDOT:PSS	$\boldsymbol{V_{oc}}$ (Volt)	$\boldsymbol{J_{sc}}$ $(\boldsymbol{mA/cm^2})$
1	1×10^{16}	1076	460.9	5×10^{19}	0.270	9.08
2	6×10^{18}	113.6	74.5	5×10^{19}	0.375	10.20

Test	n-type Silicon (cm^{-3})	MX.Output Power mW/cm^2	FF (%)	PCE (%)
1	1×10^{16}	1.87	68.7	2.29
2	6×10^{18}	2.44	63.79	2.90

Simulation results of SiNW structure with length of 4µm

Test	n-type Silicon (cm^{-3})	$\mu_n(\frac{cm^2}{V-S})$ Si	$\mu_p(\frac{cm^2}{V-S})$ Si	p-type PEDOT:PSS	$\boldsymbol{V_{oc}}$ (Volt)	$\boldsymbol{J_{sc}}$ $(\boldsymbol{mA/cm^2})$
1	1×10^{16}	1076	460.9	5×10^{19}	0.27	11.92
2	6×10^{18}	113.6	74.5	5×10^{19}	0.355	12.6

Test	n-type Silicon (cm^{-3})	MX.Output Power mW/cm^2	FF (%)	PCE (%)
1	1×10^{16}	2.27	69.24	2.7
2	6×10^{18}	2.76	61.70	3.28

Simulation results of SiNW structure with length of 8µm

Test	n-type Silicon (cm^{-3})	$\mu_n(\frac{cm^2}{V-S})$ Si	$\mu_p(\frac{cm^2}{V-S})$ Si	p-type PEDOT:PSS	$\boldsymbol{V_{oc}}$ (Volt)	$\boldsymbol{J_{sc}}$ $(\boldsymbol{mA/cm^2})$
1	1×10^{16}	1076	460.9	5×10^{19}	0.275	12.06
2	6×10^{18}	113.6	74.5	5×10^{19}	0.325	14.93

Test	n-type Silicon (cm^{-3})	MX.Output Power mW/cm^2	FF (%)	PCE (%)
1	1×10^{16}	2.30	69.35	2.73
2	6×10^{18}	2.95	60.79	3.5

Table 4.3 Simulation results of a SiNW unit cell with different lengths.

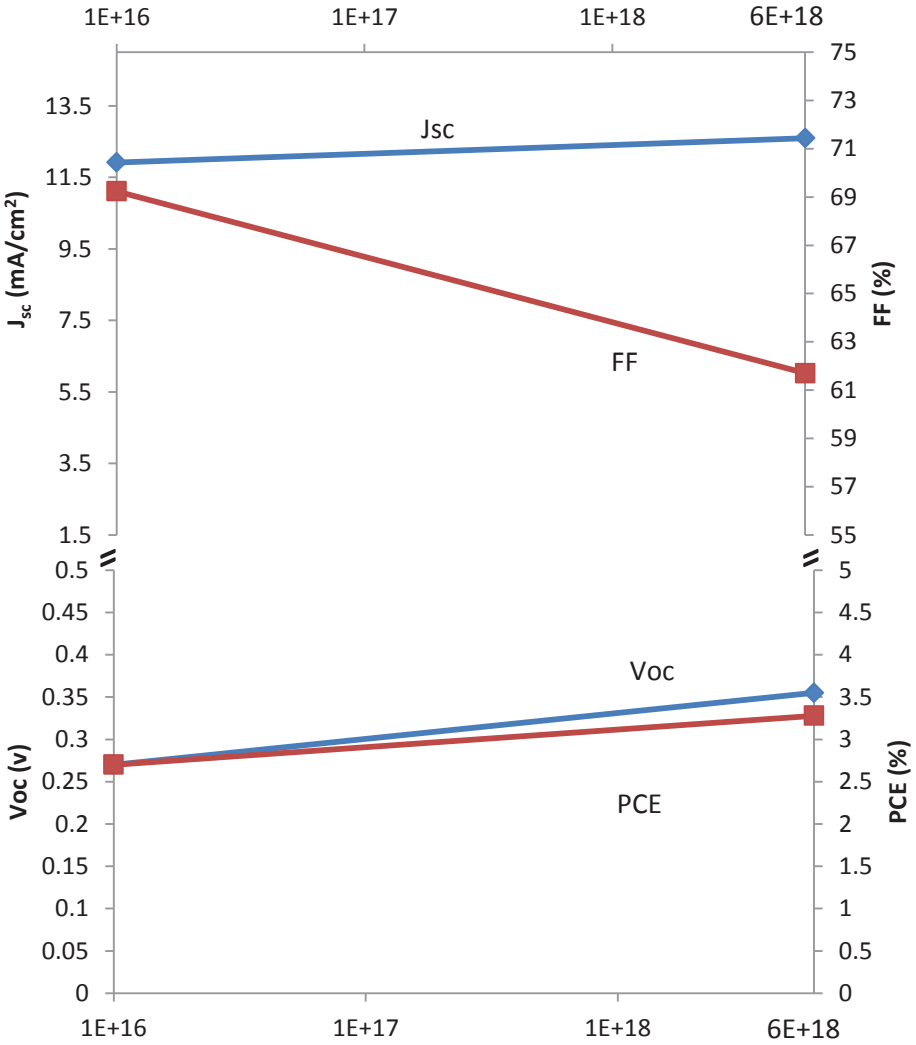

Figure 4.9 Calculated values of solar cell principal parameters based on different dopant concentrations at a constant length of 4μm.

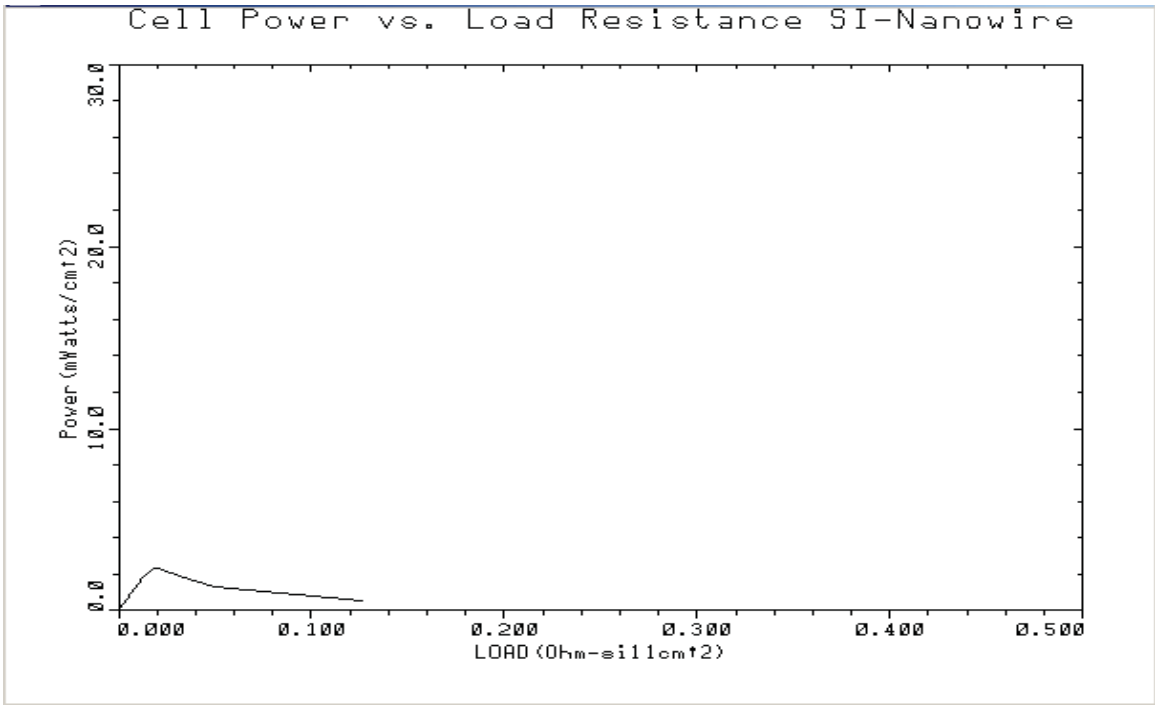

Figure 4.10 The power conversion efficiency versus load resistance for a SiNW/PEDOT:PSS solar cell with a length of 8μm and dopant concentration of $1\times10^{16}cm^{-3}$.

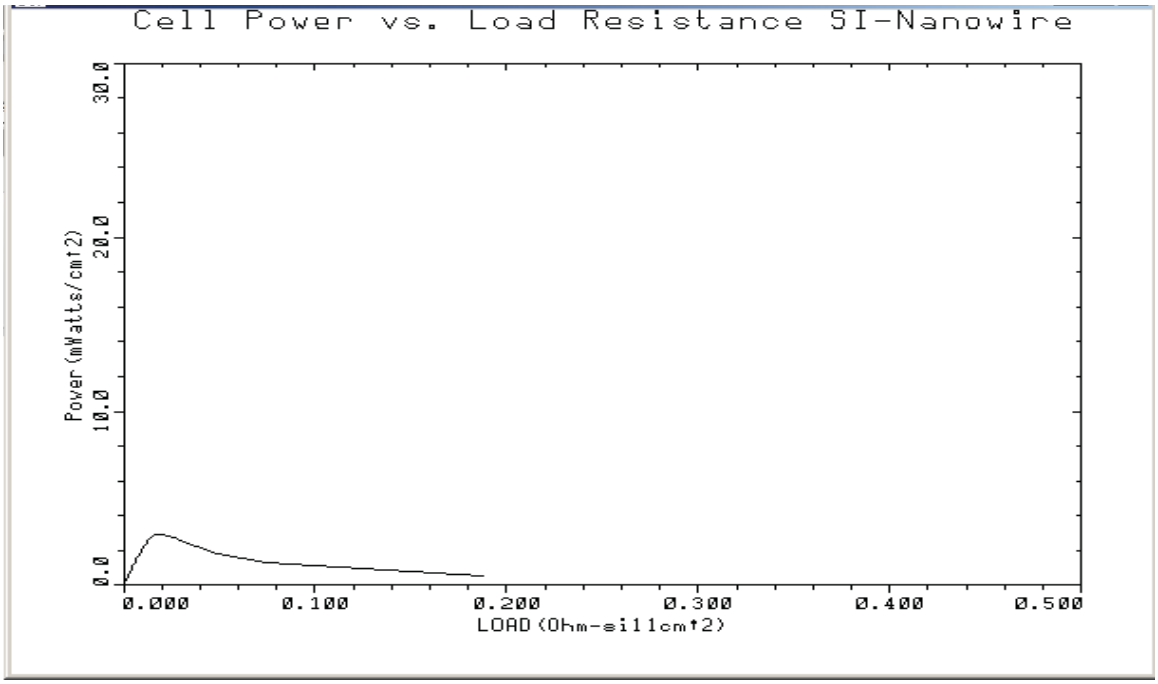

Figure 4.11 The power conversion efficiency versus load resistance for a SiNW/PEDOT:PSS solar cell with a length of 8μm and dopant concentration of $6\times10^{18}cm^{-3}$.

4.3. External quantum efficiency:

External collection efficiency of the SiNW solar cells with the dopant concentration of $1\times 10^{16}cm^{-3}$ and $6\times 10^{18}cm^{-3}$, and a length of 2 μm are plotted in Figure 4.12 and Figure 4.13 , respectively. Based on Figure 4.12, the maximum external quantum efficiency (EQE) for both of dopant concentrations ($1\times 10^{16}cm^{-3}$ and $6\times 10^{18}cm^{-3}$), is 41%, when the wavelength of the incident light is 540 nm. Note that, EQE over most of the visible spectrum is measured higher than 30%. These figures indicate that the EQE at the near infrared range decreases gradually for the unit cell of both dopant concentrations ($1\times 10^{16}cm^{-3}$ and $6\times 10^{18}cm^{3}$). Therefore, the incident light in the near infrared range should be absorbed by the bottom section of the SiNW and the light in the visible range, should be absorbed by the top section of the SiNW. In the case of the lower dopant concentration, the minority carrier has a higher lifetime so electron hole pairs (EHPs) can travel a longer distance. However, the unit cells with a higher dopant concentrations have lower lifetime so EHPs can travel a shorter distance.

Nevertheless, in the radial junction SiNW solar cell, due to the short collection length in this geometry, even carriers with low diffusion lengths can reach the junction and be collected by the electrodes. Therefore, there is no difference between the external quantum efficiencies when the dopant concentrations change from $1\times 10^{16}cm^{-3}$ to $6\times 10^{18}cm^{-3}$.

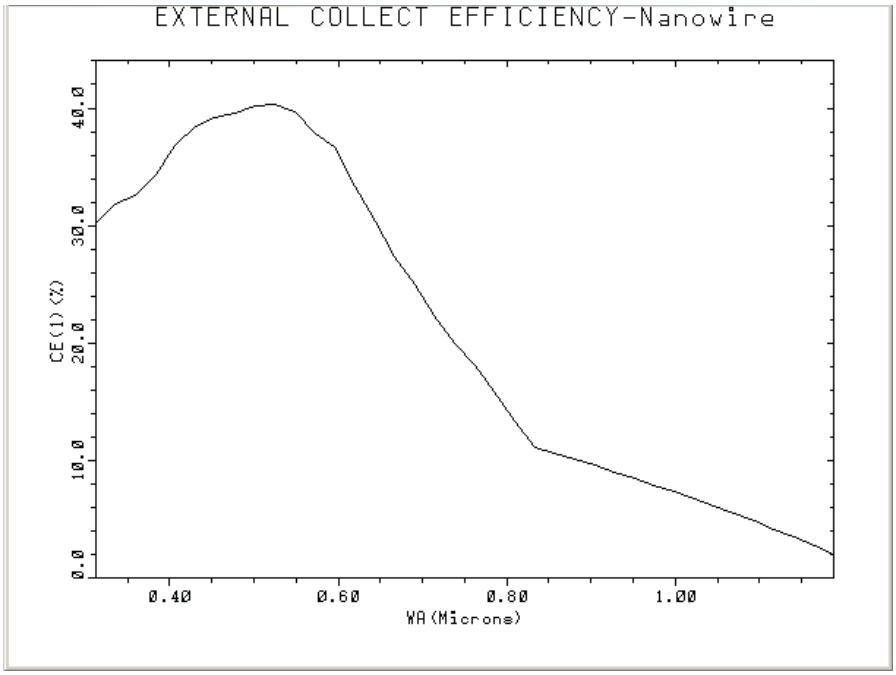

Figure 4.12 External collection efficiency of a SiNW solar cell, with a nano wire length of 2µm and dopant concentration of $1\times10^{16}cm^{-3}$.

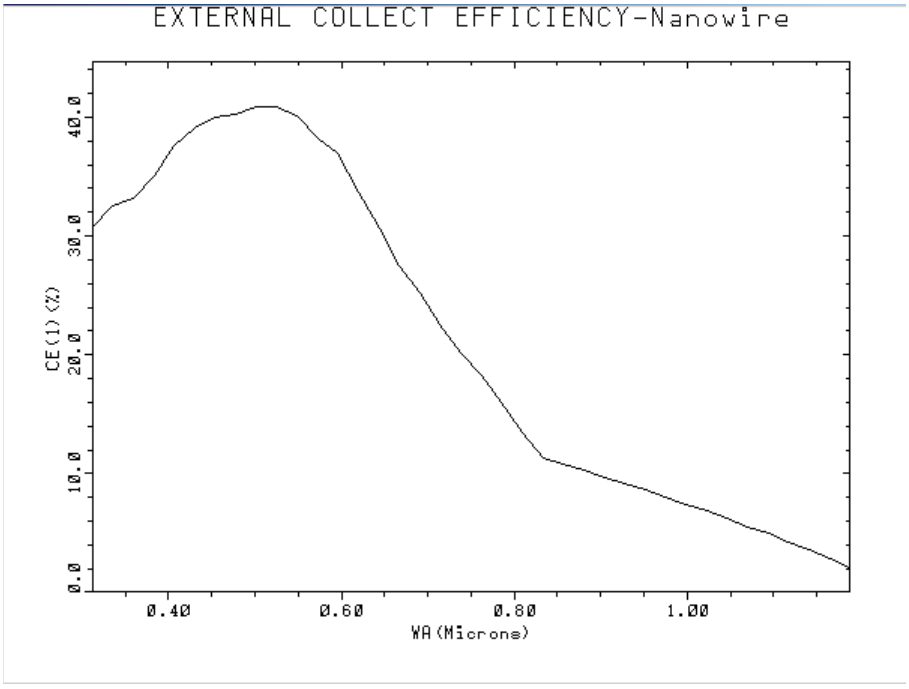

Figure 4.13 External collection efficiency of a SiNW solar cell, with a nano wire length of 2µm and dopant concentration of $6\times10^{18}cm^{-3}$.

4.4. Band Diagram

The band diagram for a unit cell of SiNW and PEDOT:PSS for two different dopant concentrations of $1\times 10^{16}cm^{-3}$ and $6\times 10^{18}cm^{-3}$ are illustrated in Figure 4.14 and Figure 4.15, respectively. The unit cell is a Si core with a diameter of 50nm, which is surrounded by the PEDOT polymer with a thickness of 20 nm. The photo-generated carriers can be separated at the junction of SiNW and the PEDOT:PSS polymer by a built-in potential. The ITO electrode collects the holes, whereas electrons are collected by the Aluminum contact. Note that, the direction of the incident light and hole transport are orthogonal in the radial junction structure.

In Figure 4.14 due to a big difference between the dopant concentration of silicon and PEDOT:PSS, we cannot find the band bending in the conduction band and valence band clearly. However, as shown in Figure 4.15, by increasing the dopant concentration of the Si, and reducing the difference between the concentration of Si and polymer, band bending can be observed. Note that, the energy band diagram of PEDOT:PSS with a band gap of 1.6 eV and electron affinity of 3.6 eV is shown in Figure 4.14.

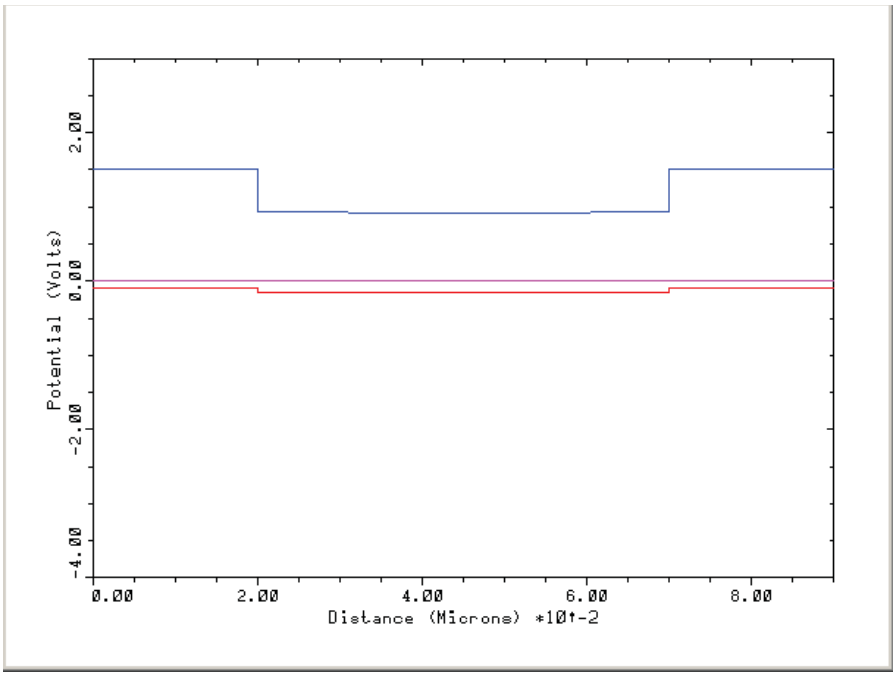

Figure 4.14 The energy band diagram of a hybrid solar cell (PEDOT:PSS/n-type Silicon) with a dopant concentration of 1×10^{16} cm^{-3}.

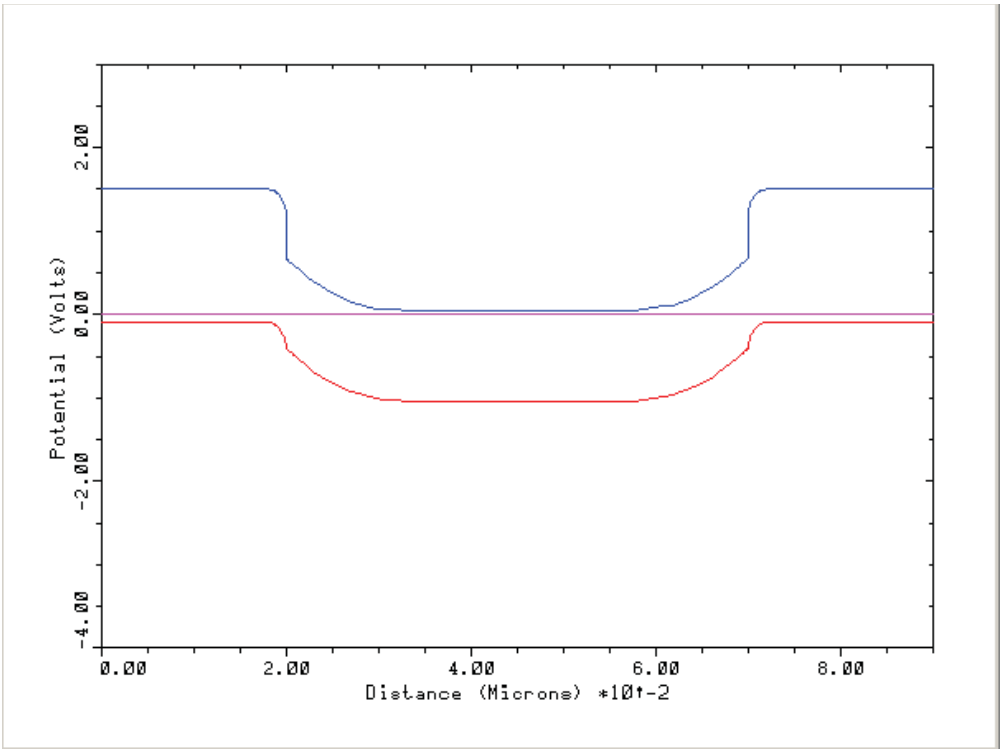

Figure 4.15 The energy band diagram of a hybrid solar cell (PEDOT:PSS/n-type Silicon) with a dopant concentration of 6×10^{18} cm^{-3}.

4.5. Photo generation

The generation rate determines the number of electrons generated at each point in the unit cell, which is related to the absorption coefficient of the material. As shown in Figure 4.16 the core of the unit cell which is silicon, has a higher photo generation rate as a result of higher absorption coefficient of silicon compared to PEDOT. Note that, the number of electron-hole pairs, which are generated either in polymer or in silicon, can be calculated by Equation 3.15. If we assume that the internal quantum efficiency is equal to 1, it means that the entire incident light has generated EHPs.

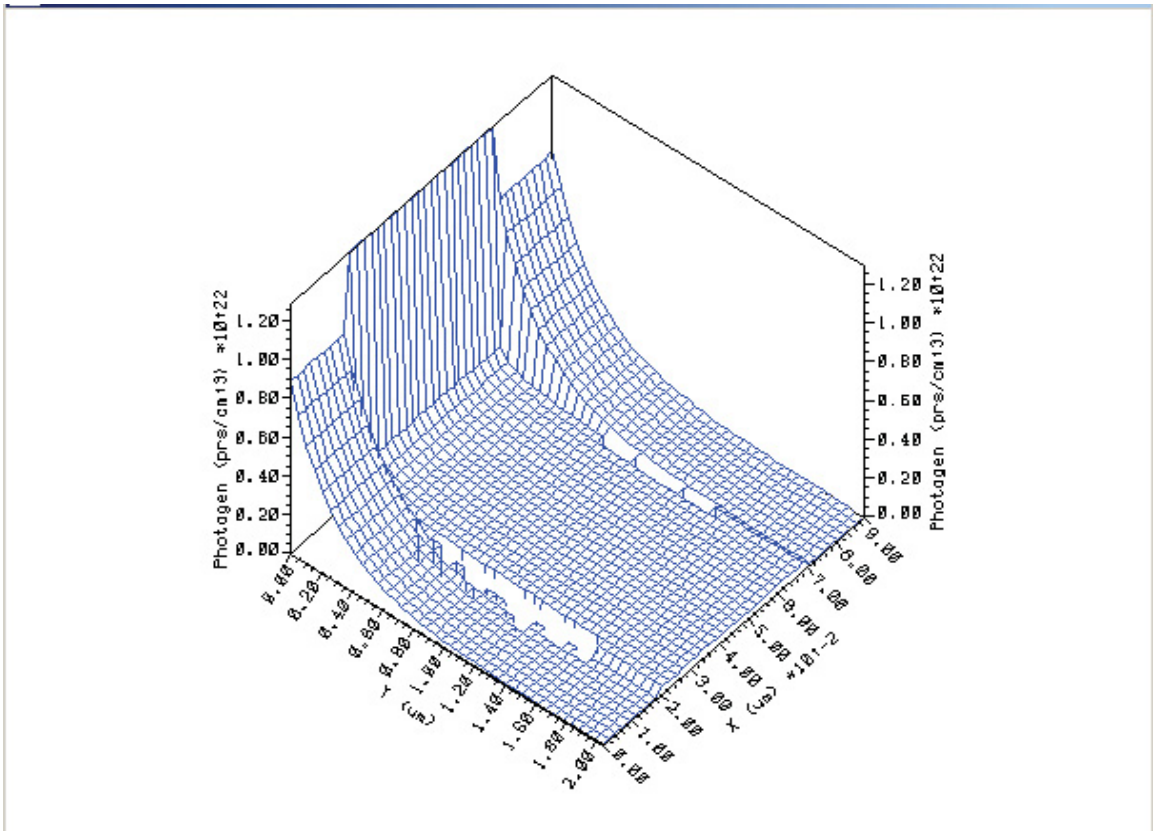

Figure 4.16 Generation rate of EHPs in a SiNW/PEDOT:PSS unit cell as a function of distance.

4.6. Conclusion

In this work, hybrid nano wire heterojunction solar cells, based on silicon and PEDOT:PSS polymer, have been studied with the device modeling software Medici. In this study, concentration of defects, the length and the dopant concentration of the SiNW, were subjected to change in order to find the electrical characterizations of the device.

For our purpose, two SiNWs with dopant concentrations of 1×10^{16}cm^{-3} and 6×10^{18}cm^{-3} were considered. For each certain dopant concentration we had three different lengths of SiNW including, 2µm, 4µm and 8µm.

In this work, it was shown that by increasing the trap density (N_r), the value of J_{sc} was remained constant, while the lifetime value (τ) has been decreased. Therefore, due to the decrease in the lifetime, there was a reduction in the open circuit voltage. Finally, the device efficiency dropped 3.9%, when the trap density increased from $1 \times 10^{12} cm^{-3}$ to $1 \times 10^{17} cm^{-3}$. This is due to a reduction in the value of open circuit voltage and constancy in the value of short circuit current.

Based on the results, it was understood that in the SiNW doped with $1\times10^{16} cm^{-3}$ and $6\times10^{18} cm^{-3}$ atoms, longer samples had better solar cell efficiencies and Fill Factors. The reason is that by increasing the length of the SiNW each nano wire can capture more photons. Thus, the short circuit current will increase. Furthermore, it can be seen that when the dopant concentration is $1\times10^{16} cm^{-3}$ the open circuit voltage (V_{OC}) is essentially independent of the length of the SiNWs. However, when the dopant concentration is $6\times10^{18} cm^{-3}$ by increasing the length of SiNW the V_{OC} decreased slightly due to an increase in the junction area. In other words, when the device is highly doped (6×10^{18}cm^{-3}), the open circuit voltage, is dependent to the junction area.

By investigating the effect of dopant concentration on SiNW samples with the same length, it was understood that SiNWs with higher dopant concentrations have better cell efficiency. Although, results show that FF decreased by increasing the dopant concentration, V_{oc} and J_{SC} showed to increase by increasing the dopant concentration from $1\times10^{16}cm^{-3}$ to $6\times10^{18}cm^{-3}$. Furthermore, external quantum efficiency for the mentioned samples was simulated. Results showed that, when the dopant concentration of the cell changed, EQE remained constant. In addition, Medici has simulated band diagrams of the Si/PDOT:PSS assembly. In the resultant figures, band bending can be observed when the dopant concentration of the Si increases to $6\times10^{18}cm^{-3}$.

Finally, photo-generation of the SiNW solar cell has been examined. Results showed that, photo generation decreases exponentially as the light goes further from the surface of the Si Nanowire to the depth of it.

CHAPTER 5

CONCLUSION

In this work, hybrid heterojunction solar cells based on planar-silicon/PEDOT:PSS polymer and SiNW/PEDOT:PSS have been simulated with the device modeling software Medici. The length, dopant concentration and the concentration of defects of these silicon-based solar cells were subjected to change in order to find the electrical characterizations.

It was shown that by increasing the trap density, the value of the short circuit current decreased in the planar Si, while remained constant in the SiNW structure. Besides, fill factor and open circuit voltage decreased for both configurations due to the reduction in the lifetime of minority carries, whereas, the power conversion efficiency dropped 3.9% in SiNW and 7.87% in the planar-silicon structure by increasing the trap densities at the same amount.

Results showed that, in both SiNW and planar-silicon structures, when the dopant density is$1 \times 10^{16} cm^{-3}$, by increasing the Si material length, the solar cell efficiency will increase. However, it was found that when Si is doped with $6 \times 10^{18} cm^{-3}$atoms, in the planar-Si structure the current density and FF remained almost the same for all of the selected lengths. While, in the SiNW structure doped with $6 \times 10^{18} cm^{-3}$atoms, increasing the length of wires contributed in improving the short circuit current and consequently efficiency.

By investigating the effect of dopant concentration on the planar configuration, it was found that Si substrates with higher dopant concentrations did not result in a better

efficiency. This is attributed to the reduction of current density in the highly doped planar-silicon layers. While in the SiNW structure, the wires with higher dopant concentrations have shown to have a better cell efficiency. The increase in the value of the open circuit voltage and short circuit current by increasing the dopant concentration is due to the short collection length in the radial SiNW/PEDOT:PSS junction solar cell.

Analysis showed that, under the same conditions such as the same thickness of the active layer and dopant concentration, the planar-Si configuration has a higher efficiency compared to the SiNW configuration, which is due to considering only one SiNW in our simulation model. Although this assumption could help us to operate the simulations, but at the same time it led to neglecting the effect of light trapping that exists in the real device configuration, which consist of arrays of SiNWs. Therefore, although Medici program is an accurate and powerful software in modeling the semiconductor devices, we were not able to show the light trapping effect through it. However, in order to make the best approximation in finding the effect of light trapping, we changed the source of light and angle of the illumination to the surface of the devise, however, results showed that these changes do not affect the short circuit current as long as the ray width covers the whole surface of the device. Nevertheless, the short circuit current decreased when the tilted angel was large enough so that, a small portion of light got out of the surface of the cell. Moreover, to operate the simulations in the nano-scale order, we had to be too much accurate in the mesh generation of the model, in order to avoid the error of convergence.

Another major problem that we faced in this study was the difficulty in finding the physical, optical and electrical properties of materials from the literatures due to ambiguity of the information, which is given in the articles.

Note that, a matter of key importance in the SiNW solar cell fabrication is the high temperature processes of the P-N junction formation. Therefore, using the PEDOT:PSS solution-based polymer as the p-type material is suggested in order to overcome the mentioned challenge.

Overall, in the planar-silicon/PEDET: PSS solar cell, the optimum device characteristics is concluded to be, the minimum possible trap density and dopant concentration in addition to the maximum acceptable Si substrate thickness. However, in the Si nano-wire structure, results showed that a device with the minimum possible trap density but at the same time maximum permissible dopant concentration and length, led to a better solar cell efficiency.

5.1. Future work

The studies in our work, tried to improve the understanding of the effect of material properties and the structure of hybrid solar cells on the principle parameters of the solar cells. However, some extra work is suggested to be done in the future to further improve the efficiency of the photovoltaic devices and decrease the fabrication costs.

Firstly, it is suggested to fabricate these two hybrid solar cells (planar and SiNW structures) and measure all the principal parameters of the solar cell and then compare the results by the results obtained from the simulations.

Moreover, it is suggested to use other polymers such as P3HT instead of PEDOT:PSS to investigate the subsequent electrical characteristics of the device. Furthermore, exploiting p-type Si instead of n-type and create the p-n junction with a proper n-type polymer, because fabricating p-type Si is easier than n-type. In addition, since in the p-type Si the minority carriers are electrons a higher short circuit current can be expected because of the lighter weight of electrons compared to holes.

REFERENCES

[1] United States Energy Information Administration, "World coal consumption by year 2011," Jan 10, 2014 (11 AM). [Online]. Available: http://www.eia.gov/.

[2] B. D. H. and E. . Slatick, "carbon dioxide Emission factors for coal," *Energy Information Administration*, 1994. .

[3] N. S. Lewis, "Toward cost-effective solar energy use.," *Science*, vol. 315, no. 5813, pp. 798–801, Feb. 2007.

[4] K.-Q. Peng and S.-T. Lee, "Silicon nanowires for photovoltaic solar energy conversion.," *Adv. Mater.*, vol. 23, no. 2, pp. 198–215, Jan. 2011.

[5] B. M. Kayes, H. a. Atwater, and N. S. Lewis, "Comparison of the device physics principles of planar and radial p-n junction nanorod solar cells," *J. Appl. Phys.*, vol. 97, no. 11, p. 114302, 2005.

[6] William Shockley1 and Hans J. Queisser1, "Detailed Balance Limit of Efficiency of p-n Junction Solar Cells.pdf," *J. Appl. Phys*, vol. 32, no. 3, p. 510, 1961.

[7] S. M. Sze, *Physics of Semiconductor Devices (3rd edition)*. 2007, pp. 227–228.

[8] C. Santa Clara, “Multicrystalline Silicon Modules to Dominate Solar PV Industry in 2014, According to NPD Solarbuzz.pdf,” *THE NPD group*,Jan 12, 2014.(10AM) [Online]. Available: http://www.solarbuzz.com/news/recent-findings/multicrystalline-silicon-modules-dominate-solar-pv-industry-2014.

[9] E. Carttidge, “Bright outlook for solar cells.pdf, *IOP*, 2007". Jan 22,2014 (3 PM) [Online]. Available: http://environmentalresearchweb.org/cws/article/news/30489.

[10] E. Bundgaard and F. Krebs, “Low band gap polymers for organic photovoltaics,” *Sol. Energy Mater. Sol. Cells*, vol. 91, no. 11, pp. 954–985, Jul. 2007.

[11] P. W. M. Blom, V. D. Mihailetchi, L. J. A. Koster, and D. E. Markov, “Device Physics of Polymer:Fullerene Bulk Heterojunction Solar Cells,” *Adv. Mater.*, vol. 19, no. 12, pp. 1551–1566, Jun. 2007.

[12] T. A. for S. Energy.LLC, “National Center for Photovoltaics,” *national laboratory of the U.S Departement of the energy (NREL)*, April 28 ,2014. (2 PM) [Online]. Available: http://www.nrel.gov/ncpv/.

[13] F. Sohrabi, A. Nikniazi, and H. Movla, *Optimization of Third Generation Nanostructured Silicon-Based Solar Cells*. 2013, pp. 1–26.

[14] G. Conibeer, “Third-generation photovoltaics,” *Mater. today*, vol. 10, no. 11, pp. 42–50, 2007.

[15] B. Ozdemir and M. Kulakci, “Silicon nanowire-poly (3, 4-ethylenedioxythiophene)-poly (styrenesulfonate) heterojunction solar cells,” *Appl. Phys.* , vol. 99, no. 11, p. 113510, 2011.

[16] A. J. Nozik, “Multiple exciton generation in semiconductor quantum dots,” *Chem. Phys. Lett.*, vol. 457, pp. 3–11, 2008.

[17] A. . Nozik, “Quantum dot solar cells,” *Physica E: Low-dimensional Systems and Nanostructures*, vol. 14. pp. 115–120, 2002.

[18] D. S. Boudreaux, F. Williams, and a J. Nozik, “Hot carrier injection at semiconductor-electrolyte junctions,” *J. Appl. Phys.*, vol. 51, no. 4, p. 2158, 1980.

[19] C. Y. Kuo and C. Gau, “Arrangement of band structure for organic-inorganic photovoltaics embedded with silicon nanowire arrays grown on indium tin oxide glass,” *Appl. Phys. Lett.*, vol. 95, no. 5, p. 053302, 2009.

[20] L. He, C. Jiang, H. Wang, and D. Lai, “Simple Approach of Fabricating High Efficiency Si Nanowire/Conductive Polymer Hybrid Solar Cells,” *IEEE Electron Device Lett.*, vol. 32, no. 10, pp. 1406–1408, Oct. 2011.

[21] M. J. Price, J. M. Foley, R. a. May, and S. Maldonado, “Comparison of majority carrier charge transfer velocities at Si/polymer and Si/metal photovoltaic heterojunctions,” *Appl. Phys. Lett.*, vol. 97, no. 8, p. 083503, 2010.

[22] W. Lu, C. Wang, W. Yue, and L. Chen, “Si/PEDOT:PSS core/shell nanowire arrays for efficient hybrid solar cells.,” *Nanoscale*, vol. 3, no. 9, pp. 3631–4, Sep. 2011.

[23] S.-C. Shiu, J.-J. Chao, S.-C. Hung, C.-L. Yeh, and C.-F. Lin, “Morphology Dependence of Silicon Nanowire/Poly(3,4-ethylenedioxythiophene):Poly(styrenesulfonate) Heterojunction Solar Cells,” *Chem. Mater.*, vol. 22, no. 10, pp. 3108–3113, May 2010.

[24] K. Q. Peng, J. J. Hu, Y. J. Yan, Y. Wu, H. Fang, Y. Xu, S. T. Lee, and J. Zhu, “Fabrication of Single-Crystalline Silicon Nanowires by Scratching a Silicon Surface with Catalytic Metal Particles,” *Adv. Funct. Mater.*, vol. 16, no. 3, pp. 387–394, Feb. 2006.

[25] L. He, C. Jiang, H. Wang, D. Lai, Y. Heng Tan, and C. Seng Tan, “Effects of nanowire texturing on the performance of Si/organic hybrid solar cells fabricated with a 2.2 μm thin-film Si absorber,” *Appl. Phys. Lett.*, vol. 100, no. 10, p. 103104, 2012.

[26] H.-J. Syu, S.-C. Shiu, and C.-F. Lin, “Silicon nanowire/organic hybrid solar cell with efficiency of 8.40%,” *Sol. Energy Mater. Sol. Cells*, vol. 98, pp. 267–272, Mar. 2012.

[27] L. He, C. Jiang, H. Wang, and D. Lai, “High efficiency planar Si/organic heterojunction hybrid solar cells,” *Appl. Phys. Lett.*, vol. 100, no. 7, p. 073503, 2012.

[28] S. Woo, J. H. Jeong, and H. K. Lyu, “Hybrid solar cells with conducting polymers and vertically aligned silicon nanowire arrays: the effect of silicon conductivity,” *Phys. B Condens. ...*, vol. 407, no. 15, pp. 3059–3062, Aug. 2012.

[29] F. Zhang, T. Song, and B. Sun, “Conjugated polymer–silicon nanowire array hybrid Schottky diode for solar cell application,” *Nanotechnology*, vol. 23, no. 19, p. 194006, May 2012.

[30] T.-G. Chen, B.-Y. Huang, E.-C. Chen, P. Yu, and H.-F. Meng, “Micro-textured conductive polymer/silicon heterojunction photovoltaic devices with high efficiency,” *Appl. Phys. Lett.*, vol. 101, no. 3, p. 033301, 2012.

[31] Synopsys, “Taurus Medici User Guide,”. September, 2008.

[32] Stuart Bowden and Christiana Honsberg, "PV CDROM," *Solar Power Labs*,Jan 2 2014 (10 AM). [Online]. Available: http://pveducation.org/pvcdrom.

[33] S. M. Sze, *Physics of Semiconductor Devices, 2nd ed*. 1981, p. 868.

[34] "Reference solar spectral irradiance: air mass 1.5," *NREL*, Feb 20, 2013.(2 PM) [Online]. Available: http://rredc.nrel.gov/solar/spectra/am1.5/.

[35] W. Shockley and H. J. Queisser, "Detailed Balance Limit of Efficiency of p-n Junction Solar Cells," *J. Appl. Phys.*, vol. 32, p. 510, 1961.

[36] B. Yaghootkar, M. Amouzgar, and M. Kahrizi, "A novel and low-cost multi-stage approach for the fabrication of silicon nano-structures," *Sensors Actuators A Phys.*, vol. 199, pp. 209–215, Sep. 2013.

[37] M. N. Amin and M. O. Alam, "Electro-optical characterisation of InP nanowire based p-n, p-i-n Infrared photodetectors," *J. Commun.*, vol. 7, no. 11, pp. 808–820, Nov. 2012.

[38] E. Garnett and M. Brongersma, "Nanowire solar cells," *Annu. Rev.*, vol. 41, no. 1, pp. 269–295, Aug. 2011.

[39] K. R. Andreas Elschner, Stephan Kirchmeyer, Wilfried Lovenich, Udo Merker, *PEDOT,Principles and Applications of an Intrinsically Conductive Polymer*. CRC Press (Nov. 2 2010), 2010.

[40] L. Groenendaal, F. Jonas, D. Freitag, H. Pielartzik, and J. R. Reynolds, "Poly(3,4-ethylenedioxythiophene) and Its Derivatives: Past, Present, and Future," *Adv. Mater.*, vol. 12, pp. 481–494, 2000.

[41] Dflanagan, "PEDOT_PSS - Wikipedia, the free encyclopedia.pdf," *Wikipedia*, April 18,2014(9AM).[Online]. http://en.wikipedia.org/wiki/PEDOT:PSS.

[42] R. Paetzold, K. Heuser, D. Henseler, S. Roeger, G. Wittmann, and A. Winnacker, "Performance of flexible polymeric light-emitting diodes under bending conditions," *Appl. Phys. Lett.*, vol. 82, p. 3342, 2003.

[43] A. N. Aleshin, S. R. Williams, and A. J. Heeger, "Transport properties of poly(3,4-ethylenedioxythiophene)/poly(styrenesulfonate)," *Synthetic Metals*, vol. 94. pp. 173–177, 1998.

[44] S. Lee, S. In, D. Mason, and N. Park, "Incorporation of nanovoids into metallic gratings for broadband plasmonic organic solar cells," *Opt. Express*, vol. 21, no. 4, pp. 4055–4060, 2013.

[45] M. . Jie Liu, “Poly (ethylenedioxythiophene) based electronic devices for sensor applications,” LOUISIANA TECH UNIVERSITY, 2008.

[46] Richard S.Muller and Theodore l.Kamins with Mansun Chan, *Device Electronics for integrated circuits*, 3rd ed. John Wiley & Sons, 2002.

[47] D. A.Neamen, *Semiconductor Physics and Devices Basic principles*, Third. Elizabeth A.Jones, 2003.